Investigation of Time Series Analysis Based Damage Detection Methodologies for Structural Health Monitoring

by

Qipei Mei

A thesis submitted in partial fulfillment of the requirements for the degree of

Master of Science

in

Structural Engineering

Department of Civil and Environmental Engineering

University of Alberta

Abstract

Structural Health Monitoring (SHM) is widely accepted as a valuable tool for monitoring, inspecting and maintaining infrastructure systems. Damage detection is one of the most critical components of SHM to identify the existence, location and severity of damage so that effective preventive actions can be taken to improve the condition of the structure. In this study, time series analysis based damage detection methods using output-only vibration data are investigated for global condition assessment of structures. The main body of the thesis falls into two key parts. In the first part, a novel damage detection method based on Auto-Regressive models with eXogenous (ARX models) and sensor clustering is proposed. Two different Damage Features (DFs) based on the difference of fit ratios and ARX model coefficients are considered in this part. Applying this method to experimental data from a steel grid type structure and a 4-span bridge type structure, it is demonstrated that the existence, location and severity could be successfully assessed by both two DFs for most of the cases. In the second part, an improved version of the previous method is developed to separate the changes in stiffness and mass of the structure using output only data. In order to verify this approach, it is first applied to a 4-DOF mass spring system and then to the shear type IASC-ASCE numerical benchmark problem. It is demonstrated that the approach can not only accurately determine the location and severity of the damage, but also distinguish between changes in stiffness and mass. This study constitutes the first approach of its kind which can distinguish between change of stiffness and mass by using output only vibration data. At the end of the thesis, the limitations of current methods, recommendations, and future work are also addressed.

Acknowledgements

First of all, I would like to express my deepest gratitude to my supervisor, Dr. Mustafa Gül, for his encouragement and guidance throughout my study at U of A. He has walked me through every stage of my thesis. This thesis could never be completed without his help and mentorship.

I am grateful to the members of our research team, Jianfeng Gu, Saeideh Fallah Nafari, Ngoan Do Tien, Branislav Kostic and Aimee De Laurentiis, for their collaboration and help. Many thanks to my friends, Ran Ding, Jian Jiang, Fei Han, Zheyuan Liu, Ran Li, who are very patient to me and makes my whole life enjoyable.

I would also like to thank the committee members of my MSc defense, Dr. J.J. Roger Cheng and Dr. Ahmed Bouferguene, for their time and great feedback.

At last, I wish to give my thanks to my beloved family and girlfriend, Jiarui Wang. It is their encouragement and support that helped me through the most difficult times.

Table of Contents

List of Figures

List of Tables

List of Nomenclature

$x_i(t)$	Displacement of the i^{th} DOF at time t
$\dot{x}_i(t)$	Velocity of the i^{th} DOF at time t
$\ddot{x}_i(t)$	Acceleration of the i^{th} DOF at time t
$\boldsymbol{M}$	Mass matrix
$\boldsymbol{C}$	Damping Matrix
$\boldsymbol{K}$	Stiffness Matrix
$Y_i(t)$	Replacement of $\dddot{x}_i(t)$ after applying the forward difference technique
$Z_i(t)$	Replacement of $\ddddot{x}_i(t)$ after applying the forward difference technique
$y_i(t)$	Replacement of $\ddot{x}_i(t+\Delta t) - \ddot{x}_i(t)$
DF_{ij}	DF for the sensor j in the i^{th} sensor cluster

CHAPTER 1:INTRODUCTION

1.1 Introduction to Structural Health Monitoring

Existing infrastructures are subjected to various potential risks, such as aging, fatigue, corrosion, overloading, etc. These potential risks result in different levels of damage which may cause the failure or even collapse of the infrastructures. As infrastructure systems age and approach (or suppress) their design life, these problems become more significant. In the past, hundreds of bridges have failed due to all kinds of reasons. One of the critical reasons is poor maintenance, such as Hayakawa wire bridge in Japan, Mianus River Bridge in the United States and Somerton Bridge in Australia, CPR Bonnybrook Bridge in Canada (Wikipedia, the free encyclopedia, 2014). Now there are over 600,000 highway bridges in the US and more than 30% of these bridges have exceeded their 50-year design life (FHWA 2011). According to FHWA (2013), among these bridges, nearly 11% are structurally deficient and 15% are functionally obsolete. In Canada, condition of the infrastructures is also downgrading (Félio et al., 2012). Mirza and Haider (2003) indicated that nearly 80% of existing bridges need repair to some extent. Recent years, many challenging bridges were successfully designed and constructed, but how to keep them safe and reliable during their life-circle is still a big problem.

Since rebuilding all the structures is out of question, Structural Health Monitoring (SHM) is considered as a valuable tool to increase safety and reliability, as well as to optimize maintenance operations during the service life of the infrastructure systems, offering considerable savings in life-cycle cost. SHM refers to a process of damage detection and condition assessment for aerospace, civil, and mechanical structures. The importance of developing robust and automated SHM systems has been widely recognized in recent decades (Bernal and Beck 2004; Lynch and Loh 2006; Inaudi and Glisic 2008; Fan and Qiao 2011).

Considering the points mentioned above, in the last few decades, the focus of structural engineers and researchers has gradually shifted from the design of structures to the maintenance of structures due to the mature and perfection of structural design theories. Owing mostly to the rapid progress of modern technologies, especially in the areas of

computer science and electrical engineering, data acquisition has become much easier than ever before. Various SHM techniques have been applied in different contexts (Hearn and Testa 1991; Hou et al. 2000; Dharap et al. 2006; Yi and Li 2012; Moaveni et al. 2012; Han et al. 2014). In particular, a number of monitoring systems have been installed on bridges (Wong 2004; Koh and Dyke 2007; VanZwol et al. 2008; Magalhães et al. 2012; Roshandeh et al. 2014) and buildings (Fritzen et al. 2000; Carpinteri and Lacidogna 2006; Jane et al. 2008; Ponzo et al. 2010; Yi et al. 2013). Most of the SHM systems can be categorized into a statistical pattern recognition frame proposed by Farrar et al. (2004). This paradigm involves four main parts:

1) Operational Evaluation: This step is mainly to investigate the purpose of the monitoring, the characteristics of the potential damage.

2) Data Acquisition, Data Fusion, and Data Cleansing: For the data acquisition process, the quantities to be measured are first determined and then the types of sensors; the second step is to decide the placement of sensors and the acquisition system. Data fusion aims to integrate data from different sensors comprehensively in order to make the system more robust and more accurate. Data cleansing is to filter and refine the data, and reduce the computational effort for the following analyses.

3) Feature Extraction and Information Condensation: Feature extraction refers to extracting the damage features (DFs) to distinguish between the baseline and damaged structures, which is usually considered as the most important part of the whole SHM process. All kinds of properties can be chosen as DFs as long as they can identify the damage. The focus of information condensation is to reduce the dimension and size of the data in the context of keeping the accuracy of damage detection.

4) Statistical Model Development for Discrimination: This final step aims to develop statistical models to operate on the DFs with the objective to expose the statistical significance for detecting the existence, location and severity of damage.

1.2 Introduction to Damage Detection Methods

Damage detection is a very critical component of SHM given that the existence and location of damage should be identified before effective preventive actions could be

taken. Generally speaking, damage refers to the changes introduced into a system which lead to a decrease in its current and future performance. In structural systems, damage may be related to changes in the material and/or geometric properties, boundary conditions and so on.

According to Rytter (1993), any damage detection method should focus on the following four objectives: 1) identifying the existence of damage; 2) localizing the damage; 3) determining the severity of damage; 4) estimating the remaining useful life. These objectives belong to four different levels and are arranged in order of difficulty. Current damage detection methods mainly concentrate on levels 1, 2 and 3. Among all the objectives, the location of damage is paramount because it is a prerequisite to conduct more detailed investigations and eventually understand the root cause of the damage.

Damage detection methods in general could be classified into two categories, local methods and global methods (Johnson et al. 2004). Local methods aim to detect specific damage in a localized region at a particular time using various techniques such as ultrasonics and X-ray (Kessler et al. 2002a; Hola and Schabowicz 2010; Cheng and Tian 2012). These localized methods belong to a totally different subject area and are not directly related to the research presented in this thesis, so the discussions presented here will not focus on this type of methods.

On the other hand, global methods, also widely known as vibration-based methods, assess the condition of the entire structure using the dynamic response of the structure. Vibration-based methods are economical and effective in assessing the overall health of the structure, although some issues, such as the following, must be resolved before they are successfully applied in reality (Beck and Bernal 2001): (1) Typical modal parameters, such as frequencies or mode shapes, are generally very insensitive to localized damage, and may not well suitable for DFs; (2) input force usually only excites the lower modes of the structure; furthermore, in most cases, the excitations are even unavailable (3) the dynamic response data are often noisy and only available at certain positions due to the limited number of sensors; and (4) an inverse problem needs to be resolved since the change of dynamic responses does not directly show the change of stiffness, mass and damping.

As a further classification, the vibration based methods could be categorized into parametric and non-parametric methods. Parametric techniques aim to develop physics-based models for damage detection. Methods based on frequency changes, mode shape changes and model updating belong to this category (Shiradhonkar and Shrikhande 2011; Siebel et al. 2012; Hamze et al. 2014). Although parametric methods can build a direct relationship between DFs and structural physical characteristics, developing such a relationship may require detailed knowledge and significant experience, which makes automation for handling large amounts of data not feasible. In addition, due to varying operational and environmental conditions, application of these techniques to real structures is also a big challenge (Catbas et al. 2007). Given these factors, non-parametric methods in combination with statistical methods have recently attracted significant attention. For these methods, with the interference of operational and environmental changes, the anomalies can be identified by analyzing DFs that may not be easily attributed to any specific physical changes (Sohn et al. 2001a; Gül and Catbas 2009; Taha 2010; Min et al. 2012; Shu et al. 2013).

Although derived based on the equation of the motion of multi-degree-of-freedom systems, the time series analysis based method used in this thesis can be considered as a non-parametric method. A time series is a sequence of data with uniform time intervals. Common time series models include Auto-Regressive (AR) models, Moving Average (MA) models, Box-Jenkins (B-J) models, etc. The robustness and ability to fit dynamic response are some of the main advantages of time series models. After the development of more than one decade, all kinds of research studies show the promising of this type of methods (Sohn et al. 2001a; Monroig and Fujino 2006; Nair et al. 2006; Gül and Catbas 2009; Wyłomańska et al. 2014). A literature review of the common vibration based damage detection methods as well as time series based damage detection methods are included in Chapter 2.

1.3 Objectives and Scope

As mentioned above, time series modeling has great potential as a tool for damage detection. However, there are still a number of issues that need to be addressed before it can be effectively used for damage detection in the context of SHM. This study has

mainly two objectives in order to step forward in this area of research. The first objective of this thesis is to develop a new, efficient and robust method for damage detection. The second objective is to develop a novel damage detection method that can distinguish the changes caused by mass and stiffness separately by using output-only vibration data. The thesis can be divided into two parts. In part 1, a new time series based method based on ARX models for damage detection is developed. Two different DFs are used. Ability of this method to detect and locate damage under free vibration is studied and verified on two experimental structures. In part 2, a further improved version of the method presented in part 1 is proposed. The novelty of this approach is that it can identify changes in the stiffness and mass of the system separately using the output-only ambient vibration data. The effectiveness of the improved method is demonstrated by using a 4-DOF mass spring system and the phase I of the IASC-ASCE numerical model. To the best of author's knowledge, this study constitutes the first approach of its kind which can distinguish between change of stiffness and mass by using output only vibration data.

1.4 Organization of the Thesis

The organization of the thesis is as follows.

Chapter 2 presents a literature review about the methods for damage detection. The first section includes the development, pros and cons of the most commonly used damage detection methods, such as those based on modal frequencies, mode shapes and model updating. The second section particularly demonstrates the history of damage detection methods based on time series modeling, and the latest research achievements in this area.

Chapter 3 demonstrates a basic introduction of time series analysis and the underlying theory of the proposed novel damage detection method using time series analysis and sensor clustering. The derivation, definition of two different DFs and process of the method are discussed.

In Chapter 4, the proposed method is verified on an experimental steel grid type large-scale benchmark problem. Four different damage cases are introduced. The method is conducted using data from free vibration. The chosen sensor clusters, the implementation of the method and the results for two different DFs along with interpretations are shown.

Besides, the influence of the impact location on the performance of the method using fit ratios as DFs is also investigated.

Chapter 5 is dedicated to test the method on a 4-span bridge structure in laboratory conditions. Seven different kinds of damage cases are introduced to this structure. Dynamic responses from free vibration are used. The results and validity of the method using two different DFs are presented.

Chapter 6 presents an improved version of the method discussed in Chapter 3. The theory and implementation of the proposed method is demonstrated. A 4-DOF numerical system under ambient vibration is introduced to conduct preliminary study.

In Chapter 7, the improved method is applied to a more realistic shear-type structure. Eight damage cases, which are caused by the different combinations of stiffness, damping and mass changes, are applied. The ability of the method to detect, locate and quantify the damage caused by stiffness and mass changes separately is presented. In addition, the relationship between damage detection results and sampling frequency is also discussed.

Finally, summary and conclusions are provided in Chapter 8. Recommendations and possible future directions are also presented.

CHAPTER 2:LITERATURE REVIEW OF DAMAGE DETECTION METHODS

SHM is a multi-disciplinary subject involving many different components, such as experimental testing, sensors, data acquisition systems, data transfer and storage, signal processing, damage detection methods, etc. Benefiting from the rapid development of advanced technologies in the area of computer science and electrical engineering, it is now more convenient and cheaper to acquire large amounts of data. However, despite being able to possess abundant data, how to properly use them to detect damage is still a big challenge. The main objective of this thesis is to develop methods for damage detection based on time series analysis. In this chapter, a detailed literature review about existing methods for damage detection is presented. For the completeness of the review, an introduction to the widely used vibration based damage detection methods in general is included in the first section, and a specific review about the history and latest accomplishment in methods based on time series analysis is presented in the second section.

2.1 Literature Review of Commonly Used Damage Detection Methods

Modal frequencies are the most basic dynamic parameters of a structure. Since they are related to physical properties of the structure, such as stiffness and mass, many researchers attempted to use these indicators to detect damage. A very brief history of the development of such damage cases is given in the next paragraphs since these methods can be considered as one of the first attempts for damage detection using vibration data.

Lifshitz and Rotem (1969) may be the first to detect damage via frequency shifts. Considering the change in moduli, which is related to the frequency, the damage in quartz particle filled resin specimens can be successfully detected. From 1980s to 1990s, research studies about frequency based methods flourished. Ju and Mimovich (1988) applied the modal frequency method along with the theory called “fracture hinge” to experimentally identify the crack damage in a cantilever beam. The results showed that the locations and intensities of the damage can be identified successfully with different

accuracies with the help of an analytic model. Hearn and Testa (1991) demonstrated a damage detection method based on examining the change in frequencies and damping coefficients. They applied their proposed method to a welded steel frame under fatigue loading and wire ropes damaged by saw-cuts. In their paper, the relationship between the change in frequency and in stiffness was derived from the equation of motion by assuming the mass does not change due to the damage. Messina et al. (1998) presented a new correlation coefficient called the Multiple Damage Location Assurance Criterion (MDLAC) which can provide useful information about the location and size of the damage. In their method, finite element model was used to obtain the sensitivity and Hessian matrices, and an updated model was not necessary. One advantage of this method was that only a few of the natural frequencies between baseline and unknown states needed to be measured. More research about damage detection method using modal frequencies can be found in an excellent review by Salawu (1997). However, despite the development for years, there are still limitations in frequency based damage detection methods. Frequency changes are usually insensitive to small damage. Therefore, very precise measurements are needed in order to make methods work. Even for such cases damage can be separated from changes caused by environmental factors only when the damage is severe. Moreover, spatial information related to the locations of damage cannot be exposed by the change of frequencies (Doebling et al. 1998). In recent years, due to the limitations mentioned above, researchers have gradually abandoned pure frequency-based methods. However, the new research combining frequency based methods with other technologies still provided some inspiration (Kim et al. 2003; Maity and Tripathy 2005; Zhong et al 2008; Hamze et al. 2014).

Similar to frequencies, mode shapes are also very important indicators of damage. They are more promising to locate the damage than the frequency based methods, because more information are included in mode shapes than in frequencies (Plankis 2012). West (1984) was probably the first to independently use information about mode shapes to locate damage. He tested a Space Shuttle Orbiter body flap before and after damage, and used modal assurance criteria (MAC) to measure the correlation between the mode shapes. In their paper, the mode shapes were first divided differently. Then, the damage was located using the change of MAC different divisions. Kam and Lee (1992) developed

an extensible method to locate cracks in a beam using frequencies and modal shapes via identifying the reduced stiffness in the elements of structures. In addition, they also used static deflection analyses to calculate the strain energy of the structure. The change of strain energy was used to estimate the size of cracks. Ahmadian et al. (2000) proposed a damage detection method based on the idea that when damage occurs in a substructure of a large structure, the participation factors of the higher modes for the corresponding substructure would change with other participation factors fixed. Therefore, the damage can be located according to two DFs derived from difference of those the mode shapes. More recently, Siebel et al. (2012) investigated the applications of two mode shape based methods, Modal Strain Energy method and Gapped Smoothing Technique, to a turbine subjected to wind excitation. The vibration data of the structure was first processed by operational modal analysis to yield mode shapes. Then the two methods were applied to the mode shape information for damage detection. Both finite element modeling and experimental analysis were conducted to verify these two methods. Overall, mode shape based methods are more feasible than frequency based methods since mode shapes can provide the spatial information of the damage and are more feasible for damage localization (Plankis 2012). However, since frequency and mode shape are both modal parameters, methods using mode shapes have some limitations very similar to frequency based methods: 1) it is difficult to excite higher modes which are more sensitive to minor damage; and 2) mode shapes are also very sensitive to operational and environmental noise.

Another noted class of vibration based methods is called model updating methods. The principle of this type of methods is to change the finite element models to simulate the measured dynamic response of baseline and damaged structures as closely as possible. (Mottershead and Friswell 1993). Comparing the updated and baseline matrices, the location and extent of damage can be estimated. Adopting different objective functions, constraints and optimization algorithms to different problems, different model updating methods can be created. Liu (1995) demonstrated a method for identifying the mass and stiffness properties by minimizing the error norm of an eigenequation formulated from the finite element model. Applying the method to a numerical truss model, the author showed that if sufficient data were provided, the element properties can be obtained

uniquely as a global minimal. Yang and Lee (1999) presented a method with two steps for damage detection. In the first step, authors first roughly estimated the potential damage regions using a substructure technique. Then, they adopted a minimization algorithm limited to the identified damage regions to quantify the severity damage. The effectiveness of their methods was proved by applying to a numerical cantilever beam. In 2006, a sensitivity based model updating method was carried out by Jaishi and Ren (2006). The damage detection scheme was to minimize the objective function derived from modal flexibility residual. By testing the method on a simulated simply supported concrete beam and experimental reinforced concrete beam, the ability of the method to detect damage was verified. One disadvantage of this method is that all the elements were used as updating parameters, which may lead to low computational efficiency. Shiradhonkar and Shrikhande (2011) used system identification and finite element model updating to detect and locate the damage in beams of a moment resistant frame using dynamic responses recorded during several strong earthquakes. Interpolation techniques were used to estimate response at unmonitored locations, and frequency domain decomposition and empirical transfer function were used to determine the frequencies and mode shapes. Just like other methods, this class of methods also has obstacles necessary to be overcome. On one hand, since damage detection techniques using model updating usually require the updating of a large number of model parameters, they may be very time consuming and strongly dependent on knowledge and experience. On the other hand, the measured matrices and dynamic data may be inaccurate due to the noise in the environment, which would result in multiple solutions for the optimization algorithms. These solutions usually cannot explain what has actually happened in structures (Plankis 2012).

In addition to the frequently used methods mentioned above, there are also many methods based on other theories, such as Hilbert Transform (Natke and Cempel 1997; Yang et al. 2004; Tang et al. 2010; Roveri and Carcaterra 2012), Ritz Vectors (Juang and Pappa 1985; Zimmerman 1999; Lam et al. 2006; Taylor and Zimmerman 2010), Principal Component Analysis (Zang and Imregun 2001; De Boe and Golinval 2003; Mujica et al. 2010; Cavadas et al. 2013), Frequency Response Functions (Sampaio et al. 1999; Kessler

et al. 2002b; Limongelli 2010; Xu et al. 2014), Canonical Variate Analysis (Hermans and van der Auweraer 1999; George et al. 2000; Salgado et al. 2014), etc.

It should be noted that the non-parametric methods based on statistical pattern recognition, such as Neural Networks (Nakamura et al. 1998; Yam et al. 2003; Jiang et al. 2011; Min et al. 2012; Shu et al. 2013) and Time Series Modelling (Sohn et al. 2001a; Monroig and Fujino 2006; Gül and Catbas 2009; Mosavi et al. 2012; Dorvash et al. 2013; Mollineaux et al. 2014), have drawn a lot of attention in recent years. Since time series modelling is the main theory used in this thesis, a detailed literature review for time series based damage detection method is presented in the following section.

2.2 Literature Review of Time Series Based Damage Detection Methods

Time series based damage detection methods are considered to be one of the promising solutions to the problems mentioned in Section 1.2 (Sohn et al. 2001a; Nair et al. 2006; Gül 2009). A typical time series includes population, stock price, temperature and other quantities that can be measured over time. Time series analyses are in general used to analyze time series data in order to extract the statistical characteristics of the data sets. Early in their development, these methods had been mainly used in economics and electrical engineering. In structural engineering, the time series model is initially used for system identification and modal analysis (Andersen 1997). Gradually, researchers found that time series analysis is a valuable tool for damage detection.

Dating back to 2000, Bodeux and Golinval (2000) illustrated an Auto-Regressive Moving-Average Vector (ARMAV) based method for system identification and damage detection on a "Steel-Quake" benchmark structure. The Prediction Error Method was used to estimate the parameters of the ARMAV model on the basis of output data. The damage was identified based on the evaluation of the uncertainties of the parameters. However, as an early study, authors only attempted to identify the existence of the damage.

In 2001, Sohn et al. (2001a) demonstrated an approach using time series analysis and outlier analysis. First, the time series analysis based on Auto-Regressive models (AR models) and Auto-Regressive models with exogenous inputs (ARX models) were carried

out. Then, an outlier analysis based on Mahalanobis distance is conducted to extract the DF. Applying this method to the strain gauge data of a surface-effect fast patrol boat, the method could distinguish different structural conditions. However, no information about location and severity was provided by this method.

Considering the low energy efficiency of transmitting raw time series data with wireless sensors, Lynch et al. (2004) developed a novel wireless sensing unit embedded with a computational core for damage detection. The processing algorithm involved in the computational core was the AR-ARX model based method proposed by Sohn et al. (2001b). To illustrate the ability of the new sensing system conducting time series analysis to detect damage, an 8-DOF laboratory structure was used where damage was detected successfully by the peak values of the ratio of the ARX model's residual error standard deviation with the saving of 50% energy.

Monroig and Fujino (2006) presented an approach using second-order ARX models derived from the equation of motion to fit acceleration data of a structure. They applied their approach to a structure similar to the ASCE benchmark problem in Bernal and Beck (2004). The promising results of their study showed that damage could be identified and located, although there were some false-positive and false-negative results.

By applying the Auto-Regressive Moving Average (ARMA) model to the vibration signals, Nair et al. (2006) proposed a new DF as a function of the first three AR coefficients. Then, a hypothesis test including the t-test was used to detect damage. Furthermore, in order to discern the location of damage, two different localization indices were introduced and the accuracies of results were compared. The results of applying the method to analytical and experimental data of the ASCE benchmark structure were encouraging since the method was able to detect and locate either minor or major damage correctly.

Gül and Catbas (2009) tested a statistical pattern recognition methodology in the context of time series analysis using different laboratory structures. The results showed that this methodology worked well in most cases. However, they also identified some issues that would have to be resolved before applying this approach in a realistic structure, such as the determination of the threshold.

Lei et al. (2010) developed a substructure approach to detect damage in large size structures. In this approach, they first divided the structure into several substructures and then applied the extended Kalman estimator and least squares estimation to estimate parameters. Both cases whether the measurements at the interfaces were available or not were considered. For verification, they applied the method to a 20-storey finite element building. The results show that the stiffness reduction can be identified accurately. However, their approach needed the mass information to be known, and there should be sensors around the unknown input and interfaces.

Gül and Catbas (2008, 2011) introduced the concept of sensor clustering to the time series based method for damage detection. Dividing the accelerometers installed on the structure into different clusters, one Auto-Regressive model with eXogenous input (ARX model) was created for each cluster. Measuring the variation of fit ratios for the ARX models, the location and severity of damage in a 4-DOF system and a steel grid structure (both simulation and experiment) was identified.

Figueiredo et al. (2011) investigated the influence of the AR order on the results of the time series based damage detection method. In their study, four different techniques - Akaike information criterion, partial autocorrelation function, root mean squared error, singular value decomposition - were used to estimate the AR order. The comparison of power spectral densities, autocorrelation functions and residual error histograms for different AR orders were shown. Eventually, testing on a three-storey frame structure, they showed that the proper AR order was very important for damage detection due to its influence in various aspects.

Loh et al. (2011) developed two methods to extract trends and set a warning threshold based on the long-term SHM data from the Fei-Tsui Arch Dam in Taiwan. The first method is the singular spectrum analysis with Auto-Regressive model (SSA-AR) and the second method is called nonlinear principal component analysis using auto-associative neural network method (NPCA-AANN). Using these two methods, the residual deformation between the recorded and estimated data was calculated, and the threshold was determined accordingly.

Xing and Mita (2012) proposed an approach, which first divided the structure into several substructures and then applied the ARMAX model derived from the equation of motion. By estimating the frequencies using ARMAX models, they could detect, locate and quantify the damage. For application, this approach was used to a 5-storey building and the approach worked well for both simulation and experiment. The disadvantage of this method is that they need to use excitation information and could not discern the changes in mass and stiffness.

Figueiredo et al. (2012) applied time series models to the data obtained using a piezoelectric active-sensing technique and extracted DFs as parameters of the models. Correlation analysis and principle component analysis were then used to determine the damaged state, and a machine learning algorithm was adopted to remove the effect of environmental variability. The experimental results from a composite plate demonstrated that damage could be correctly identified.

Mosavi et al. (2012) presented a study using Multivariate Vector Auto-Regressive (MVAR) models for damage detection. The authors first extracted the Mahalanobis distance to the coefficients of the MVAR models, and then applied the Fisher criterion to evaluate the amount of variations in DFs with respect to the healthy condition. In their study, the method was applied to a two-span continuous steel beam subjected to ambient vibrations. Damage at two locations with different severities was introduced to this beam. The results proved the validity of this technique for identifying and locating damage.

Similar to Mosavi et al. (2012), Huang et al. (2013) also demonstrated a method based on VAR models for damage detection in a 6-DOF mass spring system and a transmission tower model. After dividing the vibration signals into multiple segments and fitting them with VAR models, the diagonal elements of the models were extracted and the Mahalanobis distances were calculated. Then, the area under receiver operating characteristic curves and the deflection coefficients of Mahalanobis distance distribution were used for damage detection.

Kuwabara et al. (2013) proposed a new method for system identification and damage detection in high-rise buildings. Their method aimed to estimate the stiffness and damping of a storey using accelerations above and below the specific storey. The change

of estimated stiffness was considered as DF. In their methodology, the ARX models with constraints on transfer functions were introduced to overcome the difficulty in prediction of the function in a low frequency range.

Bao et al. (2013) presented an integrated method based on ARMA model to realize the online SHM for the subsea pipeline system. In their method, the acceleration signal was first partitioned and normalized to reduce the effect of varying loadings conditions and then auto-correlation function was considered as substitute of the input data to remove the influence of noise. At last, Mahalanobis distances between AR coefficients were measured as DFs. Their method was successfully applied to a numerical model of a submarine pipeline system subjected to ambient wave forces.

In order to save computation and communication energy, Dorvash et al. (2013) presented a method integrating the algorithm into the remote nodes of the wireless sensor network. The algorithm used in their paper is called iterative modal identification (IMID), which is an iterative process combining simulation and system identification. The Newmark's numerical method was used for simulation and ARX models were used for system identification. At last, both numerical and experimental data were used to illustrate the performance of this method.

In 2014, Yao and Pakzad (2014) created two DFs, i.e. the Mahalanobis distance of Auto-Regressive coefficients and the Cosh distance of Auto-Regressive spectra, to detect damage in a 10-DOF system. Analytical sensitivity analyses were conducted to derive the sensitivity of these DFs with respect to structural damage and measurement noise level. Theoretically, they proved that these DFs were more sensitive to damage than to noise.

Mollineaux et al. (2014) tested a 34-meter blade using both wired accelerometers and low power MEMs-based wireless accelerometers. Different degrees of damage were simulated on the trailing edge of the blade. In their paper, the performance of wireless and wired sensors was compared. Then, the methods to detect damage levels based on Auto-Regressive coefficients and wavelet transforms were investigated.

Wyłomańska et al. (2014) developed a Periodic Autoregressive Modeling (PAR) based method to overcome the difficulties of AR based method in detecting damage in structures under non-stationary operations. To validate their method, they simulated a

planetary gearbox in a bucket wheel excavator under cyclic load variation. Then, after applying four techniques, analysis of spectrograms, envelope spectra, sample autocorrelation function and periodical standard deviation, results for PAR and AR based methods were compared.

As concluded above, the researchers in this area have conducted a lot of work and made great achievements. However, due to the complexity of civil infrastructure systems, environmental and operational conditions, a number of issues still need to be resolved before they can be applied to real life structures.

In all the methods mentioned above, the order of time series models they used were determined either by experience or by fit ratio. The models would vary for different applications. In this thesis, the first new method is derived directly from the equation of motion, which has a consistent form for any application and could benefit the automation system. Based on these models, two different DFs are developed and referred as DF1 and DF2. It will be seen in the following chapters that the first proposed method could identify the location and severity of damage for two different applications successfully using either fit ratios or coefficients as DFs. Using fit ratios as DF1s, the method could provide results similar to Gül (2009), but it is simpler and more efficient. The DF2s using the difference between ARX coefficients show the potential for extensible studies. It is expected that more information could be obtained by extracting different statistical characteristics for different coefficients.

Based on the first method, the second method, which is also derived from equation of motion, is developed. With some more assumptions and using coefficients of ARMAX models as DFs, the second method could accurately quantify the severity of damage and distinguish the change caused by stiffness and mass separately under ambient vibration, which has never been done in previous research. The impacts of this method should also be emphasized since the changes in the mass and stiffness are assessed simultaneously with output-only data. This point is very useful for practical damage detection. For example, the change in the mass due to the operation traffic on a bridge may be clearly separated from the changes in the stiffness changes using the second method.

CHAPTER 3:OUTLINE OF THE TIME SERIES BASED METHOD FOR DAMAGE DETECTION AND THE UNDERLYING THEORY

3.1 Introduction to Time Series Model

Time series modelling has been widely used in different fields including SHM. In this study, time series models are used to fit the dynamic response of a structure. In this section, a brief discussion about the Auto-Regressive Moving Average model with eXogenous inputs (ARMAX model) and the Auto-Regressive model with eXogenous inputs (ARX model) used in this thesis is presented. More details of these time series models can be referred to (Ljung 1999; Box et al. 2013).

The basic form of an ARMAX model is shown in Eq. 3.1.

$$\begin{aligned} y(t) + a_1 y(t-\Delta t) + \cdots + a_{n_a} y(t-n_a\Delta t) = b_1 u(t-\Delta t) + \cdots + b_{n_b} u(t-n_b\Delta t) \\ + e(t) + d_1 e(t-\Delta t) + \cdots + d_{n_c} e(t-n_c\Delta t) \end{aligned} \tag{3.1}$$

where $y(t)$, $u(t)$ and $e(t)$ are output, input and error terms of the model, respectively, and $a_1,\cdots a_{n_a}, b_1,\cdots b_{n_b}, d_1,\cdots d_{n_c}$ are the parameters of the model. It is usually convenient to use the more concise form as in Eq. 3.2,

$$A(q)y(t) = B(q)u(t) + D(q)e(t) \tag{3.2}$$

in which, $A(q)$, $B(q)$ and $D(q)$ are the polynomials including coefficients of the model.

$$\begin{aligned} A(q) &= 1 + a_1 q^{-1} + \cdots + a_{n_a} q^{-n_a} \\ B(q) &= b_1 q^{-1} + b_2 q^{-2} \cdots + b_{n_b} q^{-n_b} \\ D(q) &= 1 + d_1 q^{-1} + d_2 q^{-2} \cdots + d_{n_c} q^{-n_c} \end{aligned} \tag{3.3}$$

where q is an back shift operator. For example, a variable $X(t)$ at time t multiplied by q^j is equal to $X(t-j\Delta t)$. The orders of the polynomials are denoted with n_a, n_b and n_c. A block diagram of the ARMAX model is shown in Figure 3.1.

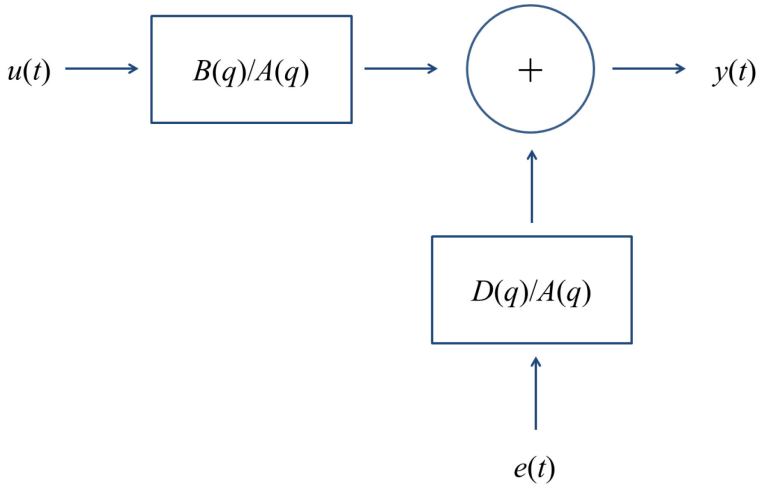

Figure 3.1. A block diagram of the ARMAX model (adapted from Ljung 1999)

Several other time series models are special cases of the ARMAX model. For example, the model is called an AR process if n_b and n_c are both zero, and an MA process if n_a and n_b are zero. If only n_c is set to zero, the model is defined as ARX model, which is used in Chapters 4 and 5. The form of an ARX model is expressed in Eq. 3.4 or Eq. 3.5. All the parameters have the same definitions as for ARMAX model. Similarly, a block diagram of the ARX can be seen in Figure 3.2.

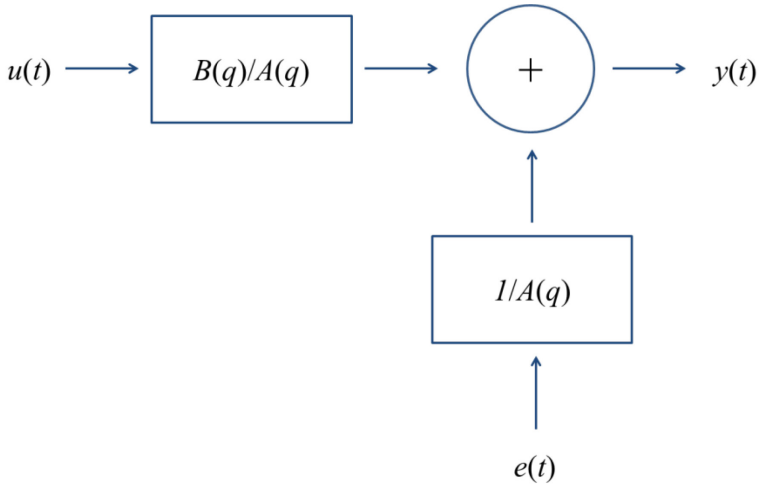

Figure 3.2. A block diagram of the ARX model (adapted from Ljung 1999)

$$y(t) + a_1 y(t-\Delta t) + \cdots + a_{n_a} y(t - n_a \Delta t) = b_1 u(t-\Delta t) + \cdots + b_{n_b} u(t - n_b \Delta t) + e(t) \tag{3.4}$$

$$A(q)y(t) = B(q)u(t) + e(t) \tag{3.5}$$

3.2 Least Squares Criterion

The first step to use an ARX model is to estimate the coefficients of it. In practice, least-squares criterion (LSC) is often used in order to estimate the coefficients of the ARX model. If data from previous time are used to represent the response at time *t,* the form in Eq. 3.6 could be obtained according to Eq. 3.4.

$$y(t) = -a_1 y(t-\Delta t) - \cdots - a_{n_a} y(t - n_a \Delta t) + b_1 u(t-\Delta t) + \cdots + b_{n_b} u(t - n_b \Delta t) + e(t) \tag{3.6}$$

The predicted value of $y(t)$ could be calculated using Eq. 3.7,

$$\hat{y}(t) = -a_1 y(t-\Delta t) - \cdots - a_{n_a} y(t - n_a \Delta t) + b_1 u(t-\Delta t) + \cdots + b_{n_b} u(t - n_b \Delta t) \tag{3.7}$$

One more concise form of Eq. 3.7 is presented below,

$$\hat{y}(t) = \varphi^T(t)\theta \tag{3.8}$$

$$\varphi(t) = [-y(t-\Delta t) \quad -y(t-2\Delta t) \quad \cdots \quad -y(t-n_a\Delta t) \quad u(t-\Delta t) \quad \cdots \quad u(t-n_b\Delta t)]^T \tag{3.9}$$

$$\theta = [a_1 \quad a_2 \quad \cdots \quad a_{na} \quad b_1 \quad \cdots \quad b_{nb}]^T \tag{3.10}$$

in which, $\varphi(t)$ is the regression vector consisting of known time series, and θ includes the coefficients to be estimated. Therefore, the error between true and predicted values of $y(t)$ can easily be derived.

$$e(t) = y(t) - \hat{y}(t) = y(t) - \varphi^T(t)\theta \tag{3.11}$$

It can be seen that $e(t)$ is actually the error term of the ARX model and it depends on the coefficients of the model. Therefore, the least square criterion could be written in Eq. 3.12.

$$V_M(\theta) = \frac{1}{M}\sum_{t=1}^{M}\frac{1}{2}[y(t) - \varphi^T(t)\theta]^2 \tag{3.12}$$

where M stands for the number of points used in the model. Since Eq. 3.12 is a quadratic criterion, analytic form of θ to minimize $V_M(\theta)$ could be derived, which is shown in Eq. 3.13.

$$\theta_M^{LS} = \arg\min V_M(\theta) = \left[\frac{1}{M}\sum_{t=1}^{M}\varphi(t)\varphi^T(t)\right]^{-1}\left[\frac{1}{M}\sum_{t=1}^{M}\varphi(t)y(t)\right] \tag{3.13}$$

Actually, there are also other search methods to determine a best model. Detailed derivations of other estimation methods can refer to Ljung (1999).

3.3 ARX Models Based on Different Sensor Clusters

The dynamic responses (accelerations, velocities and displacements) of a structure are governed by the Equation of Motion (EOM). Changing over the time and strongly depending on prior states and external inputs, these data can be considered as typical time series. Therefore, it is expected that the time series modelling is suitable to fit these data and extract the statistical characteristics. However, different orders and coefficients would lead to different ARX models and the validity of models varies a lot according to different orders. The equation of motion, which the dynamic responses of a structure should comply with, is investigated in order to determine proper orders of the ARX model. Eq. 3.14 represents the basic form of an equation of motion for an N degrees of freedom (DOFs) system.

$$\boldsymbol{M}\ddot{\boldsymbol{x}}(t) + \boldsymbol{C}\dot{\boldsymbol{x}}(t) + \boldsymbol{K}\boldsymbol{x}(t) = \boldsymbol{f}(t) \tag{3.14}$$

in which $\boldsymbol{M}$, $\mathbf{C}$, and $\boldsymbol{K}$ represent the N by N mass, damping and stiffness matrices of the system. The vectors $\ddot{\boldsymbol{x}}(t), \dot{\boldsymbol{x}}(t)$ and $\boldsymbol{x}(t)$ represent acceleration, velocity and

displacement at a certain time t. The external forcing vector on the system is denoted with $\boldsymbol{f}(t)$.

If we write Eq. 3.14 in matrix form (see Eq. 3.15), it is seen that some transformations can be conducted on this equation of motion. The first step is to write the i^{th} row of Eq. 3.15 separately (shown as Eq. 3.16). Eq. 3.17 is derived when taking the second derivative of Eq. 3.16.

$$\begin{bmatrix} m_{11} & \cdots & m_{1N} \\ \vdots & \ddots & \vdots \\ m_{N1} & \cdots & m_{NN} \end{bmatrix} \begin{Bmatrix} \ddot{x}_1 \\ \vdots \\ \ddot{x}_N \end{Bmatrix} + \begin{bmatrix} c_{11} & \cdots & c_{1N} \\ \vdots & \ddots & \vdots \\ c_{N1} & \cdots & c_{NN} \end{bmatrix} \begin{Bmatrix} \dot{x}_1 \\ \vdots \\ \dot{x}_N \end{Bmatrix} + \begin{bmatrix} k_{11} & \cdots & k_{1N} \\ \vdots & \ddots & \vdots \\ k_{N1} & \cdots & k_{NN} \end{bmatrix} \begin{Bmatrix} x_1 \\ \vdots \\ x_N \end{Bmatrix} = \begin{Bmatrix} f_1 \\ \vdots \\ f_N \end{Bmatrix} \tag{3.15}$$

$$\begin{aligned} &\left(m_{i1}\ddot{x}_1(t) + \cdots + m_{iN}\ddot{x}_N(t)\right) + \left(c_{i1}\dot{x}_1(t) + \cdots + c_{iN}\dot{x}_N(t)\right) \\ &\qquad + \left(k_{i1}x_1(t) + \cdots + k_{iN}x_N(t)\right) = f_i(t) \end{aligned} \tag{3.16}$$

$$\begin{aligned} &\left(m_{i1}\dddot{x}_1(t) + \cdots + m_{iN}\dddot{x}_N(t)\right) + \left(c_{i1}\ddot{x}_1(t) + \cdots + c_{iN}\ddot{x}_N(t)\right) \\ &\qquad + \left(k_{i1}\dot{x}_1(t) + \cdots + k_{iN}\dot{x}_N(t)\right) = \ddot{f}_i(t) \end{aligned} \tag{3.17}$$

Considering that measuring high-speed displacement and velocity data is usually not practical in real life structures, some efforts are made to eliminate these terms. The central difference technique is introduced to replace $\dddot{x}_i(t)$ with $\left(\ddot{x}_i(t+\Delta t) - \ddot{x}_i(t-\Delta t)\right) \Big/ 2\Delta t$ and $\ddot{x}_i(t)$ with $\left(\ddot{x}_i(t+\Delta t) - 2\ddot{x}_i(t) + \ddot{x}_i(t-\Delta t)\right) \Big/ (\Delta t)^2$ (Levy and Lessman 1992). Then, Eq. 3.18 is obtained with only accelerations. For free vibration, the force terms are zero since the vibration is caused by initial conditions. Rearranging Eq. 3.18 and putting $\ddot{x}_i(t+\Delta t)$ to the left of the equal sign as an output and all other terms to the right side as inputs, it is expected a form in Eq. 3.19 similar to the ARX model in Eq. 3.4.

$$\left(m_{i1}\frac{\left(\ddot{x}_1(t+\Delta t)-2\ddot{x}_1(t)+\ddot{x}_1(t-\Delta t)\right)}{(\Delta t)^2}+\cdots+m_{iN}\frac{\left(\ddot{x}_N(t+\Delta t)-2\ddot{x}_N(t)+\ddot{x}_N(t-\Delta t)\right)}{(\Delta t)^2}\right)$$
$$+\left(c_{i1}\frac{\ddot{x}_1(t+\Delta t)-\ddot{x}_1(t-\Delta t)}{2\Delta t}+\cdots+c_{iN}\frac{\ddot{x}_N(t+\Delta t)-\ddot{x}_N(t-\Delta t)}{2\Delta t}\right) \tag{3.18}$$
$$+\left(k_{i1}\ddot{x}_1(t)+\cdots+k_{iN}\ddot{x}_N(t)\right)=\ddot{f}_i(t)$$

$$\left(\frac{m_{ii}}{(\Delta t)^2}+\frac{c_{ii}}{2\Delta t}\right)\ddot{x}_i(t+\Delta t)=-\left(\frac{m_{11}}{(\Delta t)^2}+\frac{c_{11}}{2\Delta t}\right)\ddot{x}_1(t+\Delta t)-\cdots-\left(\frac{m_{i-1,i-1}}{(\Delta t)^2}+\frac{c_{i-1,i-1}}{2\Delta t}\right)\ddot{x}_{i-1}(t+\Delta t)$$
$$-\left(\frac{m_{i+1,i+1}}{(\Delta t)^2}+\frac{c_{i+1,i+1}}{2\Delta t}\right)\ddot{x}_{i+1}(t+\Delta t)-\cdots-\left(\frac{m_{NN}}{(\Delta t)^2}+\frac{c_{NN}}{2\Delta t}\right)\ddot{x}_N(t+\Delta t)$$
$$+\left(\frac{2m_{i1}}{(\Delta t)^2}-k_{i1}\right)\ddot{x}_1(t)+\cdots+\left(\frac{2m_{iN}}{(\Delta t)^2}-k_{iN}\right)\ddot{x}_N(t) \tag{3.19}$$
$$+\left(\frac{c_{i1}}{2\Delta t}-\frac{m_{i1}}{(\Delta t)^2}\right)\ddot{x}_1(t-\Delta t)+\cdots+\left(\frac{c_{iN}}{2\Delta t}-\frac{m_{iN}}{(\Delta t)^2}\right)\ddot{x}_N(t-\Delta t)$$

Comparing Eq. 3.19 with Eq. 3.4, the final form of the ARX model for the i^{th} row of the Eq. 3.15 can be seen in Eq. 3.20.

$$\ddot{x}_i(t)=b_{i1}^1\ddot{x}_1(t)+\cdots+b_{i,i-1}^1\ddot{x}_{i-1}(t)+b_{i,i+1}^1\ddot{x}_{i+1}(t)+\cdots+b_{iN}^1\ddot{x}_N(t)+$$
$$b_{i1}^2\ddot{x}_1(t-\Delta t)+\cdots+b_{iN}^2\ddot{x}_N(t-\Delta t)+b_{i1}^3\ddot{x}_1(t-2\Delta t)+\cdots+b_{i1}^3\ddot{x}_N(t-2\Delta t)+e(t) \tag{3.20}$$

Obviously, the ARX models for all the rows of Eq. 3.15 can be derived in the same way. When a structure is idealized as a multi-degree-of-freedom system, its stiffness and mass matrices are both sparse matrices and only the accelerations from some adjacent DOFs are adopted in each ARX model. Here, the sensor considered as output in the ARX model is defined as a reference channel and all the other sensors adjacent to this one are classified as the corresponding sensor cluster. Thus, for an *N*-DOF system, *N* different sensor clusters could be constructed.

To further clarify the proposed approach schematically, a simple 3-DOF mass spring system is taken as an example (shown in Figure 3.3, Figure 3.4 and Figure 3.5). For the first sensor cluster, the reference channel is the first DOF and the sensor cluster includes signals from DOFs 1 and 2. The second sensor cluster is created with the reference channel of DOF 2 and contains DOFs 1, 2 and 3 adjacent to the reference channel.

Similarly, the third sensor cluster's reference channel is DOF3 and the cluster comprises DOFs 2 and 3. For the total 3 DOFs, 3 sensor clusters are created and each ARX model corresponds to one sensor cluster.

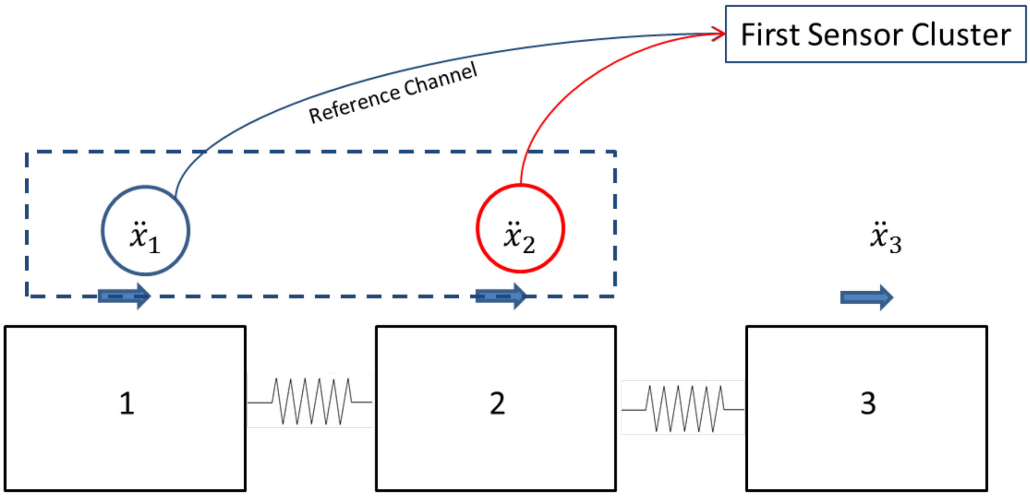

Figure 3.3. First sensor cluster for a 3-DOF mass spring system

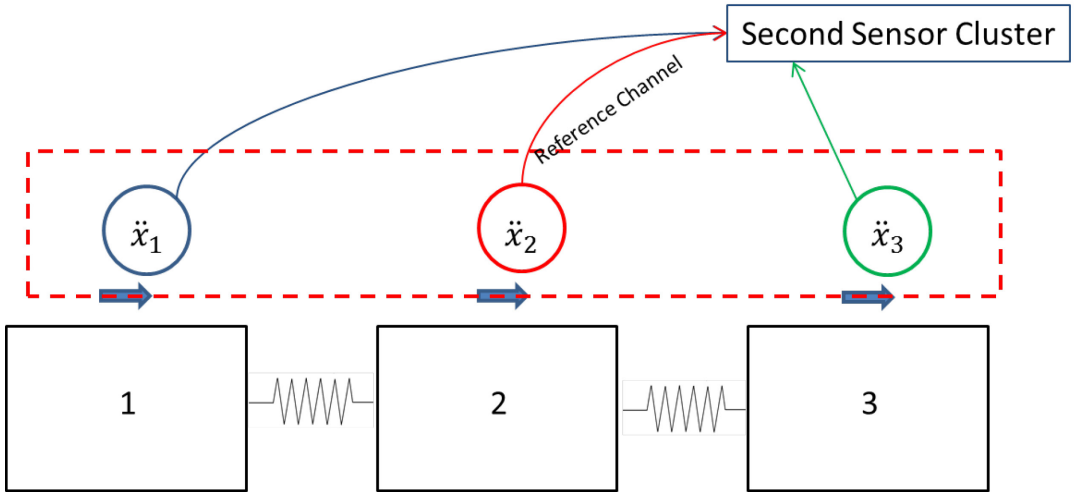

Figure 3.4. Second sensor cluster for a 3-DOF mass spring system

After creating the ARX models for the sensor clusters, two different DFs extracted from the ARX models are introduced to detect damage.

DF1 is defined as the difference of fit ratios. As shown in Eq. 3.21. FR_1^i is obtained by fitting the damaged data to the i^{th} ARX model based on baseline data, and FR_2^i is defined as the fit ratio obtained by fitting the damaged data to the i^{th} ARX model based on

damaged data. The difference between these fit ratios is expected to represent the change in the properties of the system when damage occurs.

$$DF1_i = \frac{\left|FR_1^i - FR_2^i\right|}{FR_2^i}, (i \in sensor\ clusters) \tag{3.21}$$

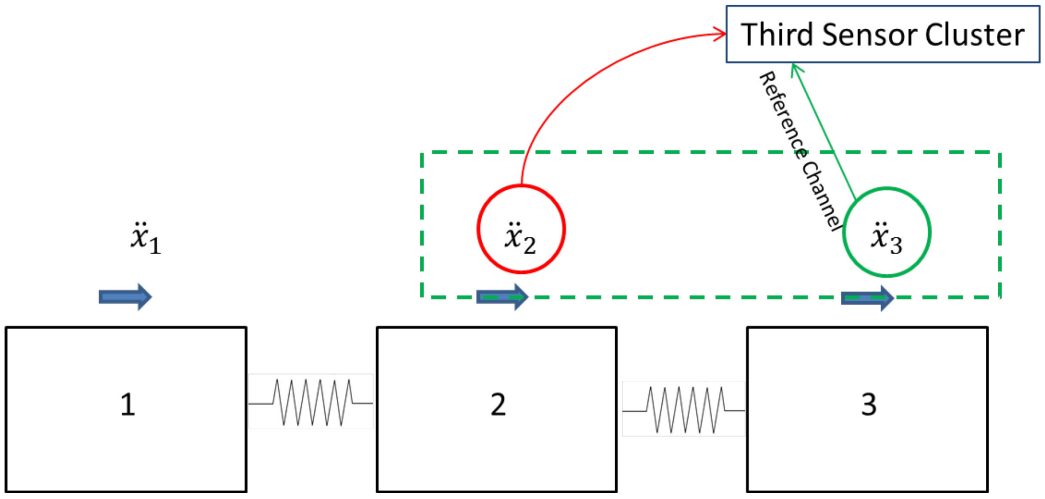

Figure 3.5. Third sensor cluster for a 3-DOF mass spring system

DF2 is based on the idea that if the ARX model can well fit the dynamic responses, the corresponding coefficients should reflect the physical properties of the structure. The damage caused by stiffness change is expected to be identified by calculating the square sum of the difference of the coefficients related to the stiffness. DF2 is defined in Eq. 3.22.

$$DF2_i = \sum_{j=1}^{N} (b_{ij,H}^2 - b_{ij,D}^2)^2 \times 100, (i \in sensor\ clusters) \tag{3.22}$$

where b_{ij}^2 stands for the coefficients for $\ddot{x}_j(t-\Delta t)$ in the i^{th} sensor cluster. The subscripts H and D represent the ARX models based on healthy and damaged data. The overall process for the method using two different DFs can be seen in Figure 3.6 and Figure 3.7.

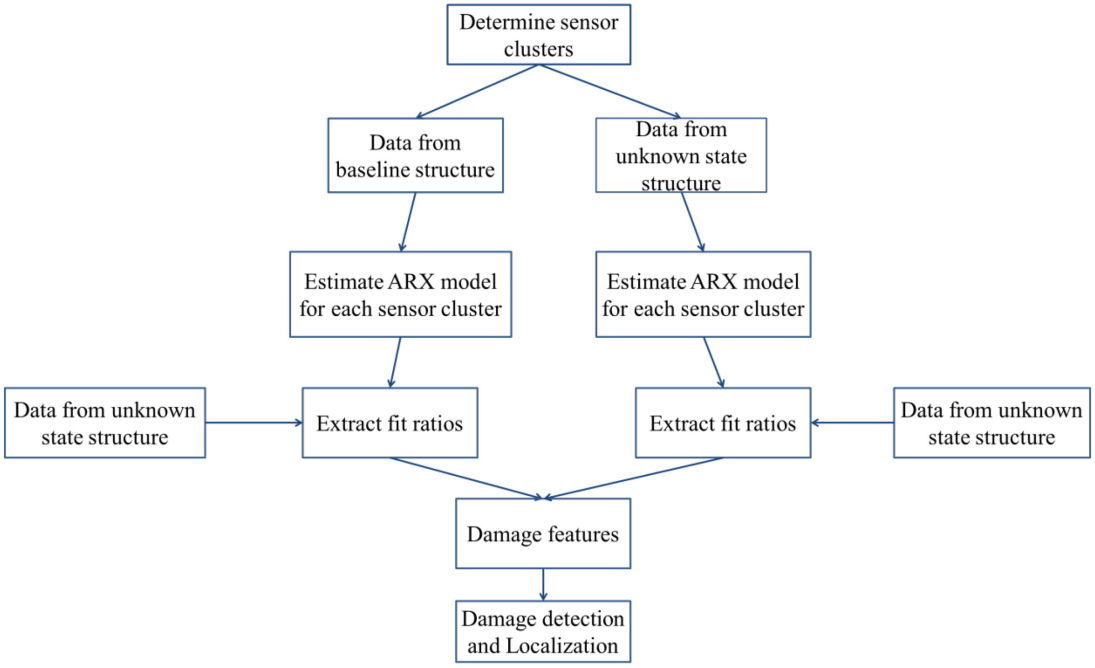

Figure 3.6. Process of the time series based method using DF1

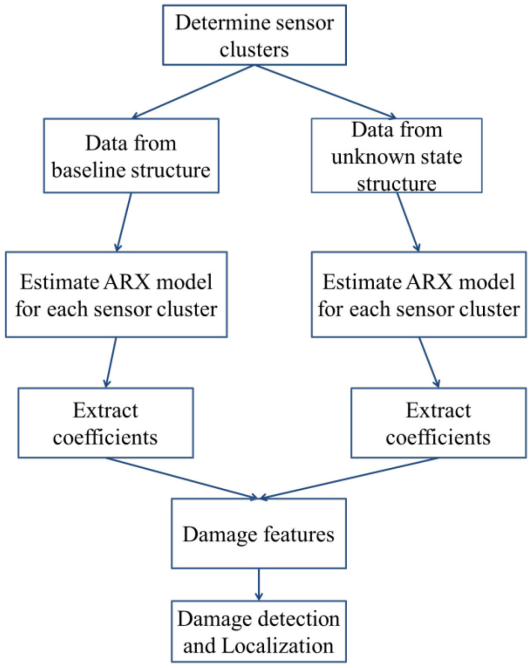

Figure 3.7. Process of the time series based method using DF2

CHAPTER 4:EXPERIMENTAL CASE STUDY I - A STEEL GRID TYPE STRUCTURE

4.1 Introduction to the Benchmark Problem and Implementation of the Method

To investigate the capabilities of the proposed approach described in the previous chapter, it is applied to experimental data obtained from a bridge health monitoring benchmark problem developed and led by a research group at the University of Central Florida. The structure chosen as the benchmark problem is a steel grid, which enables researchers to test their methods before applying to real life structures. As shown in Figure 4.1, the specimen has two clear spans with two continuous girders across the middle supports. The girders are 5.49 m in longitudinal direction and the width of the structure is 0.92 m. The whole grid is supported by six 1.07 m tall columns. More details about the specimen can be found in Catbas et al. (2006), Gül and Catbas (2008, 2011) and at the website: http://www.cece. ucf.edu/people/catbas/benchmark.htm.

Figure 4.1. Steel grid model used for experiments (Gül and Catbas 2011)

As mentioned above, this grid structure is designed to be easily modified in order to test the performance of various damage detection methods for different damaged states. In Figure 4.2, the details of the grid structure can be seen. With the specially designed

connections and supports, different boundary conditions (pin supports, roller supports, fixed supports and semi-fixed supports) and damaged states (bolts removal, supports removal, plate removal) can easily be introduced.

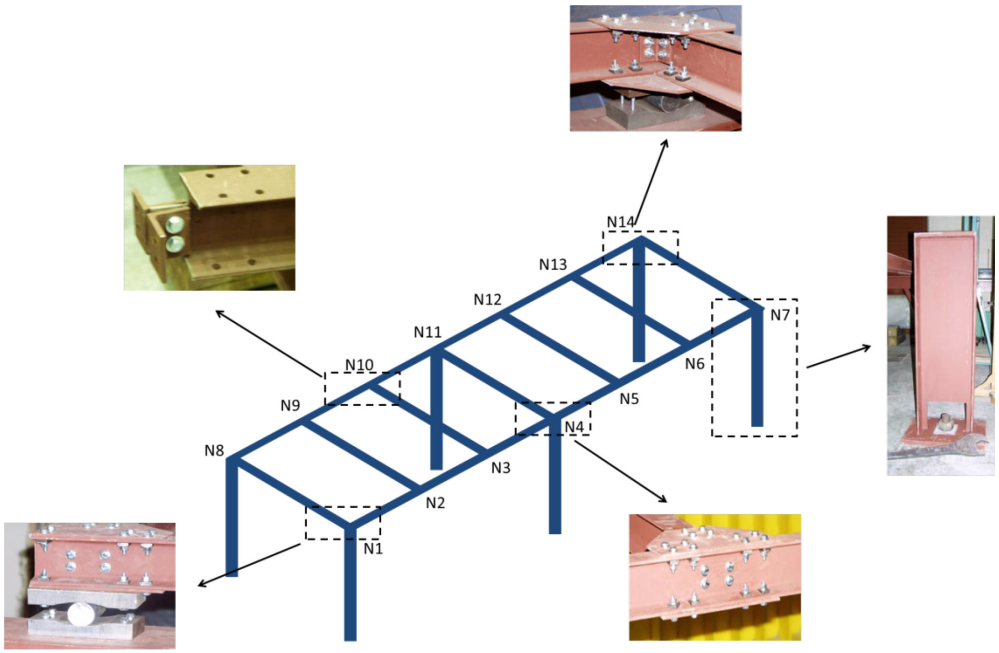

Figure 4.2. Details of the steel grid structure (adapted from Gül 2009)

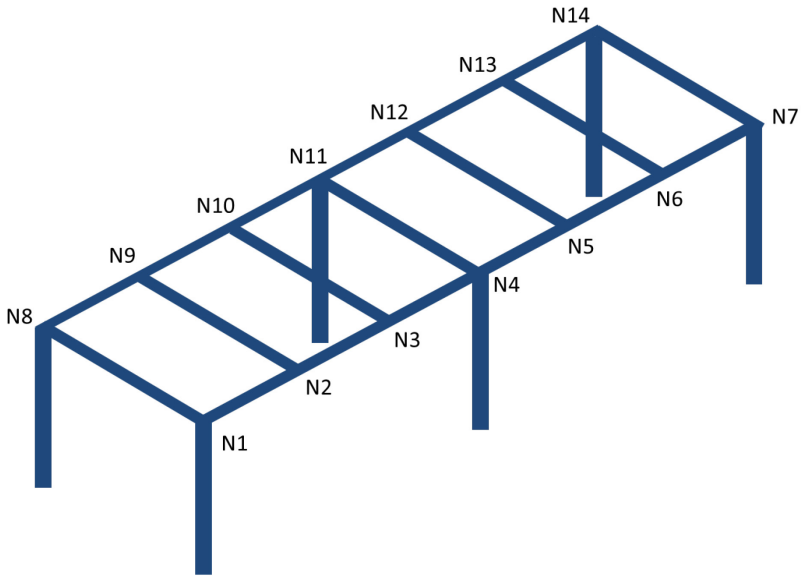

Figure 4.3. Node numbering for the steel grid specimen (adapted from Gül 2009)

The nodes which connect the girders and beams are numbered in Figure 4.3. A number of sensors could be installed on this structure. For the purpose of dynamic tests studied in

this chapter, 12 accelerometers were installed in vertical direction at each node (except N7 and N14 for practical limitations during the tests). The installation of the accelerometers is shown in Figure 4.4. The accelerometers used in this study were IPC/seismic type accelerometers. The parameters of the accelerometers were: 0.01 to 1200 Hz frequency range, 1000mV/g sensitivity and ±2.5g measurement range. A VXI system from Agilent Technologies was used as the acquisition system to record the response. MTS-Test software was used for the purpose of acquisition control (Gül 2009).

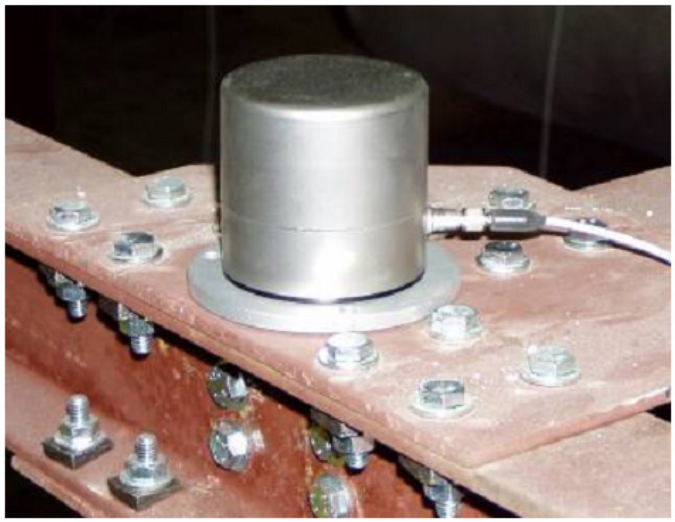

Figure 4.4. Installation of accelerometer on the structure (Gül 2009)

For this study, four different kinds of damage were introduced. The detailed photos of the damage are shown in Figure 4.5.

1) Damage Case 1: Scour (roller support removal) at N4;2) Damage Case 2: Boundary restraint (fixing the roller supports) at N7 and N14;

3) Damage Case 3: Moment release (removal of bolts) and plate removal at N3;

4) Damage Case 4: Moment release (removal of bolts) at N3 and N10.

For the experiments, impact tests were conducted to simulate free vibration. The structure was excited by an instrumented impact hammer at N2, N5, N6 and N12 separately. For each damage case, 20 tests were carried out with five continuous ones at one excitation location. The sampling frequency, 400Hz, is more than twice as the frequency for the 15th mode of the structure (Gül 2009). Thus, at least 15 modes could be identified in this

structure, which is considered as a reasonable number for damage detection of bridge type structures. Figure 4.6 shows the experimental vibration data from the baseline (undamaged) structure at all 12 nodes.

(a) Damage Case 1 (b) Damage Case 2

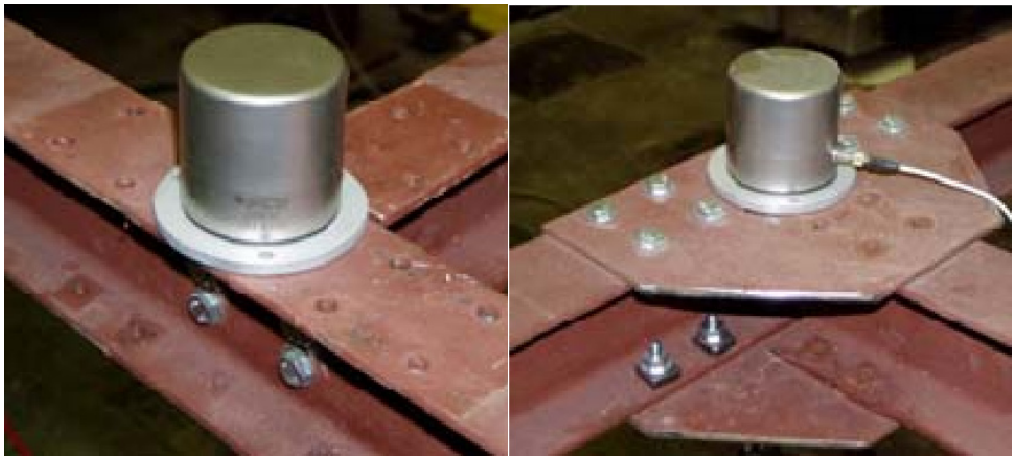

(c) Damage Case 3 (d) Damage Case 4

Figure 4.5. Detailed photos of damage simulations (Gül 2009)

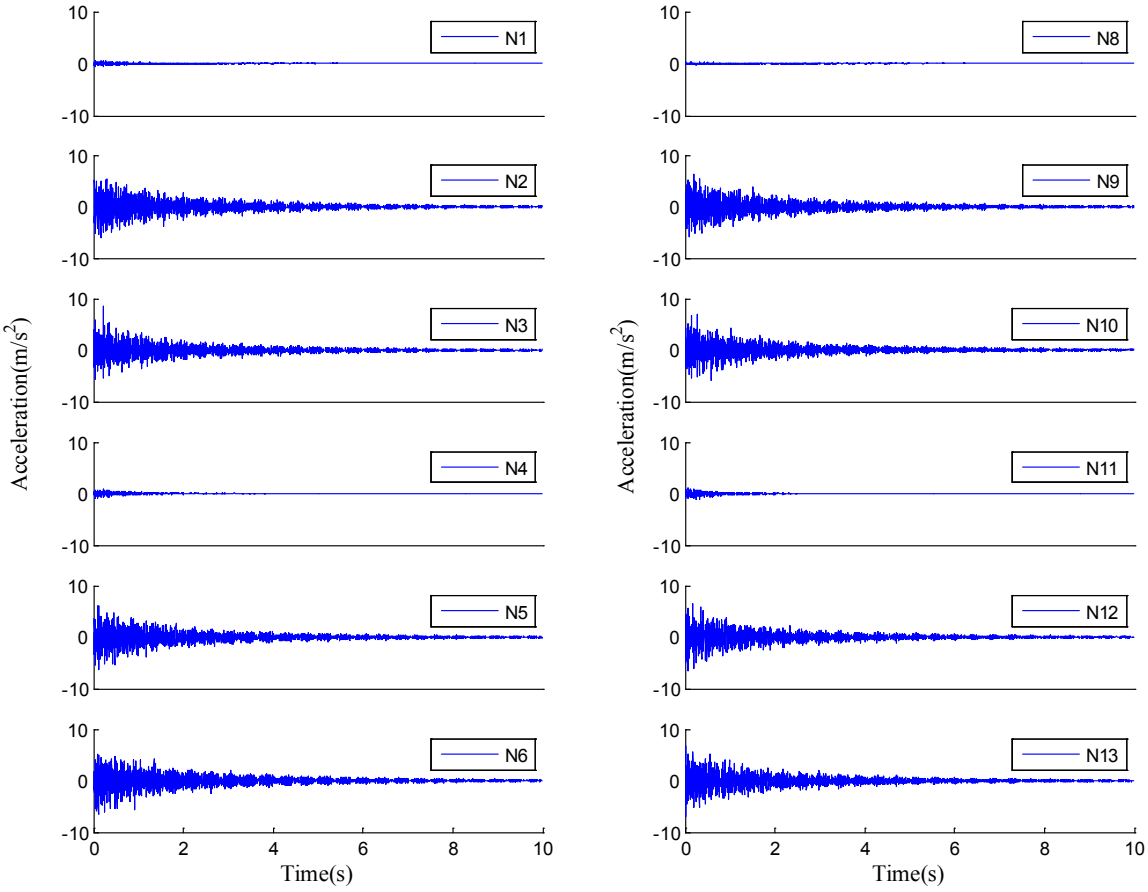

Figure 4.6. Experimental acceleration data for the baseline structure

For the implementation of the proposed damage detection method, the acceleration data from the support locations (N1, N4, N8 and N11) were not used since these nodes were almost fixed in vertical direction and experienced very small vibration, which would result in the instability in ARX models. The remaining 8 sensors can be divided into 8 different sensor clusters as shown in Table 4.1.

The following sections demonstrate the results and interpretations of the implementation of the proposed method with two different kinds of DFs. In section 4.2, the difference of fit ratios is first considered as DF1. The results for impact at N12 are taken as an example (see Figure 4.7) and for all other impact locations are used to investigate the influence of impact locations on the performance of the method. Section 4.3 presents the results

obtained by using the function of coefficients as DF2. Only results for impact at N12 are shown for the Section 4.3.

Table 4.1. Sensor clusters for the steel grid structure

Sensor Cluster	Output of the ARMAX model	Inputs of the ARMAX model
1	N2	N2, N3, N9
2	N3	N2, N3, N5, N10
3	N5	N3, N5, N6, N12
4	N6	N5, N6, N13
5	N9	N2, N9, N10
6	N10	N3, N9, N10, N12
7	N12	N5, N10, N12, N13
8	N13	N6, N12, N13

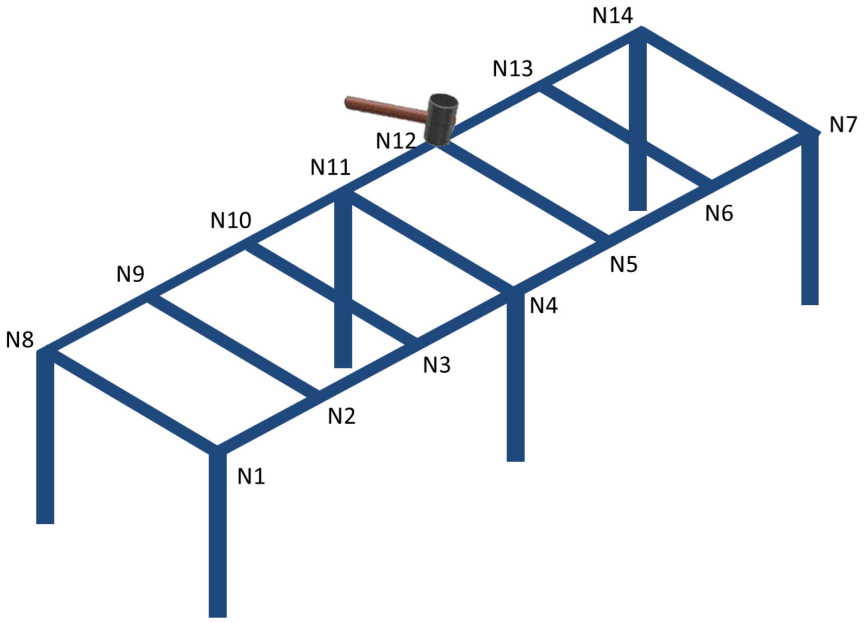

Figure 4.7. Location of the excitation

4.2 Analysis and Result Interpretations for the Method using Fit Ratios as DF1

In general, a threshold value for the baseline condition should be determined to minimize the false negative and false positive alarms. For real life applications, this threshold can be calculated by using long-term data to eliminate the noise introduced by varying environmental and operational conditions and to separate damaged state from healthy state. In this study, the threshold is determined by comparing two healthy states. Since the experimental tests used in this study are conducted in laboratory conditions, the threshold value is expected to be smaller compared to a real life application.

Considering 10 sets of healthy data as baseline state and the other 10 sets as unknown states, the DF1s can be obtained by applying the proposed damage detection method. Figure 4.8 shows all the DF1s for the healthy case. It is easy to observe that almost all the DFs are below 0.9, so here the threshold is determined as 0.9 with 79 out of the 80 points below it. Note that a more rigorous statistical analysis should be conducted for determining the threshold for real life applications.

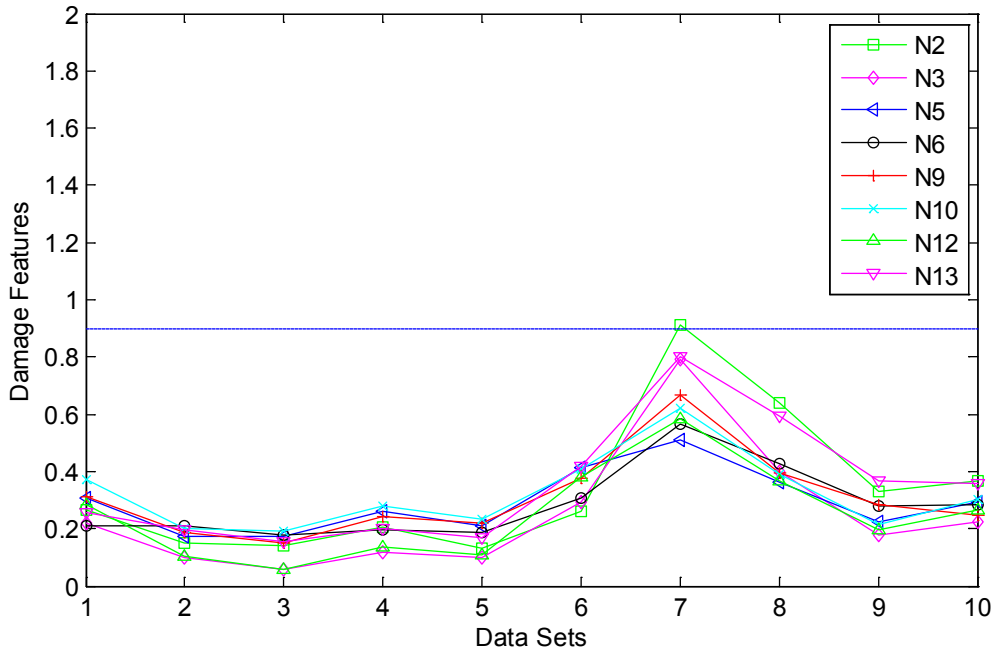

Figure 4.8. DF1s for determining the threshold under free vibration

4.2.1 Damage Case 1 (DC1): Scour (support removal) at N4

The DF1s for Damage Case 1 are presented in Figure 4.9. Since this is global damage, all the DF1s are above the threshold. Although this global damage has influence on all the nodes in the structure, the proposed method still locates the damage through the values of DF1s. It is shown in Figure 4.9 that the DF1s for N3 and N5 (actually they are very close due to the symmetry) are significantly larger than other nodes due to direct effect of the removal of roller support at N4. Interestingly, the acceleration data for N4 are not even used in any sensor clusters, but the damage is still reflected by the DF1s from the neighboring sensors. Besides, the indirect effects of the damage on N2 and N6 also lead to high DF1s at these nodes. Note that the DF1s are around 40 for N3 and N5.

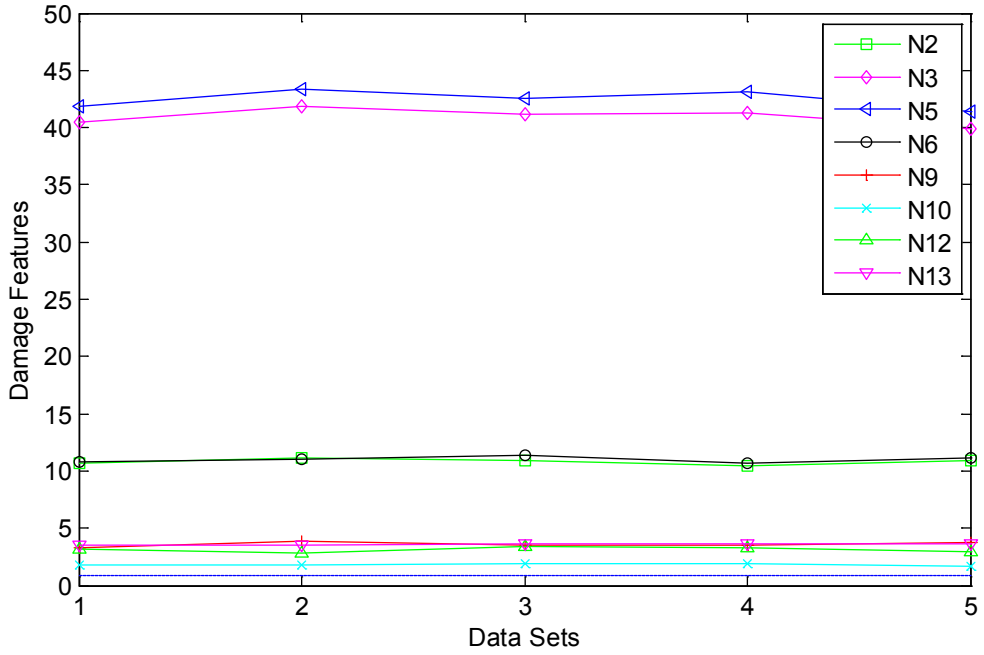

Figure 4.9. DF1s for DC1 of the steel grid structure

4.2.2 Damage Case 2 (DC2): Boundary restraint (fixing the roller supports) at N7 and N14

Damage Case 2 is a clearly less severe case than the previous one due to the removal of support at N4. All the DF1s are above the threshold also because it is global damage affecting the entire structure significantly. Due to the boundary condition change at supports N7 and N14, the DF1s for the closest nodes N6 and N13 are higher than DF1s for all other nodes (note that N7 and N14 were not instrumented). Due to the influence of damage, the nodes N5 and N12 are also higher than others (but lower than N6 and N13 because they are farther from damage). These results demonstrate that the method has ability to reflect the location of damage using the values of DF1s. Note that the DF1s for N13 are around 24 and for N6 are about 20. These values are smaller than those in damage case 1 showing that less severe damage occurs. The slight differences for DFs in N6 and N13 for different trials may be caused by some experimental variations.

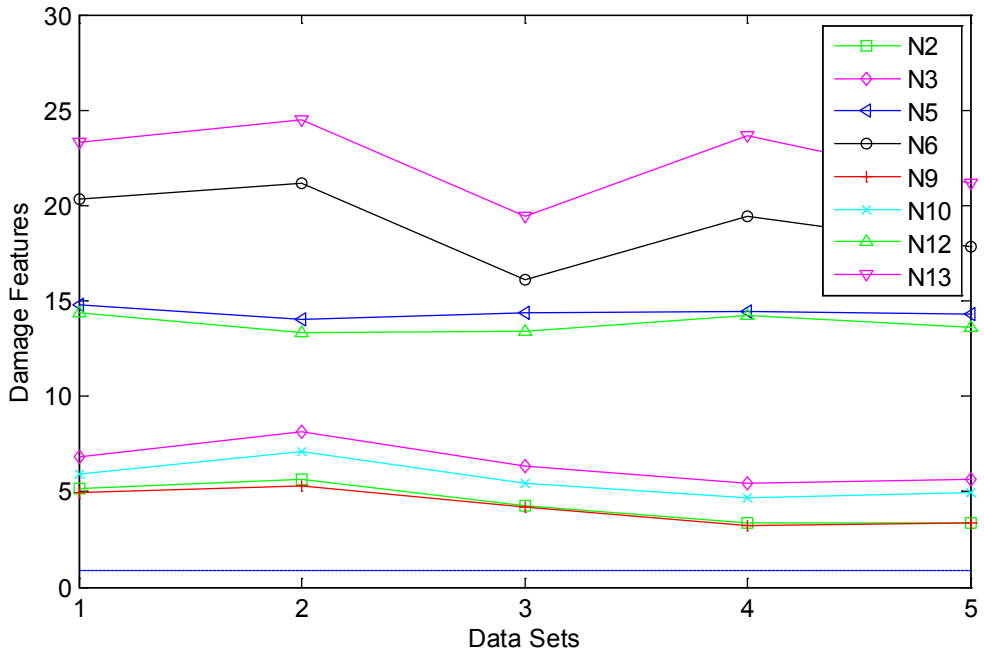

Figure 4.10. DF1s for DC2 of the steel grid structure

4.2.3 Damage Case 3 (DC3): Moment release (removal of bolts) and plate removal at N3

Damage Case 3 is localized damage due to the removal of plate and bolts simultaneously at N3. Figure 4.11 demonstrates the DF1s for each node. In this figure, only DF1s for N2, N3, N9 and N10 are above the threshold, in which the DF1s for N3 are the largest. All these evidences point out the correct location of the damage at N3. Moreover, due to the localized damage, other DF1s are below the threshold. Also note that the maximum DF1s in Damage Case 1 are around 40 and around 24 in Damage Case 2, but in this case the maximum DF1 is only about 6. This can be explained as that much less severe damage has happened in Damage Case 3. This is the case since such damage caused by removing bolts and a plate is localized and has less influence than the change of boundary conditions.

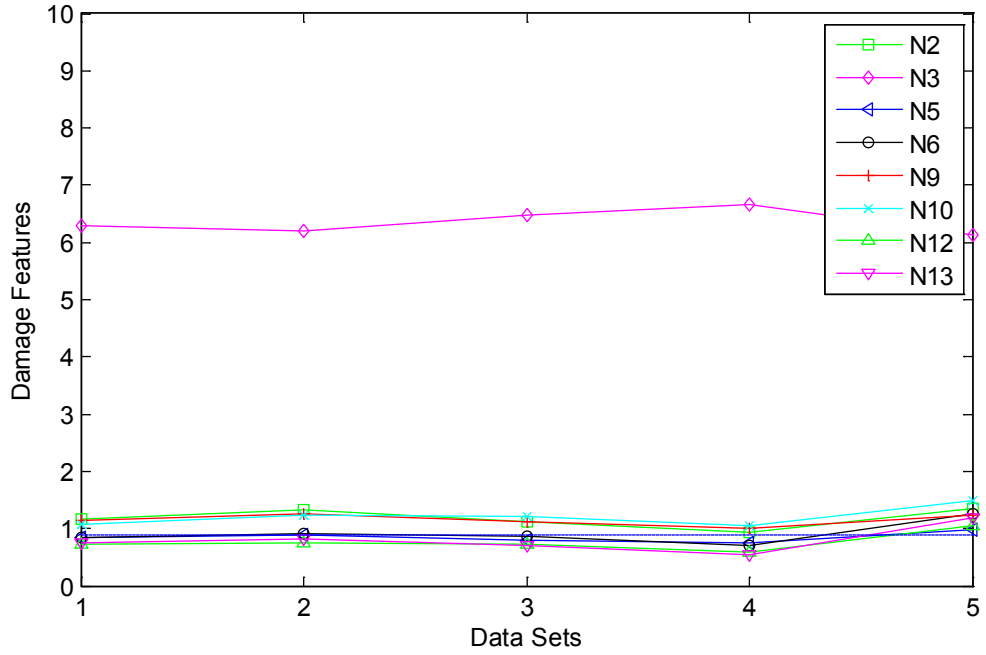

Figure 4.11. DF1s for DC3 of the steel grid structure

4.2.4 Damage Case 4 (DC4): Moment release (removal of bolts) at N3 and N10

Damage Case 4 introduces relatively minor damage by removing bolts at N3 and N10, and the DF1s for all 8 sensor clusters are demonstrated in Figure 4.12. Obviously, the removal of bolts at one node is typical localized damage, but the combination of such damage at two nodes is expected to have a more spread influence (actually, six out of eight sensors are adjacent to the damage in terms of sensor clusters). This can be the reason of why all the DF1s are above the threshold, which shows the existence of damage. In this case, the highest DF1 is about 5, the smallest in all four damage cases, which shows the severity of the damage. However, it is acknowledged that the levels of the DF1s are higher than expected and the location of damage is not well identified, but all these DF1s are very close and do not show false-positive results. The main reason to this failure can be the fact that the minor damage may have affected its adjacent nodes very similarly, which is difficult to distinguish.

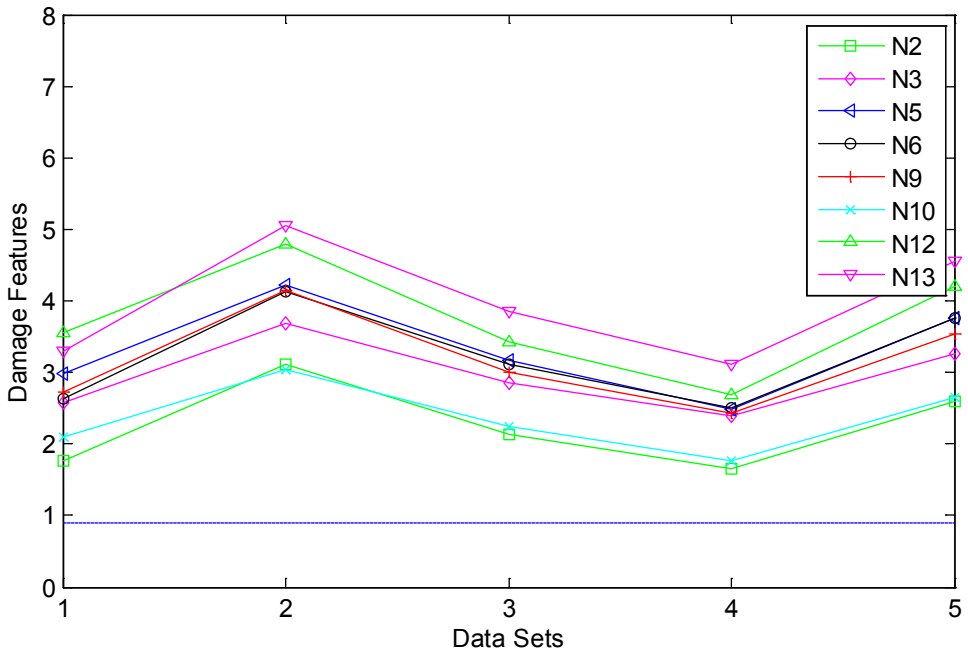

Figure 4.12. DF1s for DC4 of the steel grid structure

4.2.5 Influence of the impact location

In sections 4.2.1-4.2.4, the results obtained using the data with N12 as the impact location demonstrate that the method successfully identify, localize and estimate the severity of the damage. However, in practice, different impact locations would lead to different vibration and dynamic response from the same structure. In order to investigate the influence of impact location on the damage detection results using the time series based method, dynamic responses obtained by exciting the structure at N2, N5 and N6 are used in this section (shown in Figure 4.13).

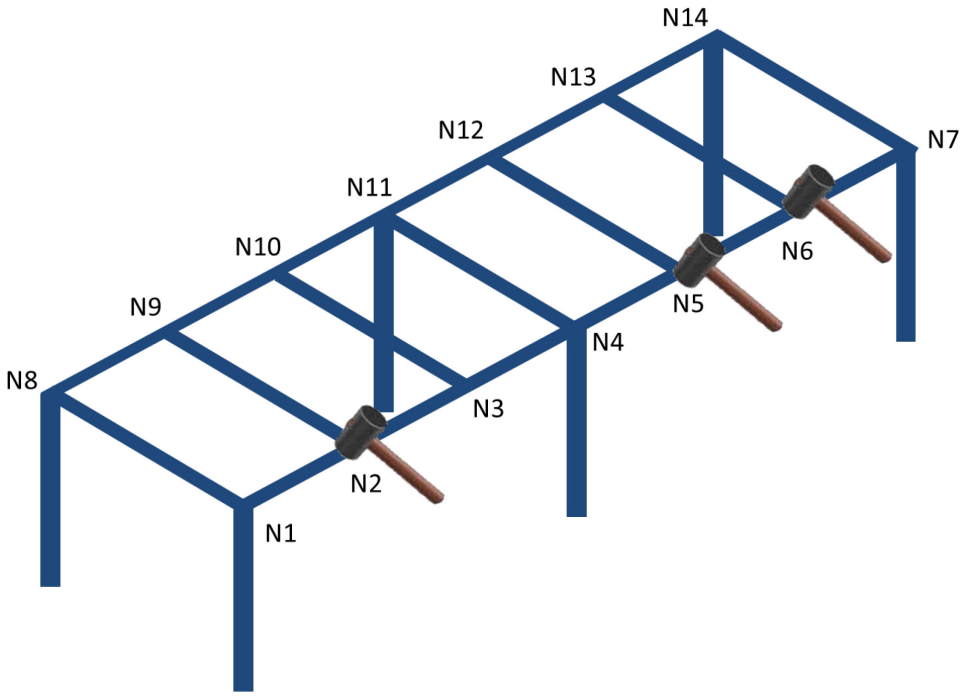

Figure 4.13. Excitations at N2, N5 and N6

Figure 4.14, Figure 4.15, Figure 4.16 and Figure 4.17 show the DF1s adopting data from different impact locations. In these figures, data sets 1-5 stands for the results for excitation at N2, data sets 6-10 represents the results for excitation at N5, and data sets 16-20 demonstrate the results for excitation at N6.

As shown in Figure 4.14, the results for support removal at N4 in Damage Case 1 are presented. Likewise, the DF1s for N3 and N5 are still the highest. The indirect effects of the damage on N2 and N6 for all three excitation locations are obvious. Although the relationship of DF1s between nodes is clear, the significance of difference still varies

according to difference impact locations. For data sets 6-10, the values of DF1s are lower than other sets, but the highest DF1 of about 45 is still larger than the one of approximately 35 in Damage Case 2. The difference of DF1s is mainly caused by the reason that the impacts at different locations excite different modes so that the goodness of fit of the ARX models would change accordingly. Fortunately, this does not affect the relationship of DF1s between sensor clusters.

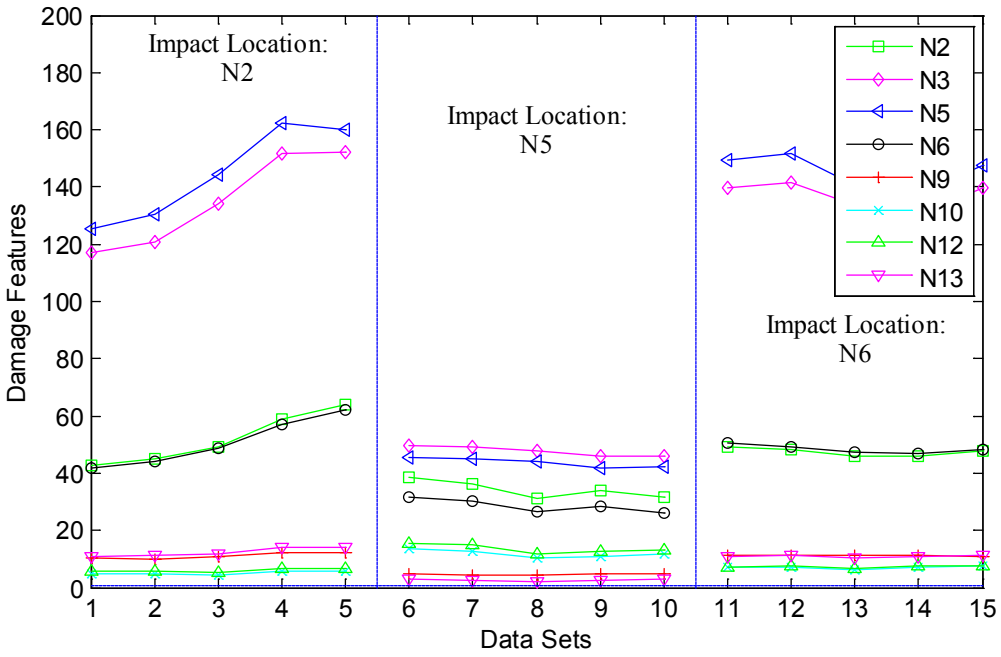

Figure 4.14. DF1s for DC1 using dynamic responses excited at N2, N5 and N6

Figure 4.17 demonstrates the DF1s obtained by applying the method to Damage Case 2. In this figure, it can be seen that the method shows the DF1s for N6 and N13 as the highest for all three impact locations despite some difference in the levels. Similarly, N5 and N12 are also standing out due to the indirect effect of the damage. All the other DF1s are relatively low. Note that for data sets 1-10 the DF1s for N3 and N10 are higher than for N2 and N9, but the case is inversed for data sets 11-15. This means the impact location may slightly affect the relationship between DFs for the nodes far from the damage.

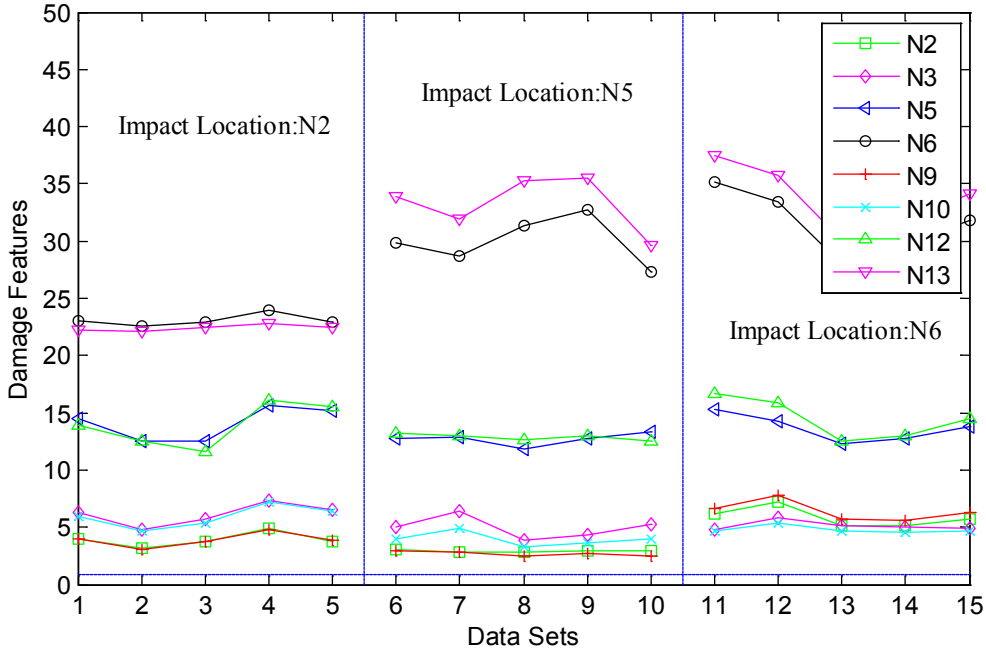

Figure 4.15. DF1s for DC2 using dynamic responses excited at N2, N5 and N6

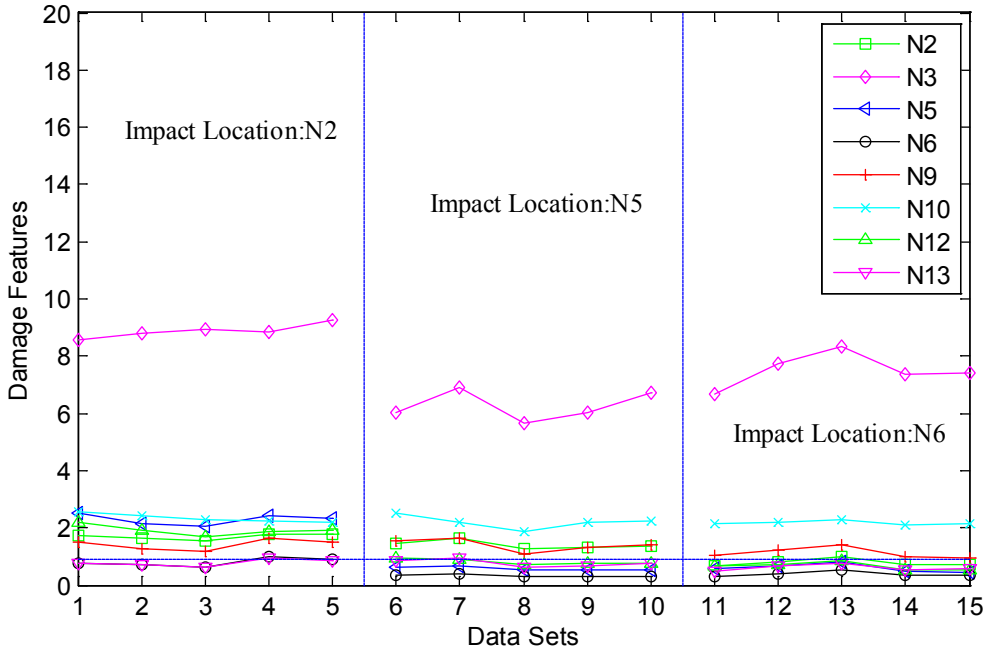

Figure 4.16. DF1s for DC3 using dynamic responses excited at N2, N5 and N6

Figure 4.16 shows the results for Damage Case 3, which is plate and bolts removal at N3. For all three impact locations, DF1s for N3 stand out exposing the correct location of damage. It is also seen that all other DF1s are relatively low, but their relations to the threshold are undetermined. When the excitation is at N2, half of the DF1s for other nodes are above the threshold, but this is not very obvious to the results for excitation at N5 and N6. This problem can be solved by determining the threshold separately for different impact locations.

In Figure 4.17, the results for Damage Case 4 (bolts removal at N3 and N10) are shown. For three different excitation locations, all the DF1s are all above the threshold, which is consistent with the results for impact at N12. However, the location of damage is still not detected for these three impact locations. This means the results cannot be improved by choosing a more proper impact location.

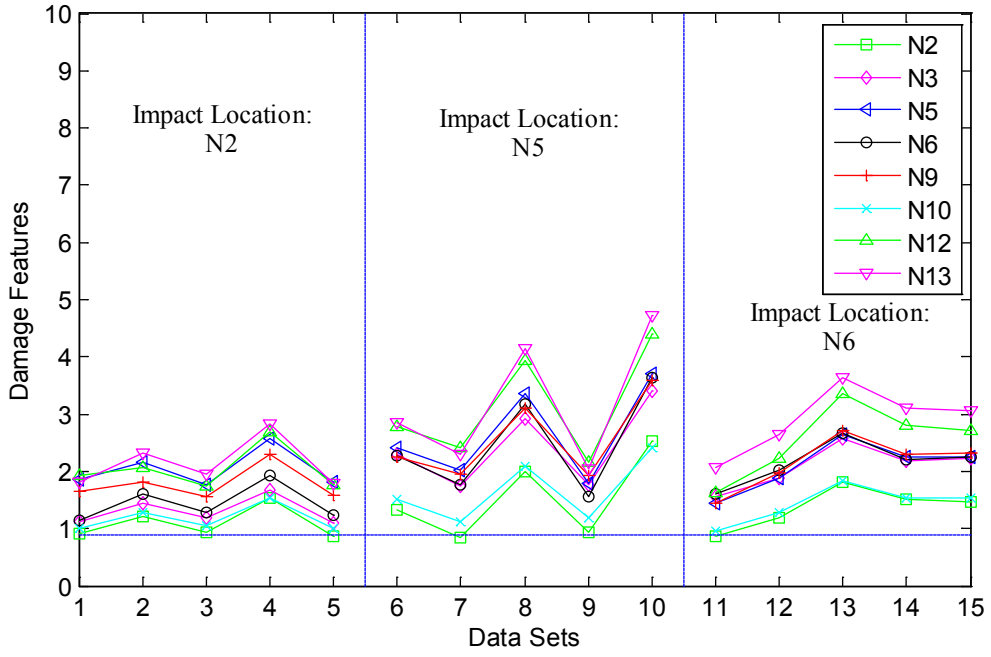

Figure 4.17. DF1s for DC4 using dynamic responses excited at N2, N5 and N6

In total, the impact locations do not have too much influence on the DF1s for the nodes closest to the damage location, which guarantees the correct detection of the damage. However, it can be seen that different impact locations still results in slightly different DF1s, which could be interpreted as better or worse results. This issue could be overcome

by carrying out tests several times for different impact locations and analyzing the results comprehensively.

4.3 Analysis and Result Interpretations for the Method using Coefficients as DF2

In this section, the extensible method using the same ARX models but different DFs is applied. In order to distinguish the damaged state from the healthy state, the threshold is introduced which is still determined by comparing two healthy states. The DF2s using the difference of coefficients are shown in Figure 4.18. According to the observation, the threshold is set to 0.5 with 79 of the 80 points below it.

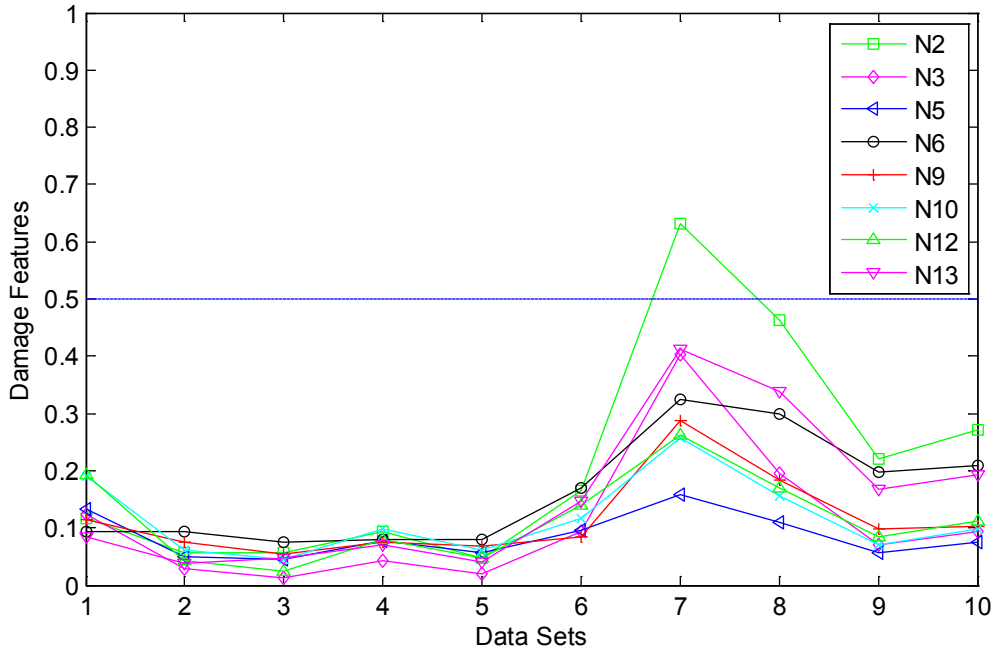

Figure 4.18. DF2s for determining the threshold under free vibration

4.3.1 Damage Case 1 (DC1): Scour (support removal) at N4

Damage Case 1 introduces damage caused by the removal of support at N4. Due to the globalization of damage, the DF2s for all the nodes are above the threshold. Among them, the DF2s for N3 and N4 are the highest because they are closest to the damage. The indirect effect at N2 and N5 are also observed. For this case, the peak value of DF2s is about 22, which shows that this damage is more severe than the change of boundary conditions in Damage Case 2 shown in the next section. Therefore, it is concluded that the method using DF2s can identify the location and estimate the severity for this case.

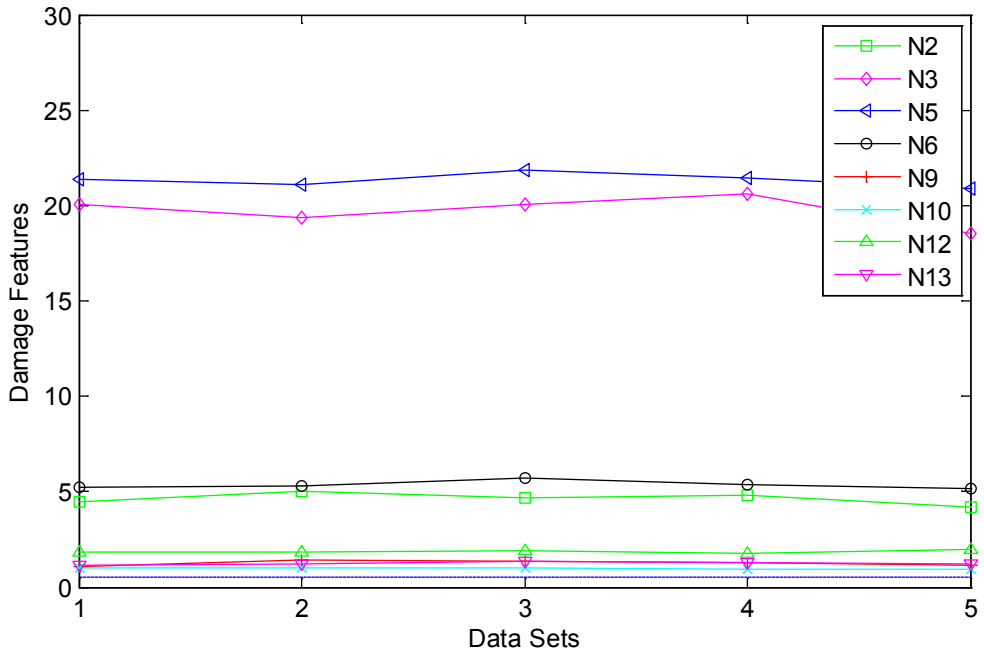

Figure 4.19. DF2s for DC1 of the steel grid structure

4.3.2 Damage Case 2 (DC2): Boundary restraint (fixing the roller supports) at N7 and N14

Figure 4.20 plots the results for Damage Case 2. It is shown that the DF2s for N6 and N13 are still higher than others because of fixing the roller supports at N7 and N14. The highest DF2 shown in this case is 8.6. N2 and N9 have the lowest DF2s since they are farthest form the damage. However, N5 and N12 do not show higher DF2s than N3 and N10 even though they are closer to the damage. Although the indirect effect is not identified, the direct influence of damage on N6 and N13 still reveal the location of damage successfully.

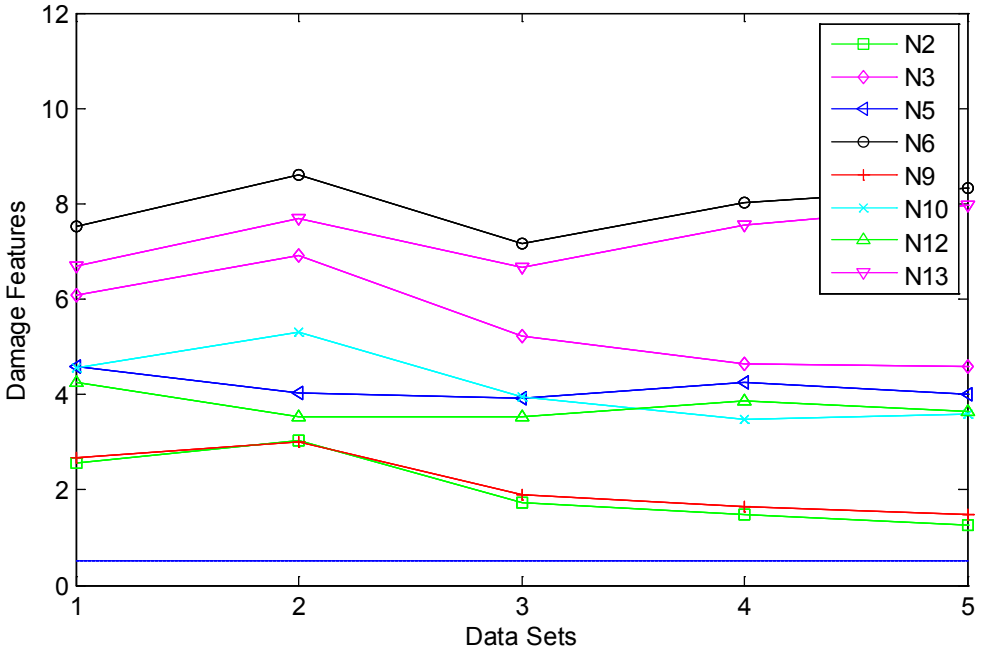

Figure 4.20. DF2s for DC2 of the steel grid structure

4.3.3 Damage Case 3 (DC3): Moment release (removal of bolts) and plate removal at N3

Figure 4.21 presents the results for the localized damage due to the removal of plate and bolts simultaneously at N3 in Damage Case 3. As shown in Figure 4.21, only the DF2s for N3 are clearly above the threshold, and all the other DF2s are around or below the threshold, which accurately locates the damage. It is noted that the maximum DF2 is 4.1, which is less than Damage Cases 1 and 2. This is consistent with the results for the first kind of DFs discussed in the previous section.

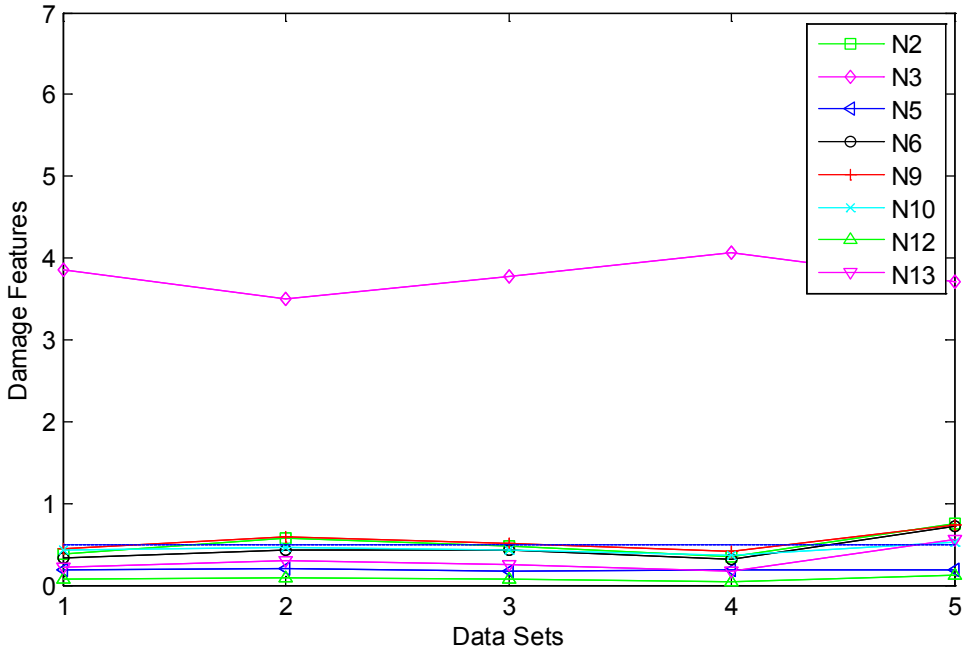

Figure 4.21. DF2s for DC3 of the steel grid structure

4.3.4 Damage Case 4 (DC4): Moment release (removal of bolts) at N3 and N10

Damage Case 4 is introduced by removing bolts at N3 and N10. The DF2s for this case are shown in Figure 4.22. It is seen that all the DF2s are above the threshold based on the same reason as in section 4.2.4. The maximum of DF2s is 3.4 showing this damage is the least severe. However, the highest DF2 is not for N3 or N10, which means that the damage is still not clearly located even if the coefficients are used as DFs.

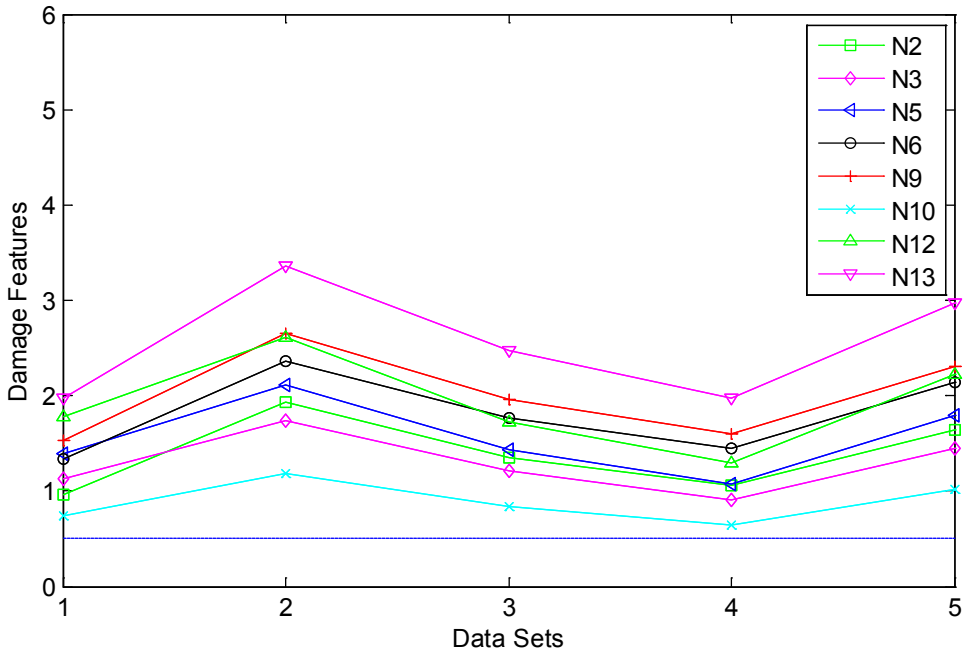

Figure 4.22. DF2s for DC4 of the steel grid structure

In this chapter, ARX models were created for sensor clusters in the steel grid type structure. Then, two different types of DFs were introduced. DF1 was based on the idea that the ARX models created for one state of the structure is no longer fit for another state. DF2 related the change in coefficients to the change in stiffness. As mentioned above, it is concluded both two kinds of DFs can identify and locate the damage in the steel grid structure and estimate the severity successfully, but DF1s using fit ratios can provide more reasonable results. Although DF2s cannot provide better results, it is extensible for future research since it directly builds a relationship between the change in coefficients and stiffness. For example, in further studies, different combinations of coefficients and different statistics methods can be used to locate damage more accurately, or distinguish between the changes in mass and stiffness.

CHAPTER 5:EXPERIMENTAL CASE STUDY II - A 4-SPAN BRIDGE TYPE STRUCTURE

5.1 Introduction to the 4-Span Bridge Type Structure

To further verify the ability of the time series based method to detect damage in different structures, a more realistic 4-span bridge type laboratory structure also developed at University of Central Florida is introduced. Same as the steel grid structure, this structure also provides a controlled environment for researchers to test different sensors, data collection systems, damage detection methods, etc. The main difference between this structure and the previous grid type structure is that it has a steel deck, which is expected to make the damage detection process more challenging.

As shown in Figure 5.1, this structure has two girders with 60.96 cm from each other. These two girds are only connected by a 3.18 mm thick, 120 cm wide steel deck using bolts and plates. Each girder has two 120 cm approach end spans and two 304.8 cm main inner spans. More details of the structure can be referred to Terrell (2011) and Zaurin (2009).

Figure 5.1. The 4-span bridge-type structure (Terrell 2011)

In this experiment, 16 PCB accelerometers were attached along the bottom of the girders. Figure 5.2 presents the installation of an accelerometer on this structure as an example. The parameters of the accelerometers were (Terrell 2011): 0.5 to 10,000 Hz frequency range, 100mV/g sensitivity and ±50g measurement range. Figure 5.3 shows the layout

and numbering of the 16 accelerometers. Note that there was no accelerometer in the approach spans since only damage at inner span was considered.

Figure 5.2. Installation of the PCB accelerometer (Terrell 2011)

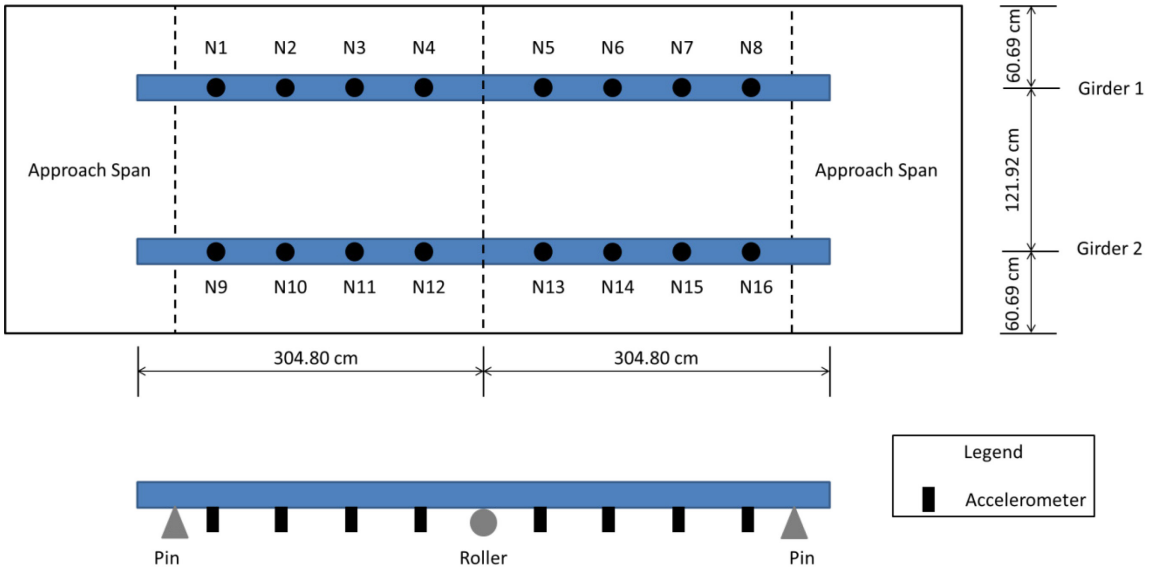

Figure 5.3. Experimental setup with locations of sensors (adapted from Terrell 2011)

The damage in this structure is mainly caused by boundary condition changes and removal of the bolts connecting the deck and girders (Figure 5.4). According to different combinations of these two changes in different locations, seven damage cases in total are introduced (Figure 5.5):

1) Damage Case 1: Change of pin connection to fixed connection at left support

2) Damage Case 2: Damage Case 1 + Change of roller connection to fixed connection at middle support
3) Damage Case 3: Change of roller connection to fixed connection at middle support
4) Damage Case 4: Removal of bolts at N4
5) Damage Case 5: Removal of bolts at N4 and N5.
6) Damage Case 6: Change of pin connection to fixed connection at right support
7) Damage Case 7: Damage Case 6 + Change of roller connection to fixed connection at middle support

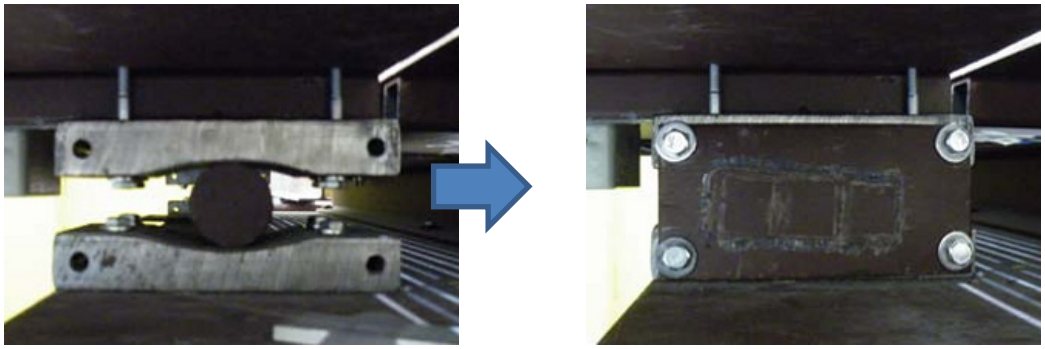

(a) Damage caused by change of boundary condition

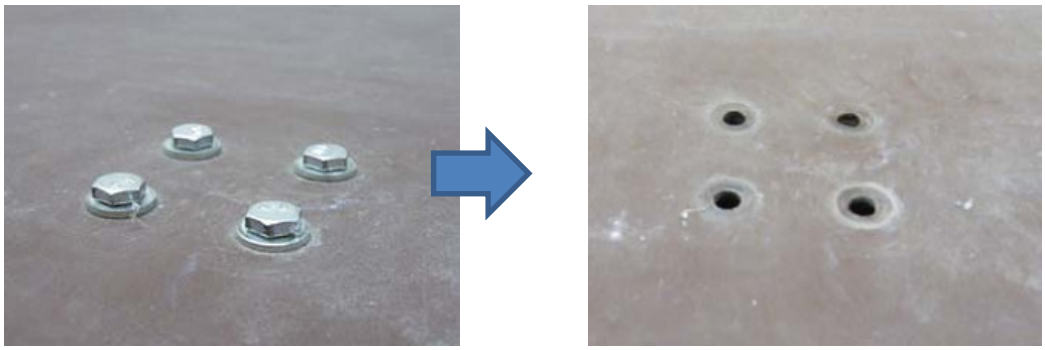

(b) Damage caused by removal of bolts

Figure 5.4. Damage introduced to the experimental structure

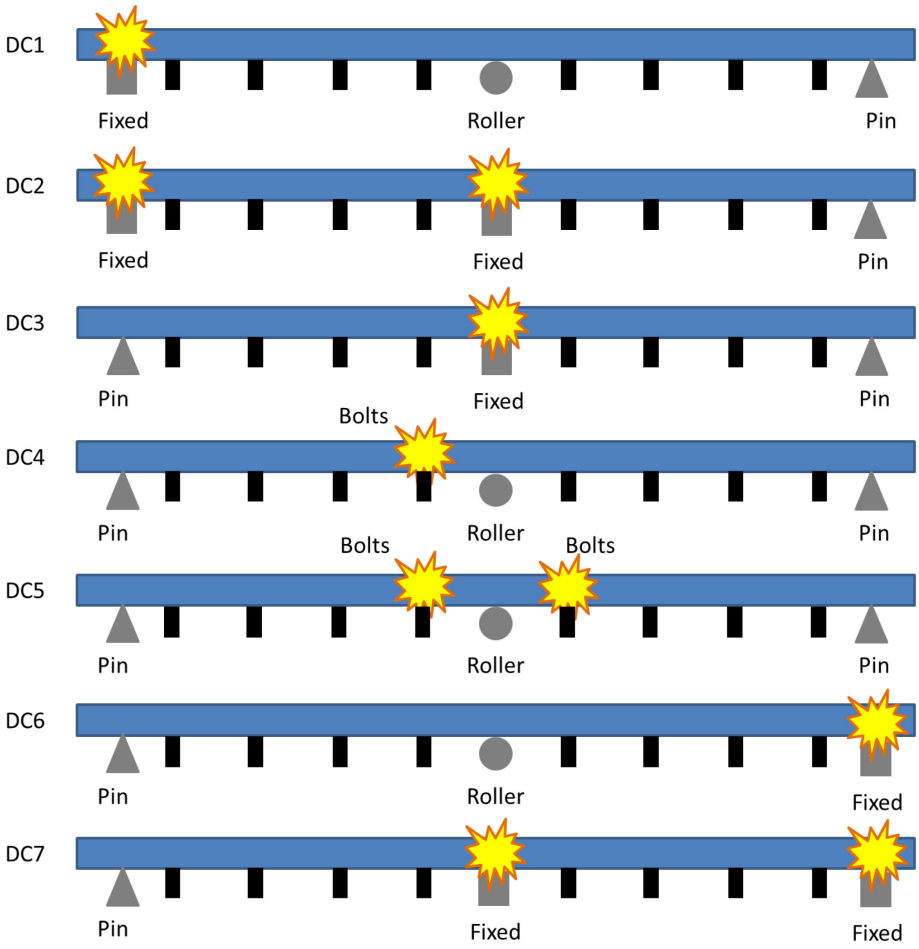

Figure 5.5. Damage cases applied to the 4-span bridge structure (adapted from Terrell 2011)

For the implementation of the proposed damage detection method, the total 16 sensors can be divided into 16 different sensor clusters (Table 5.1). As the previous case, impact tests were conducted on this structure. It is seen in Figure 5.6 that the structure was excited at 4 different locations at N3, N7, N10 and N14. The total 36 sets of data for these four different impact locations (9 trials for each location) were obtained for each damage case. The sampling frequency was 320 Hz. Figure 5.7 shows the time domain data collected from the baseline structure.

Like in the previous chapter, the ARX models are first used to fit the free responses of the structure, and then two different kinds of DFs measuring the variation of fit ratios and coefficients respectively are introduced for damage detection. Section 5.2 presents the

results and interpretations for the method using the function of fit ratios as DF1. The results for the method using the coefficients as DF2 are included in section 5.3.

Table 5.1. Sensor clusters for the 4-span bridge structure

Sensor Cluster	Output of the ARMAX model	Inputs of the ARMAX model
1	N1	N1, N2, N3, N9
2	N2	N1, N2, N3, N9, N10, N11
3	N3	N2, N3, N4, N10, N11, N12
4	N4	N3, N4, N5, N10, N11, N12
5	N5	N4, N5, N6, N12, N13, N14
6	N6	N5, N6, N7, N13, N14, N15
7	N7	N6, N7, N8, N14, N15, N16
8	N8	N7, N8, N15, N16
9	N9	N1, N2, N3, N9
10	N10	N1, N2, N3, N9, N10, N11
11	N11	N2, N3, N4, N10, N11, N12
12	N12	N3, N4, N5, N10, N11, N12
13	N13	N4, N5, N6, N12, N13, N14
14	N14	N5, N6, N7, N13, N14, N15
15	N15	N6, N7, N8, N14, N15, N16
16	N16	N7, N8, N15, N16

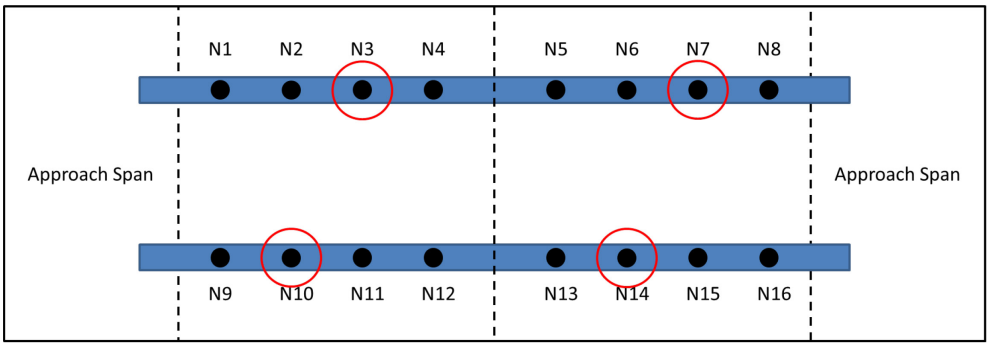

Figure 5.6. Four different impact locations

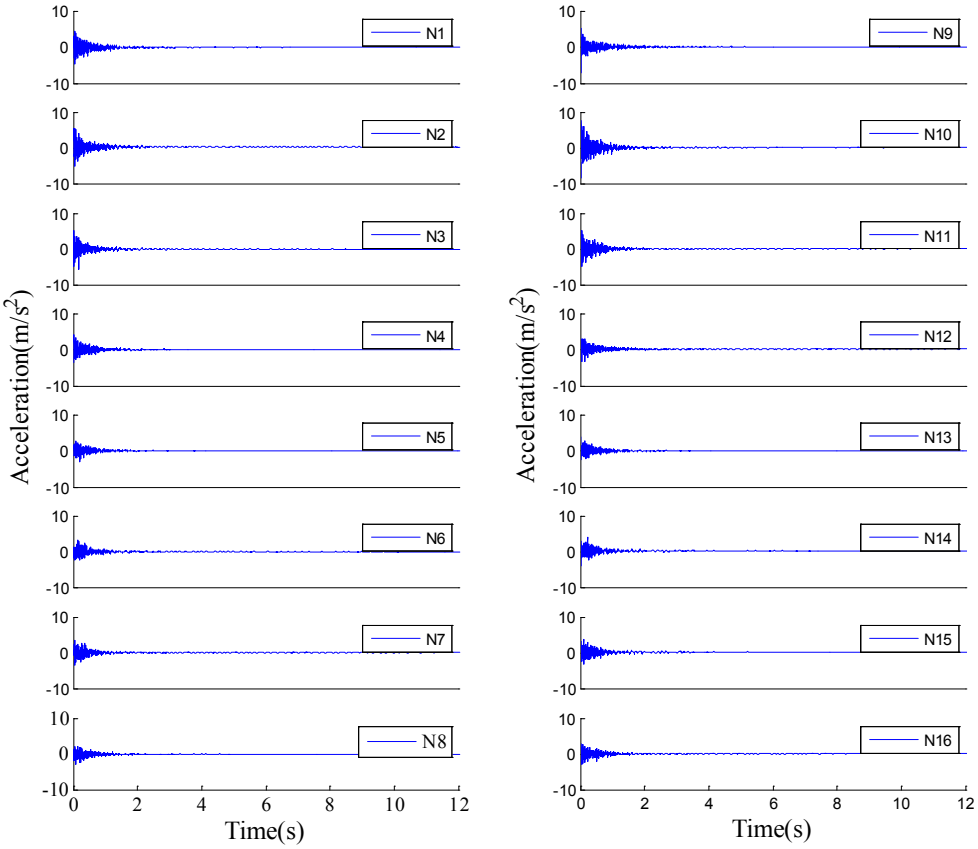

Figure 5.7. Collected acceleration data for the baseline structure

5.2 Analysis and Result Interpretations for the Method using Fit Ratios as DF1

Similar to the steel grid structure, the first step to detect damage is to determine the threshold. In this case, the threshold is still determined by comparing two groups of healthy data, each of which has 36 trials. According to Figure 5.8, almost all the DF1s are below 45. Therefore, the threshold is set to 45 with 570 out of the 576 points below it. Note that the threshold is significantly larger than the one for the steel grid structure. There are two reasons for this phenomenon: 1) this structure is more complicated so that small errors may lead to large change in DF1s; 2) these two sets of data were obtained from the first and last tests, so more errors were introduced between them. After the threshold is set, the DF1s for all the other damage cases could be compared to it.

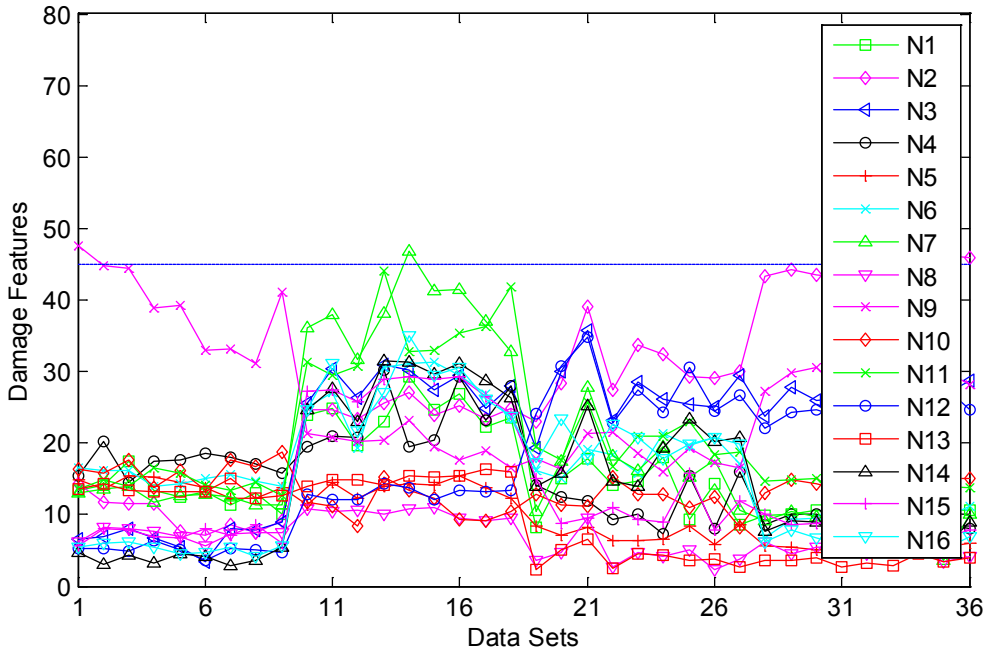

Figure 5.8. DF1s for determining the threshold (fit ratios)

Then, the same analysis as in section 4.2 can be conducted. Herein the result for Damage Case 4 is taken as an example. As shown in Figure 5.9, the DF1s for N4 are the highest due to the removal of bolts at N4. However, since there are 16 channels used in this structure and each channel has 36 points, it is very difficult to recognize and interpret the DFs clearly. In addition, the way to describe the results is also not good for a potential

automated system. In this section, in order to interpret the results clearly, the averages of the DF1s are taken for each channel. It should be noted that this is one of the simplest ways to post-process the results. Some more effective statistical methods could be applied to expect better results in the future. In addition, to represent the severity of damage more accurately, the average of all the nodes would be taken as severity indices. The logic behind it is that if one case is more severe than the other one, the entire DF1s for it would be higher.

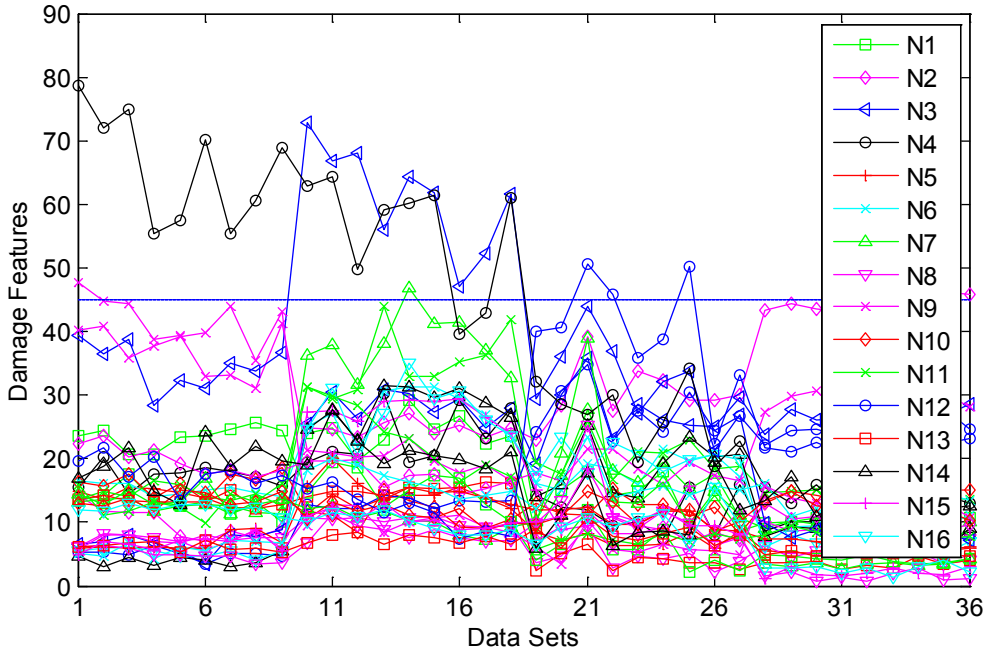

Figure 5.9. DF1s for Damage Case 4 of the 4-span bridge type structure

5.2.1 Damage Case 1 (DC1): Change of pin connection to fixed connection at left support

For the first case, the damage occurs due to the change of boundary condition at the left support. In Figure 5.10, it is shown that the DF1s for N1 and N9 are the highest, and the DF1s for other nodes gradually decrease when they are farther from N1 and N9, which implies that the damage occurs at left support. In this case, the severity index, the average of all the DF1s for 16 sensor clusters, is 26.16.

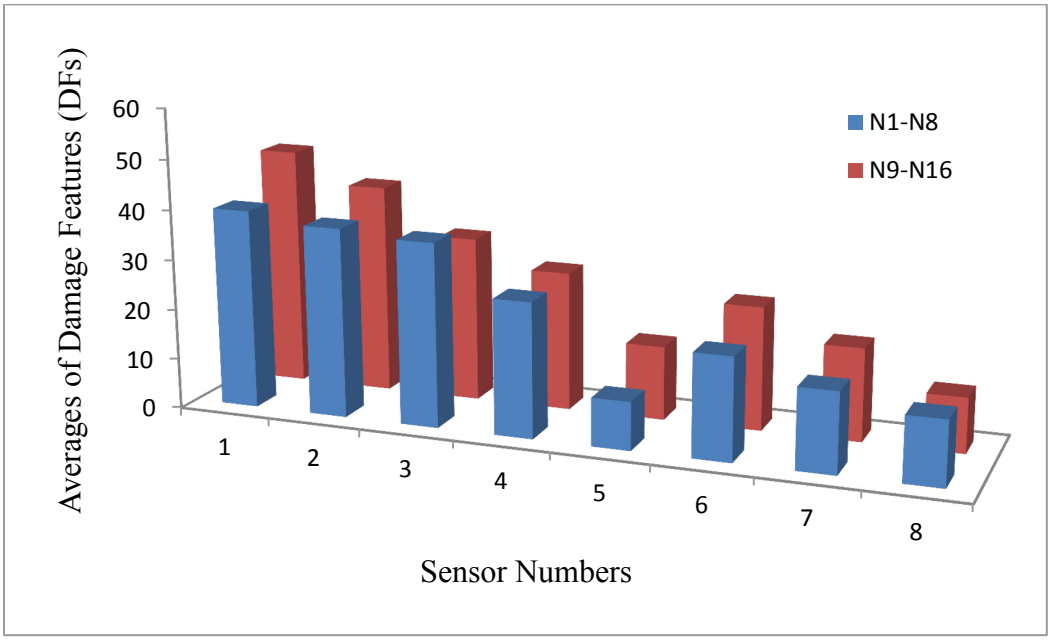

Figure 5.10. Averages of the DF1s for DC1 of the 4-span bridge model

5.2.2 Damage Case 2 (DC2): Damage Case 1 + Change of roller connection to fixed connection at middle support

Damage Case 2 is produced by applying Damage Case 1 along with boundary condition change at middle support. The highest DF1s for N1, N2, N9 and N10 shows that damage still exist at left support. As can be seen in Figure 5.11, the pattern of DF1s is very similar to the one in Damage Case 1 but the DF1s in general are higher. The DF1s for N4 and N12 near the middle support are 31.58 and 35.22, which are very close to the DF1s for N1 and N9 in Damage Case 1. In addition, the DF1s for nodes on the right span are not as low as in Damage Case 1. All these imply that damage at middle support may cause this rise. The severity index for this case is 35.04. This makes sense because the combination of damage at left and middle support is indeed more severe than boundary condition change at left support alone.

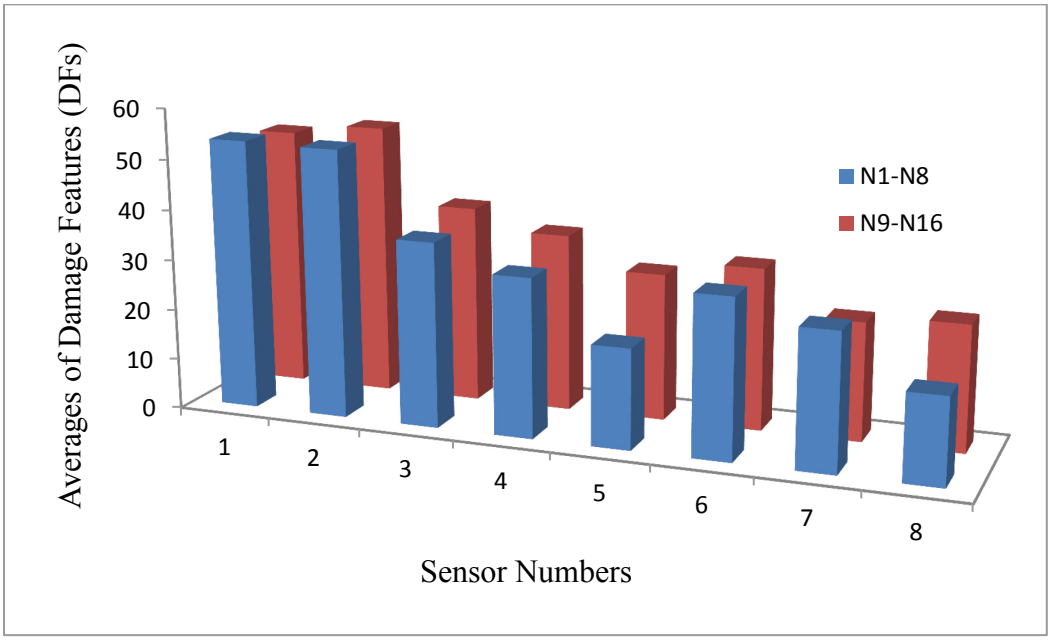

Figure 5.11. Averages of the DF1s for DC2 of the 4-span bridge model

5.2.3 Damage Case 3 (DC3): Change of roller connection to fixed connection at middle support

In Damage Case 3, only boundary condition change at middle support is applied. In Figure 5.12, it shows that the DF1 for N4 is the highest, and the DF1s for nodes adjacent to N4 are also higher than those near left and right supports. All these evidences show that damage happens at middle support. In addition, the rough symmetry of pattern also shows the location of damage. In this case, the severity index is 26.56. This value is almost the same as the one in Damage Case 1. In fact, the girder is continuous at middle support, which means the introduced fixity cannot be felt as much as fixing an end support. However, the boundary condition change is in the middle of structure, so it has influence on more nodes. Based on the two factors mentioned above, the severity index obtained by taking the average of all the DF1s shows the value similar to Damage Case 1.

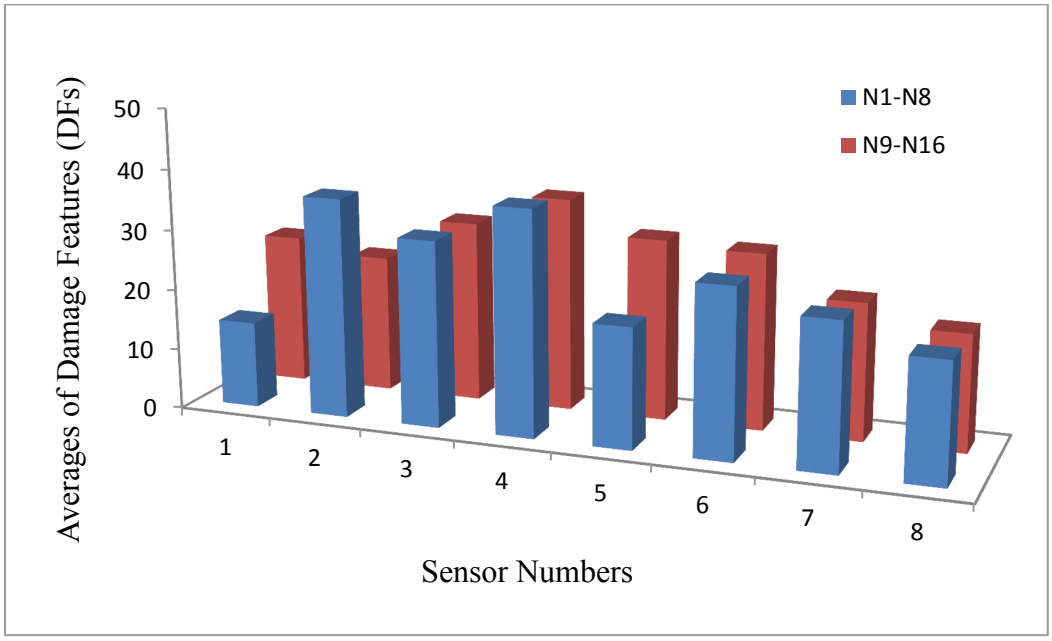

Figure 5.12. Averages of the DF1s for DC3 of the 4-span bridge model

5.2.4 Damage Case 4 (DC4): Removal of bolts at N4

The fourth Damage Case shows that four bolts are removed from the deck around N4, which is relatively minor damage compared to the others. Figure 5.13 shows the results for this damage case. It can be seen in Figure 5.13 that N3 and N4 has the highest DF1s where other nodes have the DF1s even less than half of them. This shows the localization of the damage. It is also noted that the method accurately locate the girder with damage even if two girders are directly connected by deck. The severity index for this case is only 15.29, which again demonstrates this is minor damage.

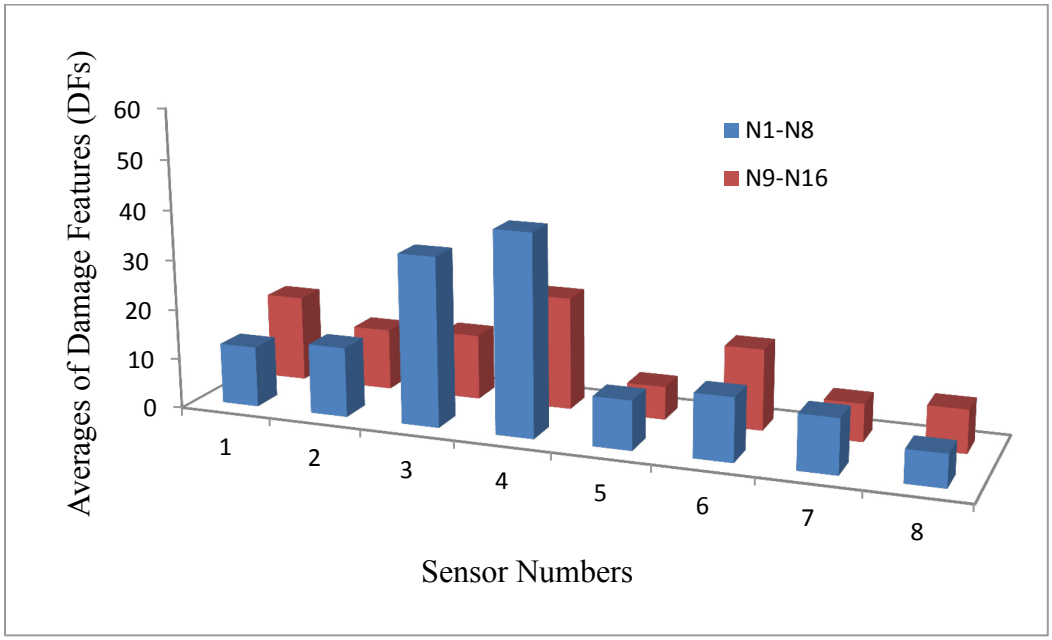

Figure 5.13. Averages of the DF1s for DC4 of the 4-span bridge model

5.2.5 Damage Case 5 (DC5): Removal of bolts at N4 and N5

Damage Case 5 involves the removal of 4 more bolts on the other span in addition to Damage Case 4. In Figure 5.14, it can be seen that high values concentrate on N4 and N5 and the values decrease as farther from the middle support, which implies the damage occurs near the middle support (N4 and N5). Compared to Damage Case 3 (boundary condition change at middle support), the damage leads to higher DF1s for N4 and N5 but much lower DF1s for the nodes near left and right supports. The severity index for this case is 38.69, which approximates to the index in Damage Case 2 and higher than in Damage Cases 1 and 3. The reason is that although the severity due to removal of 4 bolts is minor and localized, the combination of two of this kind of damage may influence on more nodes, which will increase the average of all the DF1s.

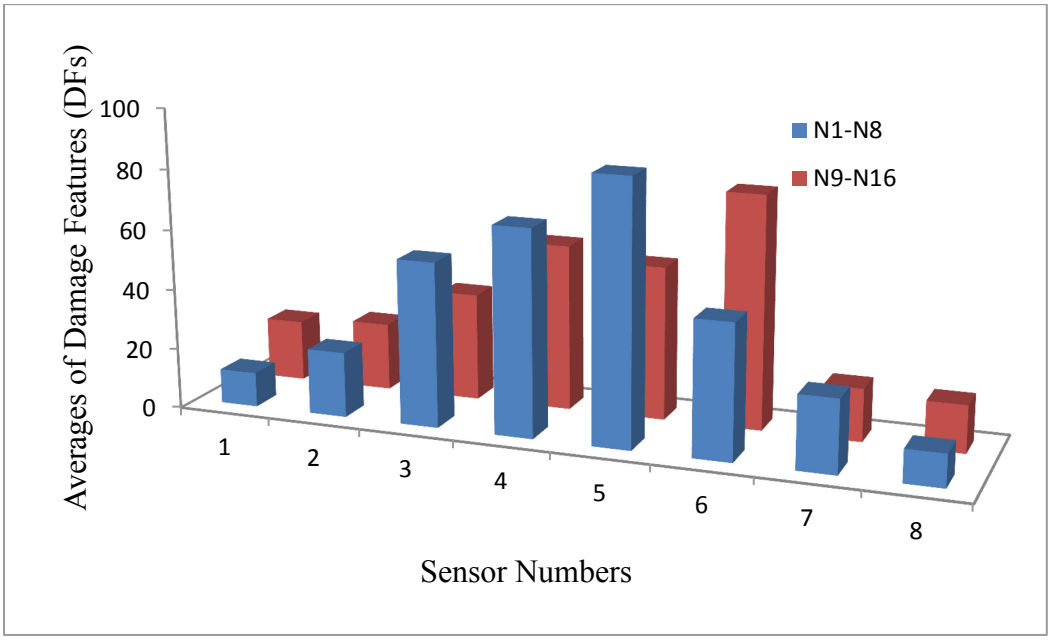

Figure 5.14. Averages of the DF1s for DC5 of the 4-span bridge model

5.2.6 Damage Case 6 (DC6): Change of pin connection to fixed connection at right support

Damage Case 6 introduces damage symmetrical to Damage Case 1, i.e., the change of boundary conditions at the right support. In Figure 5.15, similar to Damage Case 1, the highest DF1s are for the nodes closest to the right support showing the damage occurs at the right support. Likewise, the damage has limited influence on the nodes at left support. The severity index for this case is 21.46, which is slightly lower than in Damage Case 1. The reason for the asymmetry in these two damage cases is that the experimental structure and damage simulations may not be exactly symmetrical.

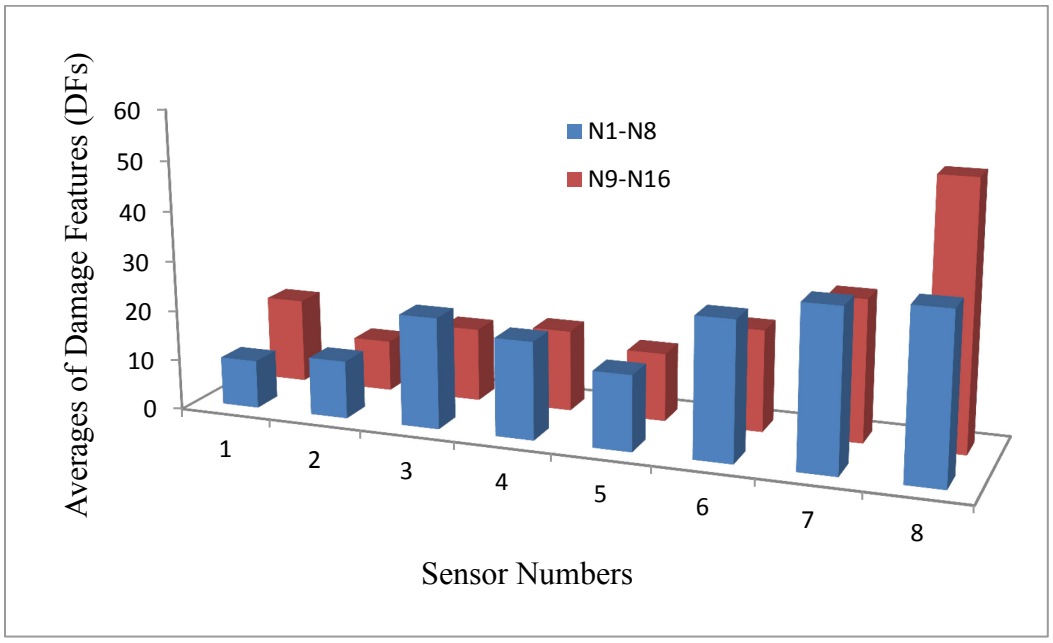

Figure 5.15. Averages of the DF1s for DC6 of the 4-span bridge model

5.2.7 Damage Case 7 (DC7): Damage Case 6 + Change of roller connection to fixed connection at middle support

Lastly, Damage Case 7 is symmetrical to Damage Case 2. It can be seen in Figure 5.16 that the DF1s near middle support and right support (N4, N8, N12 and N16) are relatively higher showing the damage is near these locations. The downward trends can be observed when nodes become father from middle and right supports. The severity index for this case is 35.21, which is very close to the one in Damage Case 2 as expected.

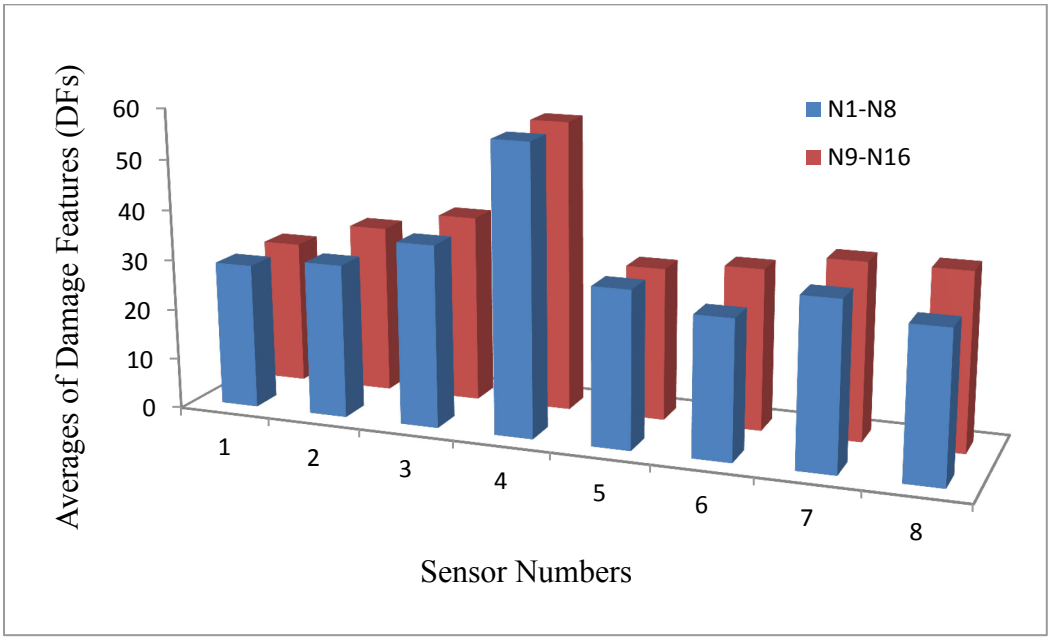

Figure 5.16. Averages of the DF1s for DC7 of the 4-span bridge model

5.3 Analysis and Result Interpretations for the Method using Coefficients as DFs

The results and interpretations for the 4-span bridge structure applying the method with coefficients as DF2 are included in this section. Similarly, in order to determine the threshold, two sets of data from healthy state are compared. According to Figure 5.8, the threshold of 25 is a reasonable value with 575 out of the 576 points below it. As in section 5.2, the severity of damage is estimated using severity index obtained by taking the average of all the DF2s for all the channels.

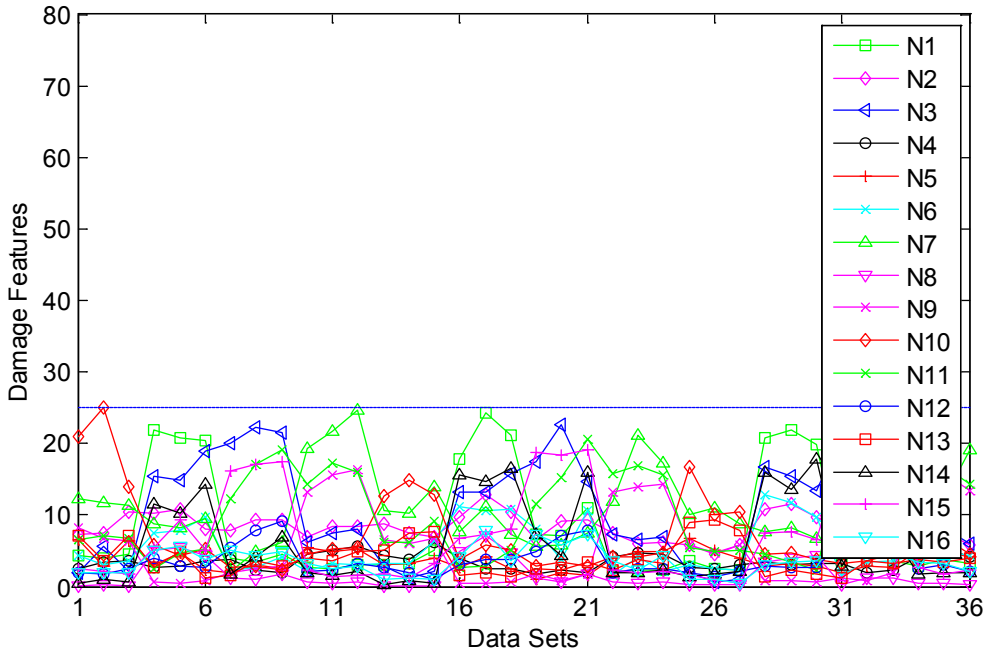

Figure 5.17. DF2s for determining the threshold

5.3.1 Damage Case 1 (DC1): Change of pin connection to fixed connection at left support

The first Damage Case introduces the damage caused by the change of boundary condition at left support. As shown in Figure 5.18, high DF2s concentrate on N2, N3, N9 and N10, which are all very close to the left support. The other nodes have relatively low DF2s since they are farther from the damage. Thus, it is most probable that damage occurs at left support despite the false negative result. Note that the DF2 at N1 is also expected to be high since it is very close to the damage location and the low DF2 identified with the methodology can be considered as a false negative.

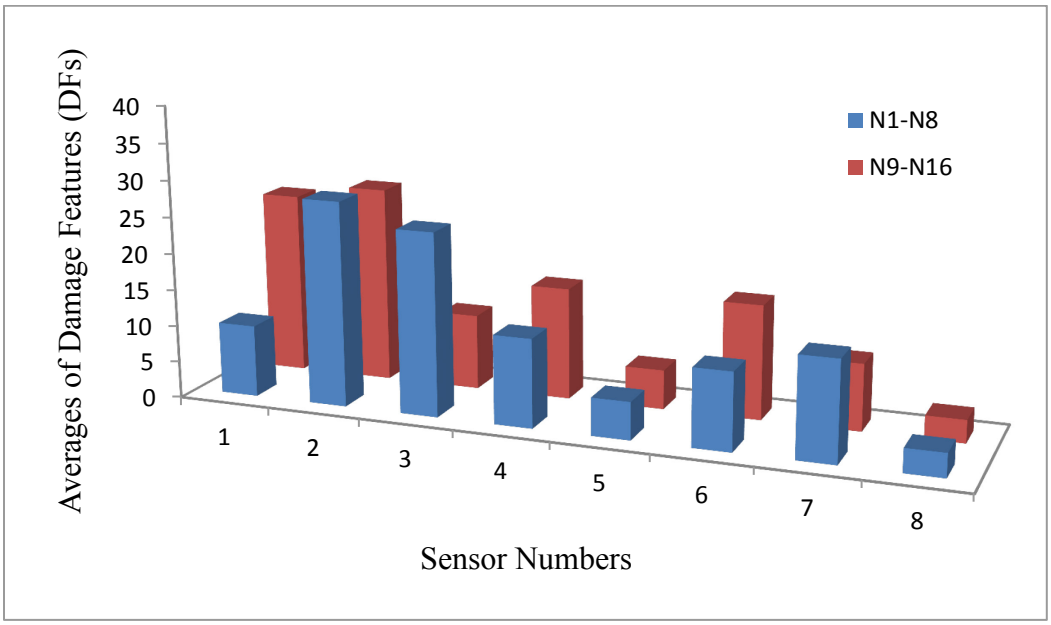

Figure 5.18. Averages of the DF2s for DC1 of the 4-span bridge model

5.3.2 Damage Case 2 (DC2): Damage Case 1 + Change of roller connection to fixed connection at middle support

Damage Case 2 consists of the damage in Damage Case 1 along with the boundary condition change at middle support. In Figure 5.19, it is seen that the DF2s for N2 and N10 are significantly high. Thus, it is believed that there is damage on the left span of the structure. Actually, since the damage is at left and middle supports, the peak values at N2 and N10 are caused by the comprehensive effects of the damage at two locations. The relatively high DF2s at N6 and N13 are due to the damage at middle span. However, the difference is not too obvious, and damage detection without knowledge of the location needs more detailed analysis. The severity index for this case is 14.61 implying that the damage in this case is slightly more severe than Damage Case 1.

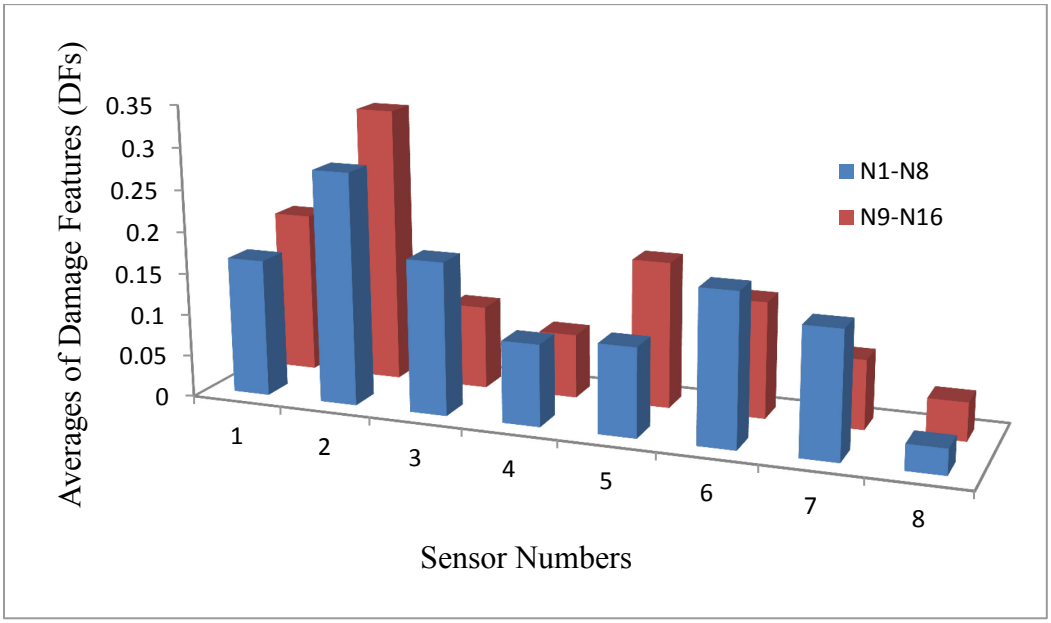

Figure 5.19. Averages of the DF2s for DC2 of the 4-span bridge model

5.3.3 Damage Case 3 (DC3): Change of roller connection to fixed connection at middle support

The change of boundary condition at middle support alone is applied in Damage Case 3. It is seen in Figure 5.20 that the difference between DF2s for different sensor is not as significant as in the previous two cases. This makes sense since the damage at middle support may affects nodes on two sides uniformly. Although a clear localization is not achieved due to the nature of the applied damage, note that the nodes near left and right supports have slightly lower DF2s than the nodes near middle support. The damage in this case is less severe than in Damage Case 2, so the severity index of 11.3 is lower than the one in Damage Case 2.

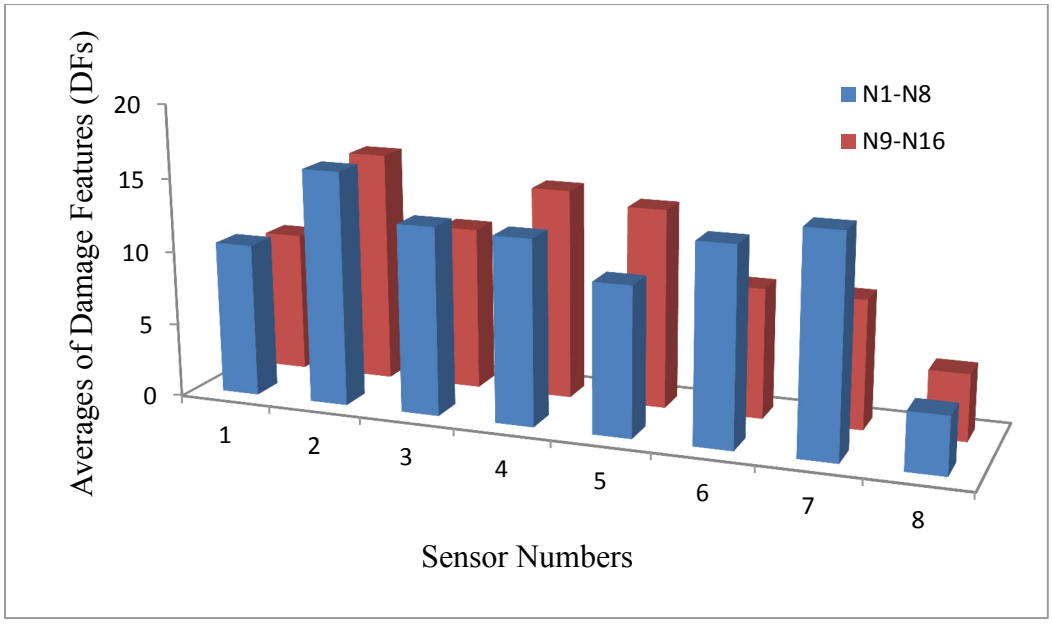

Figure 5.20. Averages of the DF2s for DC3 of the 4-span bridge model

5.3.4 Damage Case 4 (DC4): Removal of bolts at N4

In Damage Case 4, four bolts are removed at N4 to simulate minor damage. As can be seen in Figure 5.21, the DF2s for N4 and N11 (both are close to the damage at N4) are relatively high. Also the nodes on the left span have higher DF2s than the right span, which hints the localization of damage. The severity index due to this minor damage is only 9.3, which is the smallest in the first four damage cases.

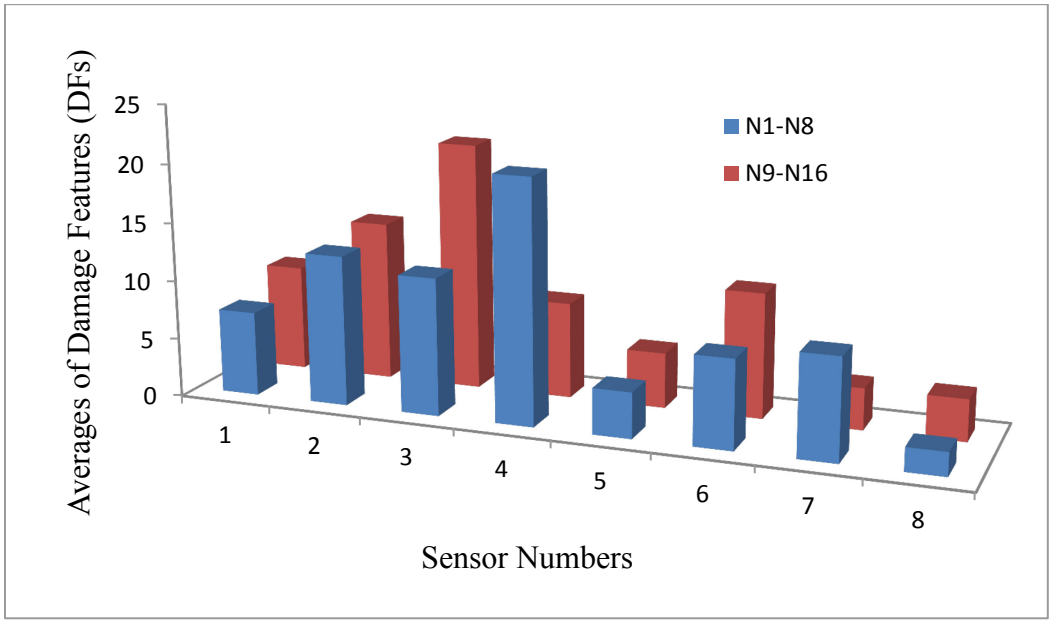

Figure 5.21. Averages of the DF2s for DC4 of the 4-span bridge model

5.3.5 Damage Case 5 (DC5): Removal of bolts at N4 and N5

In Damage Case 5, four more bolts are removed compared to Damage Case 4. As seen in Figure 5.22, the highest DF2 is for N5 and the second highest is for N3, which is consistent with the locations of damage. The nodes near left and right supports have lower DF2s since they are farther from the damage. However, the method does not show high value at N4 as in section 5.2.5. The severity index is 16.4, which is relatively higher than other cases. This is in agreement with the result for the method using fit ratios as DFs.

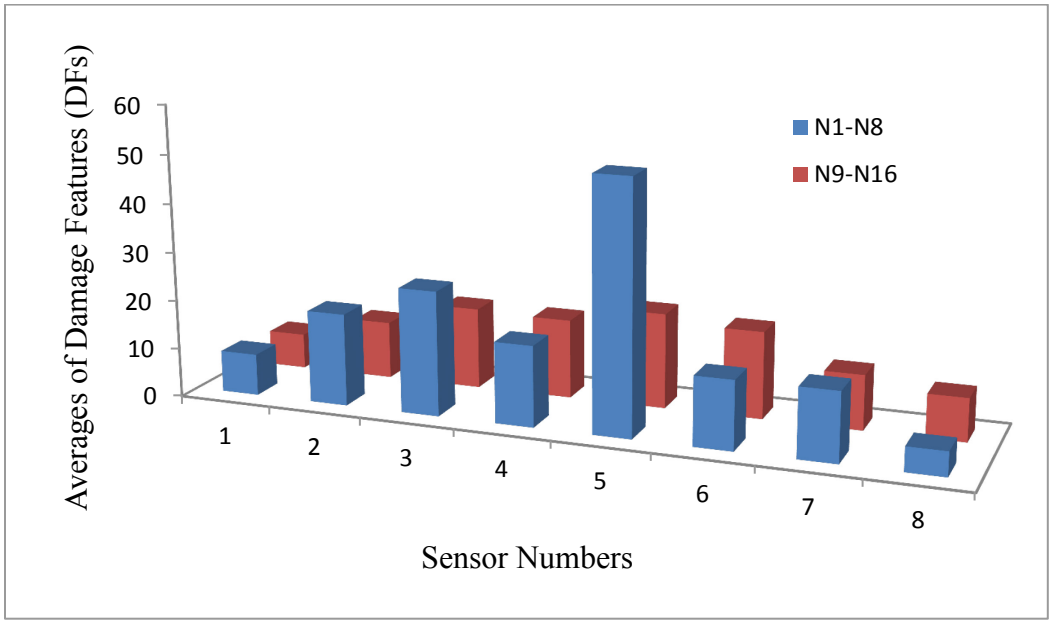

Figure 5.22. Averages of the DF2s for DC5 of the 4-span bridge model

5.3.6 Damage Case 6 (DC6): Change of pin connection to fixed connection at right support

The damage caused by boundary condition change at right support, symmetrical to the Damage Case 1, is applied in Damage Case 6. The results are shown in Figure 5.23. As expected, the high DF2s are obtained for N6, N7, N14 and N15, which are close to the right supports. Unlike the results for DF1s, the unexpected high values for N2 and N10 are observed in Figure 5.23, which should be considered as false positives. In this case, the severity index is 9.7, which is slightly smaller than in Damage Case 1. As explained before, the asymmetry in the results may be caused by the asymmetry in the structure and operations.

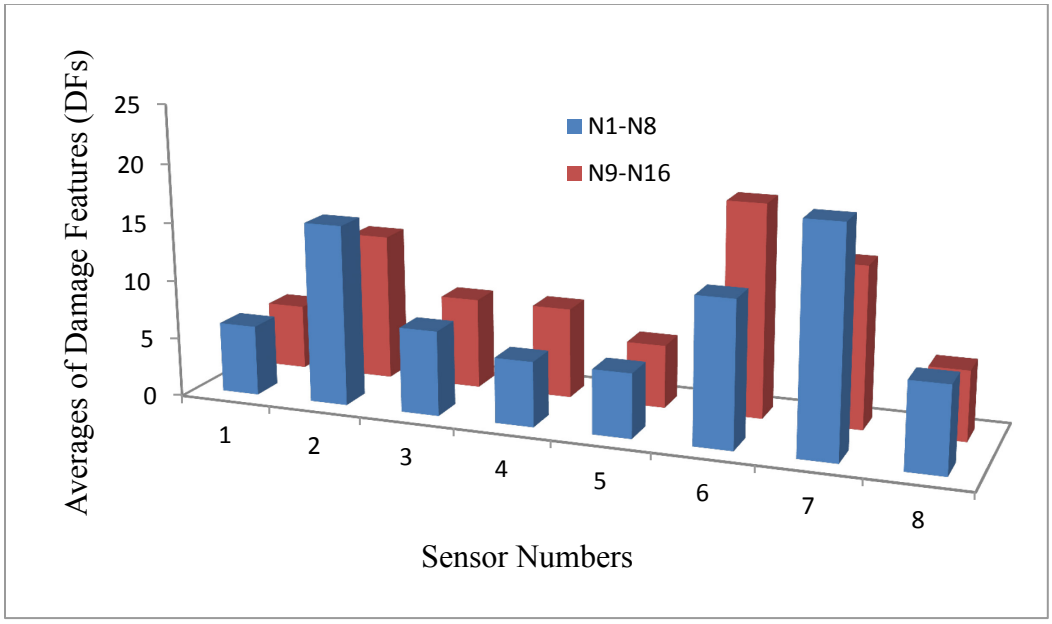

Figure 5.23. Averages of the DF2s for DC6 of the 4-span bridge model

5.3.7 Damage Case 7 (DC7): Damage Case 6 + Change of roller connection to fixed connection at middle support

Damage Case 7 includes the damage caused by the change of roller connection to fixed connection at middle and right supports. Two peaks for DF2s are observed in Figure 5.24: one is at N7 and the other one is at N13. This can be explained as the damage exists at both middle and right supports. The severity index of 13.3 demonstrates that the damage has the equivalent severity to Damage Case 2.

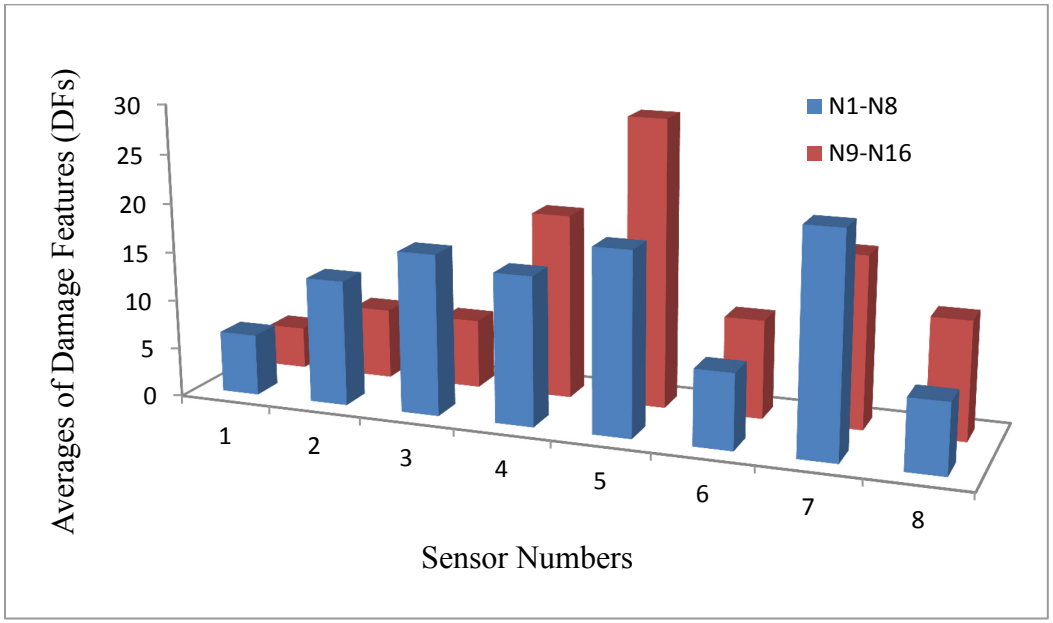

Figure 5.24. Averages of the DF2s for DC7 of the 4-span bridge model

In general, both two types of DFs can detect and locate the damage successfully in most damage cases. According to the figures above, DF1s provide better and clearer results than DF2s, especially for DCs 5, 6 and 7. The reason is that for more realistic structure, the relationships between sensors are more complicated so that the chosen DF2s obtained from the coefficients of the ARX models cannot reflect the change in stiffness as well as before. To overcome this problem, some other forms of DFs using more information (such as standard deviation and confidence intervals) and statistical methods could be used to extract the features which are more directly related to the change of stiffness.

CHAPTER 6:IMPROVEMENT OF THE PROPOSED METHOD FOR DAMAGE DETECTION

6.1 Theory for the Novel Method

In previous chapters, the feasibility of the proposed ARX based method for damage detection was demonstrated. In this chapter, an improved damage detection method based on Auto-Regressive Moving Average models with eXogenous inputs (ARMAX models) is proposed in order to detect and locate the changes in mass and stiffness properties of a system separately. The importance of such detection is that it can separate the damage (stiffness loss) from the changes caused by the mass (operational effects, such as traffic on a bridge).

The general form of an ARMAX model was shown in Eq. 3.2. For convenience, the definition of an ARMAX model is rewritten here in Eq. 6.1.

$$A(q)y(t) = B(q)u(t) + D(q)e(t) \tag{6.1}$$

$$\begin{aligned} A(q) &= 1 + a_1 q^{-1} + \cdots + a_{n_a} q^{-n_a} \\ B(q) &= b_1 q^{-1} + b_2 q^{-2} \cdots + b_{n_b} q^{-n_b} \\ D(q) &= 1 + d_1 q^{-1} + \cdots + d_{n_c} q^{-n_c} \end{aligned} \tag{6.2}$$

where the coefficients $A(q)$, $B(q)$, and $D(q)$ can be expressed in Eq. 6.2. $y(t)$ is the output, $u(t)$ is the input of the model, $e(t)$ is the error term, and $a_1,\cdots a_{n_a}, b_1,\cdots b_{n_b}, d_1,\cdots d_{n_c}$ are the parameters of the model. n_a, n_b and n_c are referred to as the orders of the parameters.

As before, in order to fit the dynamic responses of the system to ARMAX models in the context of the proposed methodology, some transformations must be conducted to the equation of motion in Eq. 3.15. First, the i^{th} row of Eq. 3.15 is considered separately as in Eq. 6.3. Re-arranging Eq. 6.3, Eq. 6.4 is obtained to represent the acceleration term of the i^{th} channel in terms of the other terms. Assuming that the structure has a lumped mass matrix, the acceleration terms on the right side are removed, since any off-diagonal

entries of the mass matrix are zero. In addition, according to our investigation, the damping terms make very little contribution to the balance of the equation. Therefore, we neglect the damping terms as in Eq. 6.5. Considering that it is usually not practical to measure the displacement data in real-life applications, efforts are made to eliminate these terms from Eq. 6.5. By taking the second derivative of Eq. 6.5, we obtain the fourth derivative of x on the left side and accelerations on the right side as in Eq. 6.6. Eq. 6.7 can then be obtained by applying the forward difference method (Levy and Lessman 1992) twice to Eq. 6.6; (the symbol, t, is added in these equations for further clarity).

$$\left(m_{i1}\ddot{x}_1 + \cdots + m_{iN}\ddot{x}_N\right) + \left(c_{i1}\dot{x}_1 + \cdots + c_{iN}\dot{x}_N\right) + \left(k_{i1}x_1 + \cdots + k_{iN}x_N\right) = f_i \tag{6.3}$$

$$\ddot{x}_i = \frac{f_i}{m_{ii}} - \frac{m_{i1}\ddot{x}_1 + \cdots + m_{i,i-1}\ddot{x}_{i-1} + m_{i,i+1}\ddot{x}_{i+1}\cdots + m_{iN}\ddot{x}_N}{m_{ii}} - \frac{c_{i1}\dot{x}_1 + c_{i2}\dot{x}_2 + \cdots + c_{iN}\dot{x}_N}{m_{ii}} - \frac{k_{i1}x_1 + k_{i2}x_2 + \cdots + k_{iN}x_N}{m_{ii}} \tag{6.4}$$

$$\ddot{x}_i = \frac{f_i}{m_{ii}} - \frac{k_{i1}x_1 + k_{i2}x_2 + \cdots + k_{iN}x_N}{m_{ii}} \tag{6.5}$$

$$\dddot{x}_i = \frac{\ddot{f}_i}{m_{ii}} - \frac{k_{i1}\ddot{x}_1 + k_{i2}\ddot{x}_2 \cdots + k_{iN}\ddot{x}_N}{m_{ii}} \tag{6.6}$$

$$\frac{\frac{\ddot{x}_i(t+2\Delta t) - \ddot{x}_i(t+\Delta t)}{\Delta t} - \frac{\ddot{x}_i(t+\Delta t) - \ddot{x}_i(t)}{\Delta t}}{\Delta t} = \frac{\ddot{f}_i}{m_{ii}} - \frac{k_{i1}\ddot{x}_1(t) + k_{i2}\ddot{x}_2(t) + \cdots + k_{iN}\ddot{x}_N(t)}{m_{ii}} \tag{6.7}$$

In Eq. 6.7, we can see that $\ddot{x}_i(t)$ appears on both sides, which may lead to trivial solutions to the parameters of the ARMAX models. To resolve this problem, we define $\ddot{x}_i(t+\Delta t) - \ddot{x}_i(t)$ as a new sequence $y_i(t)$. The final form of the equation is given as Eq. 6.8, where we can see the relation between signals in different sensors reflects a function of the system's intrinsic properties (m and k). It is therefore expected that any change in mass and stiffness will be exposed by the change in the coefficients of the ARMAX model if a proper DF is chosen based on the model coefficients.

$$\frac{y_i(t+\Delta t)-y_i(t)}{\Delta t^2}=\frac{\ddot{f}_i}{m_{ii}}-\frac{k_{i1}\ddot{x}_1(t)+k_{i2}\ddot{x}_2(t)+\cdots+k_{iN}\ddot{x}_N(t)}{m_{ii}} \tag{6.8}$$

Comparing Eq. 6.8 to the ARMAX model in Eq. 6.1, $y_i(t)$ and $\ddot{x}_i(t)$ are considered as output and input terms, respectively. The errors introduced by ignoring the damping terms and the second derivative of the excitation force can be incorporated into the error terms if we assume they are normally distributed. Therefore, the orders n_a and n_b for the ARMAX model can be chosen as 1 and 1 by comparing the corresponding output and input terms. According to the investigation, n_c is taken as 3 in order to incorporate the influence of errors caused by random ambience force, noise, and by ignoring damping terms. Finally, the ARMAX model for the i^{th} DOF can be expressed as in Eq. 6.9,

$$y_i(t+\Delta t)+a^i y_i(t)=b_1^i\ddot{x}_1(t)+b_2^i\ddot{x}_2(t)+\cdots+b_N^i\ddot{x}_N(t)+e(t)+d_1e(t-\Delta t)+d_2e(t-\Delta t) \tag{6.9}$$

The ARMAX model above is for the i^{th} row in the equation of motion. Therefore, N different ARMAX models can be established for the whole system. The same reason as before, the signal of a sensor is expected to be only related to the signals in its adjacent sensors. The ARMAX models can therefore be simplified further, such that only the reference channel and its adjacent channels are included in each ARMAX model. In this respect, the sensor clusters defined here are the same as in Chapter 2.

Building two sets of ARMAX models for the baseline and damaged (or unknown state) structures using the process described above, damage can be identified, located, and quantified by extracting proper DFs from the model coefficients. In the proposed approach, the DF is taken as the relative difference between $B(q)$ coefficients of damaged and baseline structures. The form of the DF is shown in Eq. 6.10.

$$DF_{ij}=\frac{b^i_{j,baseline}-b^i_{j,damaged}}{b^i_{j,baseline}}\times 100\%, i\in sensor\ clusters, j\in adjacent\ sensors \tag{6.10}$$

In the following sections, two case studies are presented where the proposed method is applied to two different numerical models. It is shown that damage can be accurately identified, located, and quantified using output-only acceleration data for these models.

6.2 Introduction to the 4-DOF system

In this section, preliminary investigations of the novel method are presented. To verify the approach with numerical models, a 4-DOF mass-spring system (see Figure 6.1) similar to the one used in the previous studies (Gül and Catbas 2008, 2011, Mei and Gül 2014) but with more realistic parameters is used in this thesis. The properties of this system are defined as: $m_1 = 3500kg$, $m_2 = m_3 = 2500kg$, $m_4 = 2000kg$, $k_1 = 2 \times 10^7 N/m$ and $k_2 = k_3 = k_4 = k_5 = 7 \times 10^7 N/m$. According to the relations between the blocks, the stiffness and mass matrix can be easily expressed as in Eqs. 6.11 and 6.12. Accordingly, the natural frequencies calculated through mass and stiffness matrices are 6.68Hz, 28.37Hz, 43.38Hz and 53.47Hz, respectively.

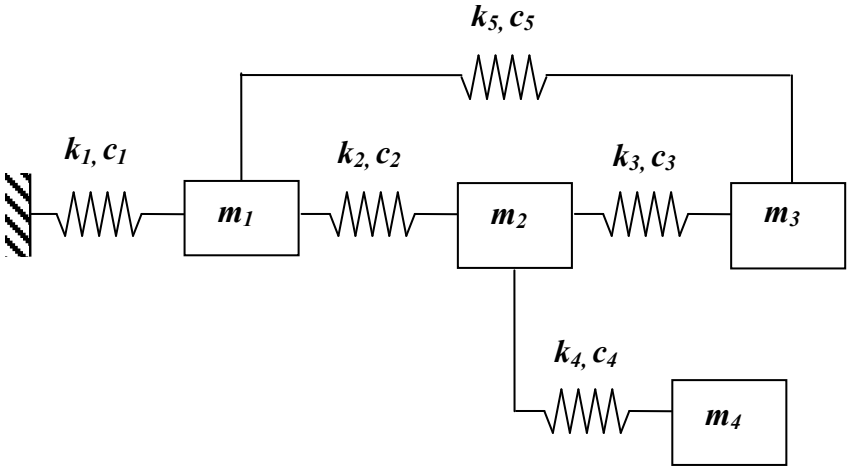

Figure 6.1. The numerical model used for verifications

$$K = \begin{bmatrix} k_1+k_2+k_5 & -k_2 & -k_5 & 0 \\ -k_2 & k_2+k_3+k_4 & -k_3 & -k_4 \\ -k_5 & -k_3 & k_3+k_5 & 0 \\ 0 & -k_4 & 0 & k_4 \end{bmatrix} = \begin{bmatrix} 160 & -70 & -70 & 0 \\ -70 & 210 & -70 & -70 \\ -70 & -70 & 140 & 0 \\ 0 & -70 & 0 & 70 \end{bmatrix} MN/m \quad (6.11)$$

$$M = \begin{bmatrix} m_1 & 0 & 0 & 0 \\ 0 & m_2 & 0 & 0 \\ 0 & 0 & m_3 & 0 \\ 0 & 0 & 0 & m_4 \end{bmatrix} = \begin{bmatrix} 3500 & 0 & 0 & 0 \\ 0 & 2500 & 0 & 0 \\ 0 & 0 & 2500 & 0 \\ 0 & 0 & 0 & 2500 \end{bmatrix} kg \tag{6.12}$$

The classic Rayleigh damping matrix is constructed assuming the damping ratio is 3% for all of the modes. The coefficients a_0=0.72 and a_1=0.0011 are solved from the first and second natural frequencies.

$$C = a_0 M + a_1 K \tag{6.13}$$

There are six damage patterns defined for this system including stiffness, mass and damping reduction: 1) reduction of 20% for stiffness k_2; 2) reduction of 20% for stiffness k_2 and k_4; 3) reduction of 20% for mass m_4; 4) 20% reduction in stiffness k_2 and 20% reduction in mass m_2; 5) reduction of 20% for damping C_{33}; 6) combination of Damage pattern 1, 3 and 5. The excitations are generated as white noise acting on all the DOFs simultaneously in order to simulate the ambient vibration. The time step for this case is 0.001s corresponding to a sampling frequency of 1000Hz, which is significantly larger than twice of the largest natural frequency 53.47Hz. In order to make the simulations more realistic, 10% noise is added to the signals at all DOFs. For each damage case, the averages and standard deviations of the DFs for ten independent trials are reported to show the repeatability.

According to the ARMAX-based approach described above, four sensor clusters with different reference channels are created for this system. The first sensor cluster is created with the first DOF as the reference channel, and it includes the first, second, and third DOFs as the adjacent DOFs. For the second sensor cluster, the second DOF is considered as the reference channel and all the DOFs are included as the adjacent channels since this DOF is connected to all the DOFs. The third sensor cluster consists of the first, second, and third DOFs and the reference channel is the third DOF. The last sensor cluster only contains the second and fourth DOFs and the reference channel is the fourth one. Creating the ARMAX models for those sensor clusters adopting the data from baseline

and damaged structures, the DFs defined in Eq. 6.10 can be extracted. The damage can be detected, located and quantified using these DFs.

6.3 Damage Detection for a 4-DOF System Using Acceleration Data Only

6.3.1 Damage Pattern 1 (DP1): $\tilde{k}_2 = 0.8k_2$

The first damage pattern simulates a reduction of 20% for stiffness k_2 between the first and second blocks. Table 6.1 is obtained by applying the DFs mentioned above. Each row of Table 6.1 represents a sensor cluster, and the four columns of the tables represent the adjacent sensors in the sensor clusters. For instance, the first row is for the first sensor cluster, which has the first DOF as the reference channel. The first sensor cluster includes the first, second, and third DOFs which are connected to it, so the fourth column of the first row is not applicable (N/A). For each entry of the table, the average and standard deviation (in the parenthesis) of 10 trials are presented in percentage. For convenience, the average of the DFs for 10 trials is simply called DF which can be indexed by their location in the table. For example, the DF in the first row and second column is defined as DF_{12}. It is observed in this table that the DFs for the third and fourth DOFs are close to zero, indicating that the damage is far from these DOFs. The non-zero DFs in the top-left corner show that the damage is related to DOF 1 and DOF 2. The magnitudes represent the contribution of the stiffness reduction. It can be seen in Table 6.1 that the DF_{21} is -18.16% and DF_{12} is -18.70%, both of which are very close to -20%, which is the applied damage. This indicates the extent of the stiffness reduction in k_2, which is between the first and second DOFs. The -8.74% and -6.61% changes for DF_{11} and DF_{22}, respectively, are caused by the fact that a 20% decrease in k_2 introduces an 8.75% decrease in the total stiffness associated with the first DOF ($0.2k_2/K_{11}$ = $0.2\times7\times10^7/(160\times10^6)$ = 8.75%), and creates a 6.67% decrease in the total stiffness associated with the second DOF ($0.2k_2/K_{22}$ = $0.2\times7\times10^7/(210\times10^6)$ = 6.67%). The standard deviations of the DFs presented in the parentheses demonstrate good repeatability of the results since most of them are very small. It is also noted that the standard deviations for low DFs (such as DF_{13} and DF_{33}) are higher. However, these relatively larger fluctuations are negligible compared to the DFs for damaged DOFs.

Especially considering the 10% artificial noise added to the data, these results are deemed very successful in locating and quantifying the damage.

Table 6.1. DFs for the DP1 (average and standard deviation of 10 trials in %)

Reference Channel	1st	2nd	3rd	4th
1st	-8.74 (0.80)	-18.16 (0.85)	-0.87 (1.84)	N/A
2nd	-18.70 (0.73)	-6.61 (0.66)	-0.18 (1.19)	0.45 (0.58)
3rd	-0.46 (1.42)	0.80 (1.77)	0.03 (0.79)	N/A
4th	N/A	0.01 (0.70)	N/A	-0.42 (0.56)

6.3.2 Damage Pattern 2 (DP2): $\tilde{k}_2 = 0.8k_2$, $\tilde{k}_4 = 0.9k_4$

Damage pattern 2 is obtained as damage pattern 1 plus the reduction of 10% to the element stiffness k_4. From Figure 6.1, we can see that k_2 is related to DOFs 1 and 2, and k_4 is related to DOFs 2 and 4. In Table 2, it is observed that DF_{11}, DF_{12}, DF_{21} are almost the same as those in Table 1, which again locate and quantify the damage caused by the reduction of k_2. Similarly, the DF_{24}, DF_{42}, DF_{44} between DOFs 2 and 4 with magnitudes of around 10% also represent the influence of the reduction of k_4. The effect of the reduction of k_2 and k_4 on the diagonal stiffness for DOF 2 is $(0.2k_2+0.1k_4)/K_{22} = (0.2+0.1) \times 7\times10^7/(210\times10^6) = 10.00\%$, which is exactly reflected by the value of DF_{22}. It should be emphasized that the reduction of -10.03% for DOF 4 is consistent with the 10% reduction in k_4 since this is the only spring connected to DOF 4. Theoretically, Table 2 should be symmetrical since the stiffness matrix is symmetrical. The slight asymmetry is mainly caused by the introduced artificial noise. Also note that in this case the standard deviations for some DFs for this damage pattern are closer to the values of DFs for damaged DOFs with 10% stiffness reduction, which may cause some false positive results. For such cases, determining a threshold based on statistical analysis of DFs obtained from multiple data sets could be very useful (Gül and Catbas 2009). Such a study is not in the scope of this article.

Table 6.2. DFs for the DP2 (average and standard deviation of 10 trials in %)

Reference Channel	1st	2nd	3rd	4th
1st	-8.83 (0.81)	-18.60 (0.92)	-0.38 (1.69)	N/A
2nd	-18.89 (0.76)	-10.05 (0.62)	-0.25 (1.17)	-9.64 (0.70)
3rd	-0.17 (1.48)	0.75 (1.71)	0.09 (0.79)	N/A
4th	N/A	-9.48 (0.60)	N/A	-10.03 (0.47)

6.3.3 Damage Pattern 3 (DP3): $\tilde{m}_4 = 0.8m_4$

In the third damage pattern, instead of stiffness reduction, the mass of the fourth DOF has a reduction of 20%. It can be seen from Table 6.3 that this reduction results in the increase for DF_{42} and DF_{44} around 23-24%, which are both in the fourth sensor cluster. These DFs are explained in Eq. 6.8, where the mass term is in the denominator and the reduction of this mass by 20% will increase the parameters of the entire sensor cluster by 1/(1-0.2)-1= 25%. It should be noted that the DFs for the change of mass are asymmetrical, with a very different layout than that for the change of stiffness. This phenomenon is considered as a main characteristic to distinguish between the change of mass and stiffness.

Table 6.3. DFs for the DP3 (average and standard deviation of 10 trials in %)

Reference Channel	1st	2nd	3rd	4th
1st	0.08 (0.84)	0.40 (1.31)	-0.96 (1.74)	N/A
2nd	0.50 (0.75)	0.39 (0.60)	-0.20 (1.15)	-0.38 (0.83)
3rd	-1.11 (1.71)	-0.41 (2.03)	0.13 (0.85)	N/A
4th	N/A	22.95 (1.44)	N/A	24.28 (0.92)

6.3.4 Damage Pattern 4 (DP4): $\tilde{k}_2 = 0.8k_2$, $\tilde{m}_2 = 0.8m_2$

Damage Pattern 4 demonstrates a damage case caused by simultaneous stiffness and mass changes at the same location. As shown in Table 6.4, the active DFs concentrate on the first and second sensor clusters. In the first row of Table 6.4, DF_{11} and DF_{12} are close to the corresponding ones in Table 6.1, which reveal the change of stiffness occurs between DOF 1 and DOF 2. The second row shows two features due to the combination of two kinds of structural changes, i.e. simultaneous stiffness and mass reductions. DF_{23}

and DF_{24} present the pattern mainly introduced by the mass change without the influence of the stiffness change. DF_{21} and DF_{22} are as a result of the superposition of these two types of damage. So, it can be concluded here that there is a stiffness reduction between DOF 1 and DOF 2 around 20% by looking at the first row. Based on this, the information presented in the last two terms of the two second row is used to evaluate the mass change, which shows the 20% mass reduction. In practice, the asymmetry of the DFs can be considered as the first step to identify the change of mass, and then specific analysis can be conducted to determine the contribution of each type of change. Although the damage and mass change can be detected as explained, it is acknowledged that the interpretation of the results becomes more challenging for such cases. Similar to the previous cases, the variation of DFs is very small, which indicates the stability of the method.

Table 6.4. DFs for the DP4 (average and standard deviation of 10 trials in %)

Reference Channel	1st	2nd	3rd	4th
1st	-8.69 (0.79)	-18.84 (1.00)	-0.52 (1.80)	N/A
2nd	0.84 (0.81)	16.29 (0.82)	24.10 (1.38)	24.88 (0.96)
3rd	-0.12 (1.41)	-0.65 (1.88)	-0.12 (0.73)	N/A
4th	N/A	-0.88 (0.80)	N/A	-0.75 (0.63)

6.3.5 Damage Pattern 5 (DP5): $\tilde{C}_{33} = 0.8C_{33}$

Since most of the civil infrastructure can be considered as lightly damped systems, the damping terms are ignored due to their small contribution to the balance of equations. However, in real life structures or even in our numerical model, small changes in damping may significantly affect the pattern of accelerations, velocity and displacement. In previous damage patterns, the damping matrix has been kept the same even when the mass and stiffness parameters are changed, and the method detects the damage correctly. Although the proposed approach ignores the damping terms and does not seek to identify the change of damping, one would still aim to determine whether or not the damping change will disturb the detection of other changes such as stiffness and mass. In this damage pattern, one element of the matrix, C_{33}, is reduced to study the influence of the change in the damping. In Table 6.5, it is demonstrated that all the DFs are very close to zero, such that the 20% reduction of C_{33} does not contribute to the DFs. It is therefore

expected that the changes of other properties can be identified separately, even if they may lead to a change of damping.

Table 6.5. DFs for the DP5 (average and standard deviation of 10 trials in %)

Reference Channel	1st	2nd	3rd	4th
1st	-0.20 (0.71)	1.80 (1.05)	0.73 (1.93)	N/A
2nd	1.37 (0.78)	-0.19 (0.63)	1.05 (1.13)	0.68 (0.62)
3rd	-0.04 (1.50)	1.48 (1.95)	-0.09 (0.74)	N/A
4th	N/A	1.20 (0.69)	N/A	-0.29 (0.54)

6.3.6 Damage Pattern 6 (DP6): $\tilde{k}_2 = 0.8k_2$, $\tilde{C}_{33} = 0.8C_{33}$, $\tilde{m}_4 = 0.8m_4$

To verify the ability to detect various damages at different locations simultaneously, the last damage pattern is introduced, which is a combination of damage patterns 1, 3, and 5. The DFs for this damage pattern are shown in Table 6.6. In the top-left corner, the DF_{11}, DF_{12}, DF_{21}, and DF_{22} are similar to the corresponding values shown in Table 6.1, which indicates that the reduction of stiffness has been detected, located, and quantified. For the fourth row, DF_{42} and DF_{44} represent the reduction of mass in the system. It can also be seen that the change of damping has no influence on the DFs. It should be noted that in this case study the symmetry and asymmetry can be considered as the main difference between DFs caused by stiffness and mass change. However, in practice, this feature may not be well observed due to the environmental noise. In future research, two independent types of DFs could be introduced to distinguish these two kinds of damage more efficiently.

Table 6.6. DFs for the DP6 (average and standard deviation of 10 trials in %)

Reference Channel	1st	2nd	3rd	4th
1st	-8.66 (0.93)	-17.82 (0.97)	-0.46 (1.74)	N/A
2nd	-17.46 (0.61)	-6.38 (0.64)	0.41 (1.18)	0.58 (0.83)
3rd	-0.76 (1.49)	0.99 (2.00)	-0.07 (0.83)	N/A
4th	N/A	24.67 (1.01)	N/A	23.83 (0.72)

6.3.7 Damage Pattern 7 (DP7): Blind test

In previous damage patterns, damage features were interpreted by the same researcher who actually simulated the damage case. In this damage pattern, we try to mimic a 'true' blind test and to locate damage without knowing where the damage is. To conduct this blind test, a random damage generator is developed. This generator could add stiffness, mass and damping change simultaneously at any location. The reductions of properties could change from 0 to 100%. Table 6.7 shows the damage features obtained by analyzing the data from this blind test and the following comments about Table 6.7 are written without really seeing the applied damage: It is seen that only DF_{22}, DF_{24}, DF_{42} and DF_{44} are negative implying that stiffness change are k_4 which is between DOF 2 and 4. Since DF_{44} is only related to k_4, it directly shows the stiffness reduction of around 60%. Except the DFs mentioned above, DF_{31}, DF_{32} and DF_{33} also deviates from zero. These asymmetrical positive values should reflect the change of mass (a decrease in the mass). The average of these 3 DFs are around 27%, so the change of mass is estimated as 27%/(1+27%)≈21%. These estimations show very high accuracy after comparing with the truly applied damage.

Table 6.7. DFs for the DP7 (average and standard deviation of 10 trials in %)

Reference Channel	1st	2nd	3rd	4th
1st	1.93 (0.22)	3.46 (0.49)	3.62 (0.32)	N/A
2nd	3.57 (0.64)	-20.22 (0.10)	1.03 (0.41)	-60.02 (0.19)
3rd	29.64 (0.52)	27.06 (0.49)	25.50 (0.22)	N/A
4th	N/A	-60.96 (0.19)	N/A	-62.04 (0.07)

CHAPTER 7:APPLICATION OF THE IMRPOVED METHOD TO THE PHASE I OF THE IASC-ASCE BENCHMARK PROBLEM

7.1 Introduction to the IASC-ASCE Benchmark Problem

In order to accelerate the development of SHM methods, some typical benchmark problems that define the realistic conditions and allow researchers to compare the performance of their respective approaches are necessary. In consideration of this, a task group supported by the International Association of Structural Control (IASC) and the Dynamics Committee of the American Society of Civil Engineers (ASCE) was formed in 1999 (Bernal and Beck 2004; Johnson et al. 2004). The structure selected by this group for investigation was a 4-storey shear type steel frame located at the Earthquake Engineering Research Laboratory of the University of British Columbia (Black and Ventura 1998). As shown in Figure 7.1, the structure is 2-bays by 2-bays and 3.6 m tall, with a 2.5 m × 2.5 m base.

A number of research groups have made efforts to apply various approaches to this benchmark problem, either numerically or experimentally. Caicedo et al. (2004) developed an approach combining natural excitation technique, eigensystem realization algorithm, and least squares method to estimate the stiffness of the ASCE benchmark structure using simulated data. With mass and acceleration information, the approach can correctly detect the location and extent of the damage. Nair et al. (2006) used the Auto-Regressive Moving Average (ARMA) model to fit either analytical or experimental vibration signals of the ASCE benchmark structure, and extracted the DF as a function of the first three auto-regressive components. In addition to the existence of damage, they also introduced localization indices to identify the location of the damage. Lynch (2005) used experimental data of the ASCE benchmark structure excited by a shaker to estimate transfer function poles using traditional system identification methods. By comparing the location of poles for an unknown state to those of the baseline state, the damage could be accurately identified. However, excitation data, which is very difficult to obtain in

realistic applications, is used in this approach. Despite these successful attempts, some challenges are still not addressed. Thus, our new approach aims to detect, locate, and quantify the damage caused by mass and stiffness changes in this structure separately using output data only.

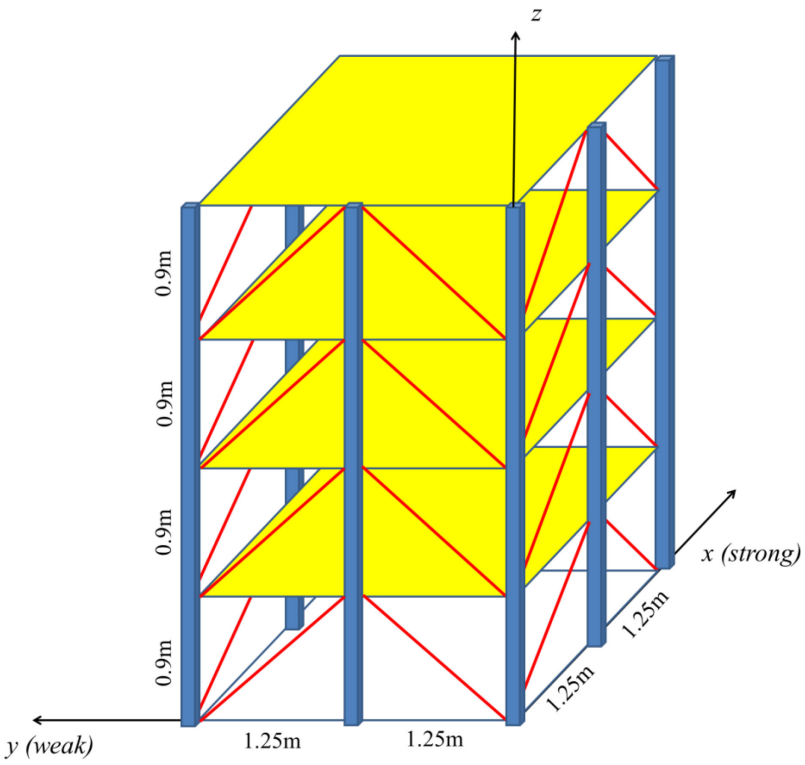

Figure 7.1. Illustration of the ASCE Benchmark Structure (adapted from Johnson et al. 2004)

As the second case study, the proposed approach is tested under simulated data in phase I of the IASC-ASCE benchmark problem using the 120 DOF finite element model. For this model, the sampling time is also 1000Hz, which is nearly twice larger than the 25th modal frequency of 481.44Hz. This means the contributions of the first 25 modes are included in the signal, which should be more than sufficient for most of vibration based damage detection techniques. Excitations in this case study are modeled as independent filtered Gaussian white noises, and are applied one per floor at the center of each floor as approximating wind or other ambient excitations. The excitations can be added either in strong (x) direction or weak (y) direction. Considering that the properties of this shear-type structure in one direction are mainly related to the vibrations in the corresponding

direction, two directions of excitation are applied separately in order to detect the damage in different directions. There are four accelerometers on each floor, two of which are to monitor the accelerations in the x direction, and the other two of which are for the y direction (Figure 7.2). To simulate the errors caused by the measurement or environment, 10% noise is imposed upon all the acceleration signals in the sensors.

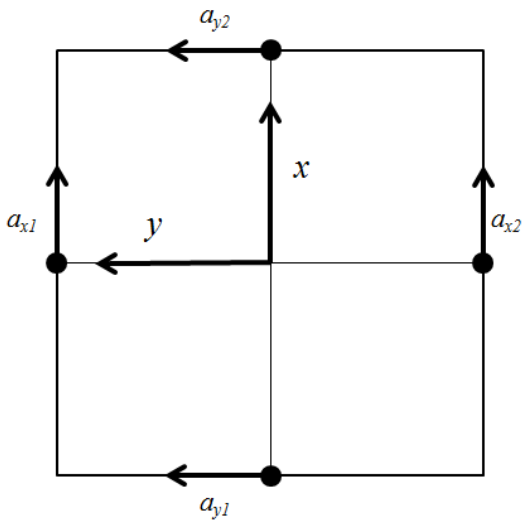

Figure 7.2. Placements and directions of sensors and excitations

There are six damage patterns defined in the benchmark problem to simulate major damage, minor damage, asymmetrical damage, etc. (Johnson et al 2004). These damage patterns are introduced by removing different braces, and mainly manifest as stiffness reduction. In addition, two damage patterns simulating the mass reduction, referred to as Damage Patterns M1 and M2, are also demonstrated in this thesis. The eight damage patterns included in this thesis are outlined below:

• Damage Pattern 1 (DP1): Removal of all braces on the first floor;

• Damage Pattern 2 (DP2): Removal of all braces on the first and third floors;

• Damage Pattern 3 (DP3): Removal of one brace on the first floor;

• Damage Pattern 4 (DP4): Removal of one brace on one side of the first and third floors;

• Damage Pattern 5 (DP5): Damage Pattern 4 + unscrewing of the left end of the north floor beam at the first floor on the west face of the structure;

• Damage Pattern 6 (DP6): Reduction of the stiffness of a brace to two-thirds of its original value;

• Damage Pattern M1 (DPM1): Reduction of mass on the fourth floor; and

• Damage Pattern M2 (DPM2): Damage Pattern M1 + Damage Pattern 1.

Note that the last two damage patterns were not included in the original benchmark damage cases; rather, they were created for this study to demonstrate the capability of the method for detection of changes in mass. As for the 4-DOF mass spring system, in order to show the robustness of the method, the averages and standard deviations of DFs for 10 independent trails are presented for each damage case in the following sections.

Figure 7.3 demonstrates the acceleration signals of the baseline structure acquired by the sensors labeled as a_{x1} in Figure 7.2. In order to obtain the translational acceleration of the floor and reduce the effect of noise, the average is taken of the two sensors in the same direction.

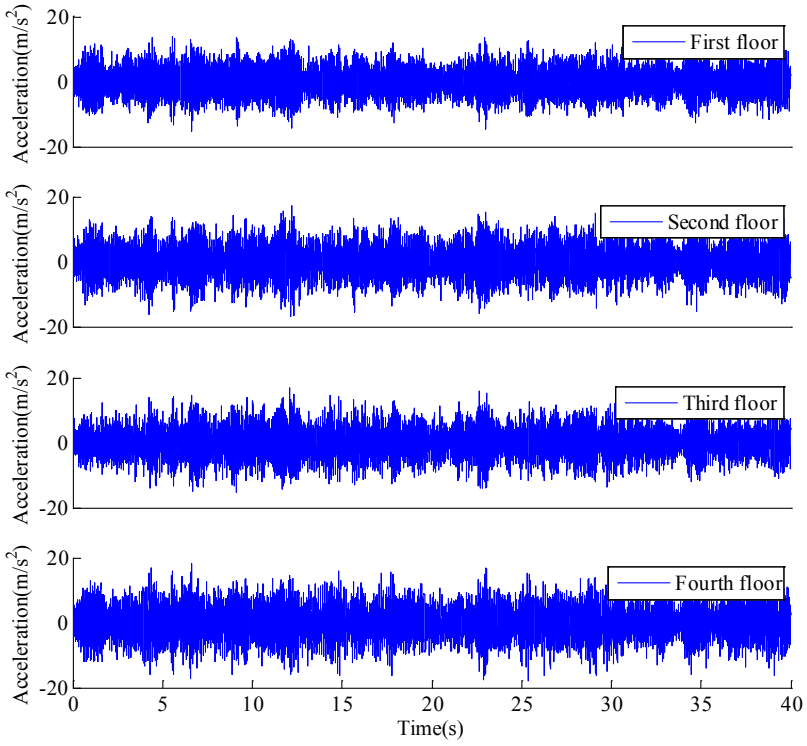

Figure 7.3. Acceleration data for each floor with 10% artificial noise

7.2 Damage Detection Using Acceleration Data Only

7.2.1 Damage Pattern 1 (DP1): All braces of the first floor are broken

The first damage pattern shows a stiffness reduction of the first floor due to the removal of all the braces on the first floor. As described above, the vibration in the *x* direction can be used to detect the change of properties in the *x* direction (strong direction), and the vibration in the *y* direction is for damage detection in the *y* direction (weak direction). The DFs calculated using the proposed method are shown in Table 7.1 for the *x* and *y* directions, respectively. As has already been discussed in previous chapters, each row in these tables represents a sensor cluster. For the *x* direction, all valid DFs except $DF_{11,x}$, which has a value of -24.64%, are very close to zero. This shows that the damage is only related to the change of properties on the first floor. Considering that the original stiffness for the first floor in the *x* direction is 2.1320×10^8 N/m, and that the damaged stiffness is 1.6497×10^8 N/m (Johnson et al. 2004), the reduction of stiffness caused by the elimination of the braces is -(2.1320-1.6497)/2.1320 = -22.60%, which is very close to the DF (-24.64%) shown in the table. This verifies that this approach is able to measure the severity of the damage quite accurately.

Table 7.1. DFs for DP1 in the IASC-ASCE benchmark problem (average and standard deviation of 10 trials in %)

Reference Channel		1st	2nd	3rd	4th
x direction	1st	-24.64 (0.10)	-0.31 (0.44)	N/A	N/A
	2nd	0.06 (0.21)	-0.19 (0.10)	1.27 (0.39)	N/A
	3rd	N/A	-0.01 (0.12)	-0.77 (0.06)	-1.21 (0.13)
	4th	N/A	N/A	-0.35 (0.17)	0.41 (0.05)
y direction	1st	-36.62 (0.07)	-0.14 (0.25)	N/A	N/A
	2nd	1.83 (0.28)	0.11 (0.13)	0.06 (0.33)	N/A
	3rd	N/A	0.06 (0.23)	0.09 (0.09)	0.09 (0.17)
	4th	N/A	N/A	-1.09 (0.21)	-0.88 (0.16)

Similarly, the DFs for the *y* direction demonstrate again that the damage occurred on the first floor. The $DF_{11,y}$ for the *y* direction is -36.62%, which is close to the stiffness

reduction in the *y* direction due to the removal of braces (-(1.3581-0.8758)/1.3581 = -35.51%), indicating that the braces have more contribution to stiffness in the *y* direction than in the *x* direction. The standard deviations for all the DFs in both directions are also shown in Table 7.1. The small values for the standard deviations demonstrate that there is little possibility that the DFs for other places would conceal the true damage.

7.2.2 Damage Pattern 2 (DP2): All braces of first and third floor are broken

Damage pattern 2 involves the removal of the braces on the first and third floors. It is thus expected that the DFs related to the first and third floors will be non-zero values. It is observed from Table 7.2 that the $DF_{11,x}$ for the first row and first column is -23.86%, which is almost the same as the corresponding value in Table 7.1, indicating that the damage for the first floor can still be located and quantified. It can also be seen that for *x* direction the four DFs between the second and third sensors reflect how the removal of the braces on the third floor influences the stiffness. The magnitudes, meanwhile, imply that the removal of the braces results in reductions of -25.48% and -29.41% in total stiffness of the second and third floors, respectively. This damage also creates an approximately 50% reduction in the stiffness between the second and third floors.

Table 7.2. DFs for DP2 in the IASC-ASCE benchmark problem (average and standard deviation of 10 trials in %)

Reference Channel		1st	2nd	3rd	4th
x direction	1st	-23.86 (0.06)	0.77 (0.36)	N/A	N/A
	2nd	2.76 (0.19)	-25.48 (0.08)	-49.71 (0.13)	N/A
	3rd	N/A	-49.21 (0.13)	-29.41 (0.09)	-4.99 (0.10)
	4th	N/A	N/A	0.85 (0.20	1.08 (0.11)
y direction	1st	-37.06 (0.06)	0.88 (0.18)	N/A	N/A
	2nd	0.09 (0.21)	-37.49 (0.08)	-73.57 (0.12)	N/A
	3rd	N/A	-73.98 (0.15)	-39.30 (0.10)	-3..47 (0.16)
	4th	N/A	N/A	-1.68 (0.25)	-1.70 (0.18)

For the *y* direction, the patterns of DFs are similar, but the absolute values are larger, which means that the braces make more contribution to the stiffness in the *y* direction. It

should also be mentioned that other DFs are not exactly zero, mostly due to the 10% noise added to the data. However, since these values are significantly smaller than the other DFs where the damage is observed, the damage is not hidden by the false-positive results. For real implementations, different statistical analyses can be conducted to define a threshold value in order to minimize such false positives and negatives as mentioned before.

7.2.3 Damage Pattern 3 (DP3): One brace of first floor is broken

Damage pattern 3 is minor compared to damage patterns 1 and 2. In damage pattern 3, only one brace of the first floor in the *y* direction is removed, which would lead to a smaller stiffness reduction in the structure. In Table 7.3, it is observed that all the DFs for the *x* direction are very close to zero. This is to be expected since the removed brace would have only provided stiffness in the *y* direction, such that its removal will not influence the stiffness in the *x* direction. For the *y* direction, it can be seen that the patterns of DFs are similar to corresponding ones in Table 7.1, since the removal of the brace only influences the stiffness for the first floor. The $DF_{11,y}$ is -10.65% which is around 1/4 of the corresponding DF in Table 7.1. Given that there are four braces in each direction on each floor, it is reasonable that removal of one brace should lead to 1/4 stiffness reduction compared to the case where all of the braces were removed.

Table 7.3. DFs for DP3 in the IASC-ASCE benchmark problem (average and standard deviation of 10 trials in %)

Reference Channel		1st	2nd	3rd	4th
x direction	1st	0.00 (0.13)	0.00 (0.39)	N/A	N/A
	2nd	0.00 (0.15)	-0.04 (0.09)	-0.02 (0.32)	N/A
	3rd	N/A	0.03 (0.13)	0.01 (0.08)	0.00 (0.13)
	4th	N/A	N/A	-0.06 (0.19)	0.06 (0.11)
y direction	1st	-10.65 (0.07)	-0.74 (0.15)	N/A	N/A
	2nd	1.20 (0.18)	-0.21 (0.13)	-0.85 (0.27)	N/A
	3rd	N/A	-0.01 (0.15)	-0.03 (0.12)	0.56 (0.15)
	4th	N/A	N/A	-0.24 (0.15)	-0.83 (0.14)

7.2.4 Damage Pattern 4 (DP4): One brace for each of the first floor and third floor is broken

Damage pattern 4 involves only minor damage compared to damage pattern 2. Only one brace is broken on each of the first (in *y* direction) and third floors (in *x* direction), which introduces an asymmetrical and torsional behavior into the structure. It can be seen in Table 7.4 that the DFs for the *x* direction related to the second and third floors have large magnitudes, whereas the corresponding DFs for the *y* direction are very close to zero. The reason for this important finding is that the removal of the brace on the third floor is only in the *x* direction, so it will not affect the DFs in the *y* direction. Also note that the DFs in the *x* direction for the second and third floors are around 1/4 of those in Table 7.2, for the same reason described with respect to damage pattern 3. Furthermore, for the *y* direction it shows the same DFs as those in Table 7.3. It is therefore observed that the proposed approach can locate and quantify damage in different directions separately, even if the structure is asymmetrical.

Table 7.4. DFs for DP4 in the IASC-ASCE benchmark problem (average and standard deviation of 10 trials in %)

Reference Channel		1st	2nd	3rd	4th
x direction	1st	-0.57 (0.11)	0.60 (0.32)	N/A	N/A
	2nd	-0.71 (0.22)	-7.83 (0.10)	-15.04 (0.25)	N/A
	3rd	N/A	-14.00 (0.17)	-7.59 (0.11)	0.22 (0.14)
	4th	N/A	N/A	0.04 (0.23)	-0.07 (0.15)
y direction	1st	-10.79 (0.07)	-1.00 (0.14)	N/A	N/A
	2nd	1.29 (0.20)	-0.15 (0.12)	-0.86 (0.29)	N/A
	3rd	N/A	-0.06 (0.15)	0.02 (0.10)	0.59 (0.16)
	4th	N/A	N/A	-0.11 (0.13)	-0.78 (0.11)

7.2.5 Damage Pattern 5 (DP5): Damage Pattern 4 + unscrewing of the left end of the north floor beam at the first floor on the west face of the structure

Damage pattern 5 is very close to damage pattern 4. In addition to the brace removals in damage pattern 4, only one beam is unscrewed on the first floor. From Table 7.5, it can

be observed that the DFs are almost the same as those in Table 7.4, which indicates that the damage pattern 4 is detected and the damage introduced by the unscrewing of the beam is hidden. According to Johnson et al. (2004), it is observed that the difference between the stiffness matrices for damage patterns 4 and 5 is quite small. We thus conclude that the reason the unscrewing of the beam cannot be detected is that the damage is not noticeably reflected in the change in stiffness of the finite element model.

Table 7.5. DFs for DP5 in the IASC-ASCE benchmark problem (average and standard deviation of 10 trials in %)

Reference Channel		1st	2nd	3rd	4th
x direction	1st	-0.55 (0.09)	0.69 (0.21)	N/A	N/A
	2nd	0.63 (0.18)	-7.85 (0.08)	-14.92 (0.32)	N/A
	3rd	N/A	-14.05 (0.16)	-7.61 (0.15)	0.25 (0.15)
	4th	N/A	N/A	0.08 (0.16)	-0.10 (0.15)
y direction	1st	-10.82 (0.09)	-0.79 (0.26)	N/A	N/A
	2nd	1.44 (0.27)	-0.49 (0.13)	-0.75 (0.27)	N/A
	3rd	N/A	-0.14 (0.16)	0.09 (0.13)	0.47 (0.18)
	4th	N/A	N/A	-0.11 (0.17)	-0.71 (0.09)

7.2.6 Damage Pattern 6 (DP6): Area of one brace of the first storey is reduced to its 2/3

Damage pattern 6 is very close to damage pattern 1, which involves stiffness reduction for the first floor. However, damage pattern 6 is even smaller than pattern 1, since no braces are removed but instead the stiffness of one brace on the first floor is reduced to 2/3 of its original value. Similarly, it can be seen in Table 7.6 that the DFs for the *x* direction are very small, which means that the damage is not in the *x* direction. For the *y* direction, a -3.12% reduction in $DF_{11,y}$ is identified, which demonstrates the slight stiffness reduction on the first floor. The magnitude of -3.12% here is approximately 1/3 of the -10.65% magnitude in Table 7.3, which exactly reflects the severity of the damage (1/3 stiffness reduction in the brace). All of the other DFs in this table are close to zero even if the variability is considered. The standard deviation and averages of the DFs are so small that this small damage is not concealed. It is also noted that the variation of DFs

in Case Study II is smaller than in Case Study I. The main reason is that the type of structure is simpler (shear type) so that the chosen sensor clusters are more accurate.

Table 7.6. DFs for DP6 in the IASC-ASCE benchmark problem (average and standard deviation of 10 trials in %)

Reference Channel		1st	2nd	3rd	4th
x direction	1st	0.02 (0.13)	0.03 (0.43)	N/A	N/A
	2nd	0.00 (0.15)	0.04 (0.09)	-0.02 (0.32)	N/A
	3rd	N/A	0.03 (0.13)	0.01 (0.08)	0.00 (0.13)
	4th	N/A	N/A	-0.06 (0.19)	0.07 (0.11)
y direction	1st	-3.12 (0.08)	-0.09 (0.19)	N/A	N/A
	2nd	-0.06 (0.23)	0.09 (0.10)	0.04 (0.20)	N/A
	3rd	N/A	0.17 (0.23)	0.05 (0.12)	-0.02 (0.17)
	4th	N/A	N/A	0.20 (0.19)	-0.17 (0.18)

7.2.7 Damage Pattern M1 (DPM1): Mass of fourth floor is reduced by 20%

From the results for damage patterns 1-6, it is demonstrated that the change of stiffness can be very accurately detected, located, and quantified using the proposed approach. In this section, a reduction of 20% to the mass on the fourth floor is introduced to test the capability of the methodology for identification of mass changes. It can be seen in Table 7.7 that the DFs for the fourth sensor cluster for both *x* and *y* directions are very large (around 25%) while the other values are very close to zero. The same as before, the magnitude of 25% in the DFs for 20% reduction in the mass could be deduced from Eq. 6.8, where the mass term is in the denominator. It should be noted that the DFs for the change of mass are asymmetrical, just as shown for the mass spring system, and same in both *x* and *y* directions, which can be considered as the main differences between change of mass and change of stiffness.

Table 7.7. DFs for DPM1 in the IASC-ASCE benchmark problem (average and standard deviation of 10 trials in %)

Reference Channel		1st	2nd	3rd	4th
x direction	1st	-0.63 (0.09)	0.05 (0.16)	N/A	N/A
	2nd	-0.75 (0.18)	-0.01 (0.08)	0.27 (0.32)	N/A
	3rd	N/A	1.02 (0.16)	-0.16 (0.11)	-0.90 (0.13)
	4th	N/A	N/A	26.20 (0.17)	26.34 (0.14)
y direction	1st	-1.06 (0.06)	-0.28 (0.20)	N/A	N/A
	2nd	1.18 (0.17)	-0.26 (0.13)	-1.03 (0.31)	N/A
	3rd	N/A	-0.71 (0.19)	-0.67 (0.12)	-0.16 (0.15)
	4th	N/A	N/A	24.20 (0.25)	23.22 (0.15)

7.2.8 Damage Pattern M2 (DPM2): Damage Pattern 1 + Damage Pattern M1

From previous sections, the capability of this approach to identify and quantify change of mass and change of stiffness, respectively, has been verified. Now damage consisting of changes of both mass and stiffness is introduced by combining damage pattern 1 and damage pattern M1. The DFs for this damage pattern are demonstrated in Table 7.8. The $DF_{11,x}$ and $DF_{11,y}$ related to the first floor are close to the corresponding DFs in Table 7.1, indicating that a change of stiffness is detected. Similarly, The $DF_{43,x}$, $DF_{44,x}$, $DF_{43,y}$ and $DF_{44,y}$, which demonstrate the change of mass, are the same as those in Table 7.7. It is noted that a change of mass and stiffness can be distinguished by the characteristic that the DFs for mass change are not symmetrical, i.e., that change affects only rows in the table. It is therefore concluded that the proposed approach is able to accurately identify, locate, and quantify damage, and to distinguish change of mass and change of stiffness separately, even when they occur simultaneously. Having said this, it is acknowledged that noticing these symmetrical and asymmetrical changes in real-life data may not be as easy but these findings are still very valuable for separating the stiffness and mass changes using output-only data in SHM applications.

Table 7.8. DFs for DPM2 in the IASC-ASCE benchmark problem (average and standard deviation of 10 trials in %)

Reference Channel		1st	2nd	3rd	4th
x direction	1st	-24.06 (0.11)	-0.93 (0.47)	N/A	N/A
	2nd	-0.91 (0.20)	0.27 (0.09)	0.65 (0.26)	N/A
	3rd	N/A	0.57 (0.19)	-0.41 (0.18)	1.77 (0.16)
	4th	N/A	N/A	24.29 (0.22)	26.41 (0.13)
y direction	1st	-36.94 (0.05)	0.05 (0.19)	N/A	N/A
	2nd	0.78 (0.29)	-0.82 (0.13)	-0.60 (0.25)	N/A
	3rd	N/A	-0.92 (0.39)	-0.42 (0.14)	1.03 (0.20)
	4th	N/A	N/A	23.69 (0.40)	23.63 (0.23)

7.3 Influence of Sampling Time

For real life application, the sampling frequency would affect the accuracy of the collected data and thus the damage detection results. In this section, the relationship between sampling frequency and damage features for *x* direction in damage pattern 1 is investigated as an example. In Figure 7.4, only some typical DFs related to the damage are presented. It is seen that the $DF_{11,x}$, which directly shows the severity of damage in the previous sections, is very stable as the sampling frequency changes. However, other DFs vary as the sampling frequency increases. When sampling frequency is smaller than 400 Hz, DF_{12} and DF_{21} show significant non-zero values. Although these DOFs are still close to the damage on the first floor, this is not observed when sampling frequency is large. As the sampling frequency grows, these DFs gradually converge to zero. Thus, it is demonstrated here that the sampling frequency would indeed influence the results to some extent as expected. In practice, it is important to design the instrumentation plan accordingly to maximize the accuracy of the collected data.

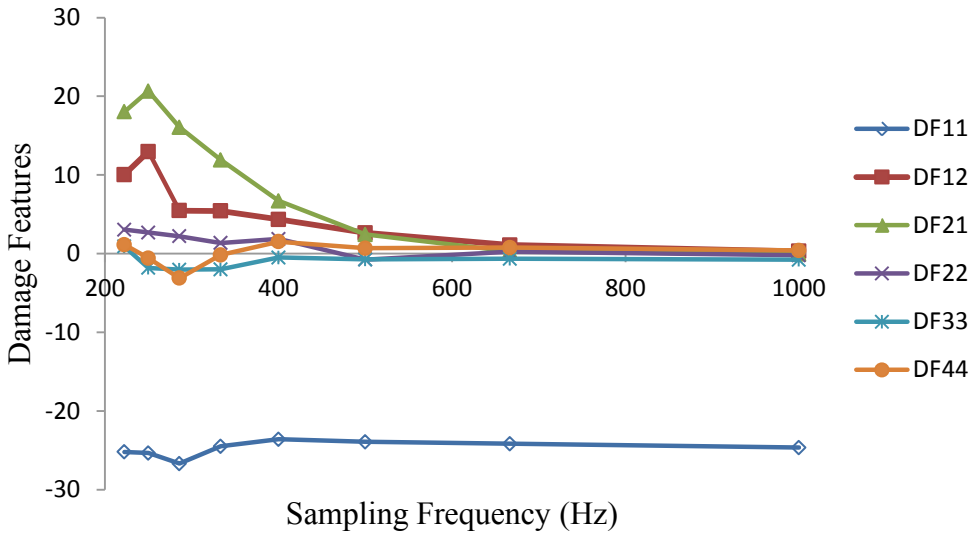

Figure 7.4. Relationship between sampling frequency and damage detection results for *x* direction in damage pattern 1

CHAPTER 8:SUMMARY AND CONCLUSIONS

In this thesis, two damage detection methods using time series modelling and sensor clustering were proposed and developed. It is shown that both methods could detect damage by analyzing output only data from baseline and damaged structures. The main body of the thesis can essentially be summarized in two parts: 1) the development of a novel time series based method for damage detection and its applications to two experimental studies; 2) the improvement of the first method to enable it to identify the change of stiffness and mass separately.

In the first part, the proposed novel time series based method is first presented in Chapter 3. After conducting transformations and applying central difference technique to the equation of motion, the ARX models are used to fit the dynamic responses from free vibrations. Two different DFs are introduced for the purpose of damage detection. The difference between fit ratios of the ARX models is considered as DF1 based on the idea that if damage occurs, the ARX models created from one state will be no longer suitable for another state due to the change of the relationship between different DOFs. For DF2, the distance between the coefficients of the corresponding ARX models are used to detect damage considering that the stiffness matrix is related to these coefficients.

To verify this method, experimental studies for a steel grid type structure and a more realistic 4-span bridge type structure were presented in Chapters 4 and 5. For each structure, the comparison of the results obtained from two DFs is included. The first structure has two clear spans with two continuous girders across the middle supports. Four kinds of damage caused by the change of boundary conditions and the removal of components were applied to this structure. The results demonstrated that the damage could be identified and located correctly and the severity of the damage could be assessed using both types of DFs for most of the cases.

The second structure is a 4-span bridge model with two girders and a steel deck. Seven different damage cases were applied to this structure. In order to present the results clearly, the averages of the DFs for 36 trials were taken to show the location of damage, and the averages of all the DFs were calculated as severity index to expose the severity of

damage. Using both DFs, the damage was identified and located and the severity was estimated correctly. However, it was also noted that there is still some difference between the performances of the methods using two DFs for some damage cases.

In the second part, an improved version of the previous method is developed. In Chapter 6, the theory of the improved method along with a preliminary study on a 4-DOF system is presented. For this method, with the assumption of lumped mass and normally distributed excitations, ARMAX models adopting output-only vibration data are created for different sensor clusters. In this way, an anomaly can be identified by considering the damage features extracted from the difference between coefficients of ARMAX models created for baseline and damaged structures.

The improved method was first applied to a 4-DOF mass spring system for proof of concept. The parameters of the system were chosen by considering realistic structures, and it was directly solved using numerical algorithms developed in MATLAB. The combinations of changes in mass, stiffness and damping were considered as damage scenarios. The results showed that the method can simultaneously identify, locate and quantify the damage due to different stiffness and mass changes.

All the DOFs were used to create ARMAX models in the 4-DOF system, which is impossible for real life structures. To further investigate the validity of this method for sparse sensor networks and more realistic structure, the phase I of the shear type IASC-ASCE benchmark problem was investigated in Chapter 7. The structure selected by the IASC-ASCE group for investigation was a 4-storey and 2-bays by 2-bays shear type steel frame. Six original damage cases caused by the removal or weakening of braces and two additional damage cases developed for changing mass were applied to this structure. It was shown that the proposed damage detection method can identify, locate and quantify damage very accurately for all cases except damage case 5, which was a very minor damage case.

The proposed methods have the following unique advantages compared to the previous methods such as the one proposed by Gül (2009):

1. Since the ARX models are developed based on the equation of motion, the order of the models is fixed for any application, which would facilitate development of an automated SHM system;
2. The proposed methods use ARX/ARMAX models with an order of at most 2 for the exogenous input terms, which could significantly improve the computational efficiency.
3. The second proposed method can detect and locate the change of stiffness and mass separately. This constitutes the first approach of its kind which can distinguish between change of stiffness and mass by using output only vibration data.
4. The second proposed method can very accurately determine the severity of an anomaly. On a theoretical level, it achieves level 3 damage identification as defined in Rytter (1993).
5. The second method could exclude the influence of damping change, which highlights the damage caused by mass and stiffness changes.

8.1 Recommendation for Future Work

Two methods proposed and developed in this thesis are very promising for damage detection in structures. Despite the successful damage detection for two experimental studies and one widely used numerical benchmark model, the methods still have some limitations and are not verified on real life structures.

For future attempts, the most immediate step is to carry out experimental studies of the first method under ambient vibration. Current research demonstrated satisfactory performance on a steel grid type structure and a 4-span bridge type structure using output-only data from free vibration, which demonstrates that the ARX models could fit the dynamic response correctly. However, for real life structures, it is very difficult to conduct impact test to obtain free responses due to practical limitations. In contrast, ambient responses excited by traffic effects are more commonly used. The preliminary studies have shown that the first method could be directly applied to ambient data without any change despite some false-positive results. In addition, some efforts can be made on looking for different DFs based on the developed ARX models (such as difference

between the distances of other coefficients). These points were not in the scope of this thesis and more investigations can be conducted in future.

Secondly, the second method is very promising since it can distinguish the changes in mass and stiffness separately. The characteristic is useful to eliminate the the operational effects, e.g. traffic crossing the bridge, which could cause the change of mass alone. However, this part of study is now only conducted on numerical models. Experimental research for shear type structures and more general structures can be carried out in the future.

Thirdly, it should be noted here that the proposed methods do not need the baseline structure to be healthy. Any damage relative to the baseline structure could be highlighted by the signature of DFs. In real life monitoring of existing structures, the real time vibration data are recorded, and the data from the true health condition are often unavailable. In practical operations, it may be more practical to automatically conduct analysis over time and observe the pattern of the DFs to detect the damage by analyzing these patterns. Corresponding implementations may need the help of statistical models and unsupervised learning, e.g. outlier analysis. This area is included in our research plan.

Fourth, the experimental studies presented for the first method still concentrate on simplified lab structures. For future studies, more factors should be considered and parametric studies considering different boundary conditions, sampling frequencies, damping, and forms of structures should be conducted. Also, the structures including plates and shells may be more complicated due to complex force transmission paths. This direction of study needs to be investigated as well. In addition, only 2D layout of sensor networks is studied so far. The applicability of methods adopting spatial layout of sensor networks will be tested.

Finally, it is widely acknowledged that the change of vibration properties due to temperature effects sometimes is more prominent than that caused by a medium degree of damage in real life structures. Relevant studies about compensating the influence of the varying temperature are also included in our future research plans.

REFERENCES

Ahmadian, H., Mottershead, J. E., and Friswell, M. I. (2000). "Damage location indicators from substructure mode shapes." *Inverse Problems in Engineering*,8(4), 309-323.

Andersen, P. (1997). "Identification of civil engineering structures using ARMA models." Ph.D. Thesis, Aalborg University, Aalborg, Denmark.

Bao, C., Hao, H., and Li, Z. X. (2013). "Integrated ARMA model method for damage detection of subsea pipeline system." *Engineering Structures*, 48, 176-192.

Beck, J., and Bernal, D. (2001). "A benchmark problem for structural health monitoring." *Experimental Techniques*, 25(3), 49-52.

Bernal, D., and Beck, J. (2004). "Preface to the special issue on phase I of the IASC-ASCE structural health monitoring benchmark." *Journal of Engineering Mechanics*, *ASCE,* 130(1), 1–2.

Black, C. J., and Ventura, C. E. (1998). "Blind Test on Damage Detection of a Steel Frame Structure." *Proceedings of the 16th International Modal Analysis Conference (IMAC XVI)*, Santa Barbara, CA, USA, 1, 623-629.

Bodeux J, and Golinval J. (2000). "ARMAV model technique for system identification and damage detection." *Proceedings of the European COST F3 Conference on System Identification and Structural Health Monitoring*, Madrid, Spain, 303–312.

Box, G. E., Jenkins, G. M., and Reinsel, G. C. (2013). "Time Series analysis: Forecasting and Control, 4th Edition." John Wiley & Sons, Hoboken, NJ, USA.

Caicedo, J. M., Dyke, S. J., and Johnson, E. A. (2004). "Natural excitation technique and eigensystem realization algorithm for Phase I of the IASC-ASCE benchmark problem: simulated data." *Journal of Engineering Mechanics, ASCE*, 130(1), 49-60.

Carpinteri, A., and Lacidogna, G. (2006). "Damage monitoring of an historical masonry building by the acoustic emission technique." *Materials and Structures*, 39(2), 161-167.

Catbas, F. N., Caicedo, J.M., and Dyke, S.J. (2006). "Development of a benchmark problem for bridge health monitoring." *the 3rd International Conference on Bridge Maintenance, Safety and Management (IABMAS 2006)*, Porto, Portugal.

Catbas, F. N., Ciloglu, S., Hasancebi, O., Grimmelsman, K., and Aktan, A. (2007). "Limitations in structural identification of large constructed structures." *Journal of Structural Engineering*, *ASCE,* 133(8), 1051–1066.

Catbas, F. N., Gül, M., and Burkett, J. L. (2008). "Damage assessment using flexibility and flexibility-based curvature for structural health monitoring." *Smart Materials and Structures*, 17 (1): 015024.

Cavadas, F., Smith, I. F., and Figueiras, J. (2013). "Damage detection using data-driven methods applied to moving-load responses." *Mechanical Systems and Signal Processing*, 39(1), 409-425.

Cheng, L., and Tian, G. Y. (2012). "Comparison of non-destructive testing methods on detection of delaminations in composites." *Journal of Sensors*, 2012, 1-7.

De Boe, P., and Golinval, J. C. (2003). "Principal component analysis of a piezosensor array for damage localization." *Structural health monitoring*, 2(2), 137-144.

Dharap, P., Koh, B. H., and Nagarajaiah, S. (2006). "Structural health monitoring using ARMarkov observers." *Journal of Intelligent Material Systems and Structures*, 17(6), 469-481.

Doebling, S. W., Farrar, C. R., and Prime, M. B. (1998). "A summary review of vibration-based damage identification methods." *Shock and vibration digest*, 30(2), 91-105.

Dorvash, S., Pakzad, S. N., and Cheng, L. (2013). "An iterative modal identification algorithm for structural health monitoring using wireless sensor networks." *Earthquake Spectra*, 29(2), 339-365.

Fan, W., and Qiao, P. (2011). "Vibration-based damage identification methods: a review and comparative study." *Structural Health Monitoring*, 10(1), 83-111.

Farrar, C. R., Hemez, F. M., Shunk, D. D., Stinemates, D. W., Nadler, B. R., and Czarnecki, J. J. (2004). "A review of structural health monitoring literature: 1996-2001." *by Los Alamos National Laboratory*.

Félio, G., Ferreira, B., McNally, C., Robertshaw, R., Andres, R., Siu, K., Buda, M., Thompson, A., and Lounis, Z. (2012). "Canadian infrastructure report card, volume 1: 2012, municipal roads and water systems," *by Canadian Construction Association, Canadian Public Works Association, Canadian Society for Civil Engineering, and Canadian Public Works Association*.

Federal Highway Administration (FHWA) (2011). "Bridge preservation guide." *by US Department of Transportation.* Report No. FHWA-HIF-11042, McLean, VA.

Federal Highway Administration (FHWA) (2013). "Deficient Bridges by State and Highway System." http://www.fhwa.dot.gov/bridge/nbi/no10/defbr13.cfm (Accessed August 8, 2014).

Figueiredo, E., Figueiras, J., Park, G., Farrar, C. R., and Worden, K. (2011). "Influence of the autoregressive model order on damage detection." *Computer‐Aided Civil and Infrastructure Engineering*, 26(3), 225-238.

Figueiredo, E., Farinholt, K. M., Lee, J. R., Farrar, C. R., and Park, G. (2012). "Use of time-series predictive models for piezoelectric active-sensing in structural health monitoring applications." *Journal of Vibration and Acoustics*, 134(4), 041014.

Fritzen, C.P., Bohle, K., and Stepping, A. (2000). "Damage detection in structures with multiple cracks using computational models," *Proceedings of the European COST F3 Conference on System Identification and Structural Health Monitoring*, Madrid, Spain, 191–200.

George, D., Hunter, N., Farrar, C., & Deen, R. (2000, February). "Identifying damage sensitive features using nonlinear time series and bispectral analysis." *Proceedings of the 18th International Modal Analysis Conference (IMAC XVIII)*, San Antonio, TX, USA, 1796-1802.

Gül, M., and Catbas, F.N. (2008). "A new methodology for identification, localization and quantification of damage by using time series modeling", *26th International Modal Analysis Conference (IMAC XXVI)*, Orlando, FL, USA.

Gül, M., and Catbas, F. N. (2009). "Statistical pattern recognition for structural health monitoring using time series modeling: theory and experimental Verifications." *Mechanical Systems and Signal Processing*, 23(7), 2192-2204.

Gül, M. (2009). "Investigation of damage detection methodologies for structural health monitoring." Ph.D. dissertation, University of Central Florida, Orlando, FL, USA.

Gül, M., and Catbas, F.N. (2011). "Structural health monitoring and damage assessment using a novel time series analysis methodology with sensor clustering." *Journal of Sound and Vibration*, 330(6): 1196-1210.

Hamze, A., Gueguen, P., Roux, P., and Baillet, L. (2014). "Damage detection and localisation using mode-based method and perturbation theory." In *7th European Workshop on Structural Health Monitoring(EWSHM 2014)*, Nantes, France.

Han, L. Z., Zhang, J. Q., and Yang, Y. (2014). "Optimal placement of sensors for monitoring systems on suspension bridges using genetic algorithms." *Applied Mechanics and Materials*, 530, 320-331.

Hearn, G., and Testa, R. B. (1991). "Modal analysis for damage detection in structures." *Journal of Structural Engineering*, *ASCE*, 117(10), 3042-3063.

Hermans, L., and van der Auweraer, H. (1999). "Modal testing and analysis of structures under operational conditions: industrial applications." *Mechanical Systems and Signal Processing*, 13(2), 193-216.

Hoła, J., and Schabowicz, K. (2010). "State-of-the-art non-destructive methods for diagnostic testing of building structures–anticipated development trends." *Archives of Civil and Mechanical Engineering*, 10(3), 5-18.

Hou, Z., Noori, M., and Amand, R. (2000). "Wavelet-based approach for structural damage detection." *Journal of Engineering Mechanics*, *ASCE*, 126(7), 677–683.

Huang, Z., Liu, G., Todd, M., and Mao, Z. (2013). "Damage detection using vector auto-regressive models." *Proc. SPIE 8695, Health Monitoring of Structural and Biological Systems*, San Diego, CA, USA, 86953E.

Inaudi, D., and Glisic, B. (2008). "Overview of 40 bridge monitoring projects using fiber optic sensors." *Conference CD, 4TH International Conference on Bridge Maintenance, Safety and Management (IABMAS '08),* Seoul, Korea.

Jaishi, B., and Ren, W. X. (2006). "Damage detection by finite element model updating using modal flexibility residual." *Journal of Sound and Vibration*, *290*(1), 369-387.

Jang, W. S., Healy, W. M., and Skibniewski, M. J. (2008). "Wireless sensor networks as part of a web-based building environmental monitoring system." *Automation in Construction*, 17(6), 729-736.

Jiang, S. F., Zhang, C. M., and Zhang, S. (2011). "Two-stage structural damage detection using fuzzy neural networks and data fusion techniques." *Expert systems with applications*, 38(1), 511-519.

Johnson, E., Lam, H., Katafygiotis, L., and Beck, J. (2004). "Phase I IASC-ASCE structural health monitoring benchmark problem using simulated data." *Journal of Engineering Mechanics, ASCE*, 130(1), 3–15.

Ju, F. D., and Mimovich, M. E. (1988). "Experimental diagnosis of fracture damage in structures by the modal frequency method." *Journal of Vibration, Acoustics Stress and Reliability in Design*, 110(4), 456-463.

Juang, J. N., and Pappa, R. S. (1985). "An eigensystem realization algorithm for modal parameter identification and modal reductions." *Journal of Guidance and Control Dynamics*, 8(5), 620-627.

Kam, T. Y., and Lee, T. Y. (1992). "Detection of cracks in structures using modal test data." *Engineering Fracture Mechanics*, 42(2), 381-387.

Kessler, S. S., Spearing, S. M., and Soutis, C. (2002a). "Damage detection in composite materials using lamb wave methods." *Smart Materials and Structures*, 11(2), 269.

Kessler, S. S., Spearing, S. M., Atalla, M. J., Cesnik, C. E., & Soutis, C. (2002b). "Damage detection in composite materials using frequency response methods." *Composites Part B: Engineering*, 33(1), 87-95.

Kim, J.T., Ryu, Y.S., Cho, H.M., and Stubbs, N. (2003). "Damage identification in beam-type structures: frequency-based method vs. mode-shape based method." *Engineering Structures*, 25(1), 57-67.

Koh, B. H., and Dyke, S. J. (2007). "Structural health monitoring for flexible bridge structures using correlation and sensitivity of modal data." *Computers & structures*, 85(3), 117-130.

Kuwabara, M., Yoshitomi, S., and Takewaki, I. (2013). "A new approach to system identification and damage detection of high-rise buildings." *Structural Control and Health Monitoring*, 20(5), 703-727.

Lam, H. F., Yuen, K. V., and Beck, J. L. (2006). "Structural health monitoring via measured Ritz vectors utilizing artificial neural networks." *Computer‐Aided Civil and Infrastructure Engineering*, 21(4), 232-241.

Lei, Y., Xu, Z. Q., Ni, P. H., and Mao, Y. K. (2010). "A substructure approach for damage detection of large size structures under limited input and output measurements." *Proceedings of the 12th International Conference on Engineering, Science, Construction, and Operations in Challenging Environments-Earth and Space, ASCE,* Honolulu, Hawaii, USA, 2595-2604.

Levy H, and Lessman F. (1992). "Finite Difference Equations." Dover Publications, Mineola, NY, United States.

Lifshitz, J. M., and Rotem, A. (1969). "Determination of reinforcement unbonding of composites by a vibration technique." *Journal of Composite Materials*,3(3), 412-423.

Limongelli, M. P. (2010). "Frequency response function interpolation for damage detection under changing environment." *Mechanical Systems and Signal Processing*, 24(8), 2898-2913.

Liu, P. L. (1995). "Identification and damage detection of trusses using modal data." *Journal of Structural Engineering*, *ASCE,* 121(4), 599-608.

Ljung, L. (1999). "System identification: theory for the user." Prentice Hall, Upper Saddle River, NJ, USA.

Loh, C. H., Chen, C. H., and Hsu, T. Y. (2011). "Application of advanced statistical methods for extracting long-term trends in static monitoring data from an arch dam." *Structural Health Monitoring*, 10(6), 587-601.

Lynch, J. P., Sundararajan, A., Law, K. H., Kiremidjian, A. S., and Carryer, E. (2004). "Embedding damage detection algorithms in a wireless sensing unit for operational power efficiency." *Smart Materials and Structures*, 13(4), 800.

Lynch, J. (2005). "Damage characterization of the IASC-ASCE structural health monitoring benchmark structure by transfer function pole migration." *Proceedings of the*

*ASCE Structures Congress and the Forensic Engineering Symposium***,** New York, NY, 845-854.

Lynch, J. P., and Loh, K. J. (2006). "A summary review of wireless sensors and sensor networks for structural health monitoring." *Shock and Vibration Digest*, 38(2), 91-130.

Magalhães, F., Cunha, A., and Caetano, E. (2012). "Vibration based structural health monitoring of an arch bridge: from automated OMA to damage detection." *Mechanical Systems and Signal Processing*, 28, 212-228.

Maity, D., and Tripathy, R.R. (2005). "Damage assessment of structures from changes in natural frequencies using genetic algorithm." *Structural Engineering and Mechanics*, 19(1), 21-42.

Min, J., Park, S., Yun, C. B., Lee, C. G., & Lee, C. (2012). Impedance-based structural health monitoring incorporating neural network technique for identification of damage type and severity. *Engineering Structures*, *39*, 210-220.

Mei, Q., and Gül, M. (2014). "A novel sensor clustering-based approach for simultaneous detection of stiffness and mass changes using output-only data." *Journal of Structural Engineering, ASCE*, under review.

Messina, A., Williams, E. J., and Contursi, T. (1998). "Structural damage detection by a sensitivity and statistical-based method." *Journal of Sound and Vibration*, 216(5), 791-808.

Monroig, E., and Fujino, Y. (2006). "Damage Identification Based on a Local Physical Model for Small Cluster of Wireless Sensors." In *the 1st Asia-Pacific Workshop on Structural Health Monitoring*, Yokohama, Japan.

Mottershead, J. E., and Friswell, M. I. (1993). "Model updating in structural dynamics: a survey." *Journal of sound and vibration*, 167(2), 347-375.

Mirza, S.M. and Haider, M. (2003). "The state of infrastructure in Canada: implications for infrastructure planning and policy," *Infrastructure Canada*, 29(1), 17-38.

Moaveni, B., Hurlebaus, S., and Moon, F. (2012). "Special issue on real-world applications of structural identification and health monitoring methodologies." *Journal of Structural Engineering*, *ASCE*, 139(10), 1637-1638.

Mollineaux, M., Balafas, K., Branner, K., Nielsen, P., Tesauro, A., Kiremidjian, A., and Rajagopal, R. (2014). "Damage detection methods on wind turbine blade testing with wired and wireless accelerometer sensors." In *7th European Workshop on Structural Health Monitoring(EWSHM 2014)*, Nantes, France.

Mosavi, A. A., Dickey, D., Seracino, R., and Rizkalla, S. (2012). "Identifying damage locations under ambient vibrations utilizing vector autoregressive models and Mahalanobis distances." *Mechanical Systems and Signal Processing*, 26, 254-267.

Mujica, L. E., Rodellar, J., Fernandez, A., and Guemes, A. (2010). "Q-statistic and T2-statistic PCA-based measures for damage assessment in structures." *Structural Health Monitoring*, 10: 539-553.

Nakamura, M., Masri, S. F., Chassiakos, A. G., and Caughey, T. K. (1998). A method for non‐parametric damage detection through the use of neural networks." *Earthquake engineering & structural dynamics*, 27(9), 997-1010.

Nair, K. K., Kiremidjian, A. S., and Law, K. H. (2006). "Time series-based damage detection and localization algorithm with application to the ASCE benchmark structure." *Journal of Sound and Vibration*, 291(1), 349-368.

Natke, H. G., and Cempel, C. (1997). "Model-Aided Diagnosis Based on Symptoms." *DAMAS 97, Structural Damage Assessment using Advanced Signal Processing Procedures*, Sheffield, UK, 363–375.

Plankis, A. (2012). "Structural health monitoring MEMS sensors using elasticity-based beam vibrations." M.S thesis, Colorado State University, Fort Collins, CO, USA.

Ponzo, F. C., Ditommaso, R., Auletta, G., and Mossucca, A. (2010). "A fast method for structural health monitoring of Italian reinforced concrete strategic buildings." *Bulletin of earthquake engineering*, 8(6), 1421-1434.

Roshandeh, A. M., Poormirzaee, R., and Ansari, F. S. (2014). "Systematic data management for real-time bridge health monitoring using layered big data and cloud computing. *International Journal of Innovation and Scientific Research*, *2*(1), 29-39.

Roveri, N., and Carcaterra, A. (2012). "Damage detection in structures under traveling loads by Hilbert–Huang transform." *Mechanical Systems and Signal Processing*, *28*, 128-144.

Salawu, O. S. (1997). “Detection of structural damage through changes in frequency: a review.” *Engineering structures*, 19(9), 718-723.

Salgado, R., Cruz, P. J., Ayala, G., and Zamora, S. A. (2014). “Performance of damage detection methods used in bridge structures through dynamic tests in steel beams.” *American Journal of Civil Engineering*, *2*(2), 18-26.

Sampaio, R. P. C., Maia, N. M. M., and Silva, J. M. M. (1999). “Damage detection using the frequency-response-function curvature method.” *Journal of Sound and Vibration*, 226(5), 1029-1042.

Shiradhonkar, S. R., and Shrikhande, M. (2011). “Seismic damage detection in a building frame via finite element model updating.” *Computers and Structures*, 89(23), 2425-2438.

Shu, J., Zhang, Z., Gonzalez, I., & Karoumi, R. (2013). The application of a damage detection method using Artificial Neural Network and train-induced vibrations on a simplified railway bridge model. *Engineering structures*, *52*, 408-421.

Siebel, T., Friedmann, A., Koch, M., and Mayer, D. (2012). “Assessment of mode shape-based damage detection methods under real operational conditions.” In *6th European Workshop on Structural Health Monitoring (EWSHM 2012), Dresden, Germany*.

Sohn, H., Farrar, C. R., Hunter, N. F., and Worden, K. (2001a). “Structural health monitoring using statistical pattern recognition techniques.” *Journal of Dynamic Systems, Measurement, and Control*, 123(4), 706-711.

Sohn, H., and Farrar, C. R. (2001b). “Damage diagnosis using time series analysis of vibration signals.” *Smart materials and structures*, 10(3), 446.

Taha, M. M. R. (2010). “A neural-wavelet technique for damage identification in the ASCE benchmark structure using phase II experimental data.” *Advances in Civil Engineering*, 2010, 1-13.

Taylor, S. G., and Zimmerman, D. C. (2010). “Improved experimental Ritz vector extraction with application to damage detection.” *Journal of Vibration and Acoustics*, 132(1), 011012.

Tang, J. P., Chiou, D. J., Chen, C. W., Chiang, W. L., Hsu, W. K., Chen, C. Y., and Liu, T. Y. (2010). "A case study of damage detection in benchmark buildings using a Hilbert-Huang Transform-based method." *Journal of Vibration and Control*, 17(4), 623-636.

Terrell, T. (2011). "Structural health monitoring for damage detection using wired and wireless sensor clusters." MSc thesis, University of Central Florida, Orlando, FL, USA.

Rytter, A. (1993). "Vibration based inspection of civil engineering structures," Ph. D. Dissertation, Aalborg University, Aalborg, Denmark.

VanZwol, T. R., Cheng, J. R., and Tadros, G. (2008). "Long-term structural health monitoring of the Crowchild Trail Bridge." *Canadian Journal of Civil Engineering*, 35(2), 179-189.

West, W.M. (1984). "Illustration of the use of modal assurance criterion to detect structural changes in an orbiter test specimen." in *Proc. Air Force Conference on Aircraft Structural Integrity*, 1–6.

Wikipedia， the free encyclopedia, (2014). "List of bridge failures." http://en. wikipedia. org/ wiki/List_of_bridge_failures (Accessed Sep 23, 2014).

Wong, K. Y. (2004). "Instrumentation and health monitoring of cable‐supported bridges." *Structural Control and Health Monitoring*, 11(2), 91-124.

Wyłomańska, A., Obuchowski, J., Zimroz, R., and Hurd, H. (2014). "Periodic Autoregressive Modeling of Vibration Time Series From Planetary Gearbox Used in Bucket Wheel Excavator." In *Cyclostationarity: Theory and Methods* (pp. 171-186). Springer International Publishing.

Xing, Z., and Mita, A. (2012). "A substructure approach to local damage detection of shear structure." *Structural Control and Health Monitoring*, 19(2), 309-318.

Xu, Y. L., Chen, B., Ng, C. L., Wong, K. Y., and Chan, W. Y. (2010). "Monitoring temperature effect on a long suspension bridge." *Structural Control and Health Monitoring*, *17*(6), 632-653.

Xu, Y. L., Huang, Q., Zhan, S., Su, Z. Q., and Liu, H. J. (2014). "FRF-based structural damage detection of controlled buildings with podium structures: Experimental investigation." *Journal of Sound and Vibration*, 333(13), 2762-2775.

Yao, R., and Pakzad, S. N. (2014). "Damage and noise sensitivity evaluation of autoregressive features extracted from structure vibration." *Smart Materials and Structures*, 23(2), 025007.

Yam, L. H., Yan, Y. J., and Jiang, J. S. (2003). "Vibration-based damage detection for composite structures using wavelet transform and neural network identification." *Composite Structures*, 60(4), 403-412.

Yang, S.M., and Lee, G.S. (1999). "Effects of modeling error on structure damage diagnosis by two-stage optimization," *Structural Health Monitoring 2000*, Fu-Kuo Chang ed, CRC Press, Boca Raton, FL, USA, 871–880.

Yang, J. N., Lei, Y., Lin, S., and Huang, N. (2004). "Hilbert-Huang based approach for structural damage detection." *Journal of engineering mechanics*, *ASCE,* 130(1), 85-95.

Yi, T. H., and Li, H. N. (2012). "Methodology developments in sensor placement for health monitoring of civil infrastructures." International Journal of Distributed Sensor Networks, 2012, 1-11.

Yi, T. H., Li, H. N., and Gu, M. (2013). "Recent research and applications of GPS‐based monitoring technology for high‐rise structures." *Structural Control and Health Monitoring*, 20(5), 649-670.

Zang, C., and Imregun, M. (2001). "Structural damage detection using artificial neural networks and measured FRF data reduced via principal component projection." Journal of Sound and Vibration, 242(5), 813-827.

Zaurin, R. (2009). "Structural health monitoring with emphasis on computer vision, damage indices and statistical analysis." Ph.D. Dissertation, University of Central Florida Orlando, FL, USA.

Zhong, S., Yadiji, S.O., and Ding, K. (2008). "Response-only method for damage detection of beam-like structures using high accuracy frequencies with auxiliary mass spatial probing." *Journal of Sound and Vibration*, 311(3), 1075–1099.

Zimmerman, D.C. (1999). "Looking into the crystal ball: The continued need for multiple viewpoints in damage detection." *DAMAS 99, Structural Damage Assessment using Advanced Signal Processing Procedures*, Dublin, Ireland, 76–90.